JOURNAL OF THE AERONAUTICAL SCIENCES

VOLUME 14 JANUARY, 1947 NUMBER 1

CONTENTS

A Method for Simplifying the Calculations of the Natural Frequencies for a System Consisting of *n* Rigid Rotating Discs Mounted on an Elastic Shaft ..... JOHN L. BOGDANOFF 5

Analytic Definition of a Retractable Landing Gear Axis of Rotation .. ROY A. LIMING 19

Exact and Approximate Solutions of Two-Dimensional Oblique Shock Flow ..... EDMUND V. LAITONE 25

The Bending of Rotor Blades ..... ALEXANDER H. FLAX 42

Systematic Wing Section Development ..... GEORGE S. SCHAIRER 51

Force Measurements by Means of Resistance Wire Strain Gages ..... W. C. RANDELS AND V. C. PLANE 59

Letters to the Editor 23, 24

Published by the
INSTITUTE OF THE AERONAUTICAL SCIENCES, INC.

JOURNAL OF THE AERONAUTICAL SCIENCES

Editor: HUGH L. DRYDEN, *Associate Director, National Bureau of Standards*

Associate Editor: ROBERT R. DEXTER *Associate Editor:* BERNEICE H. JARCK

The Institute of the Aeronautical Sciences publishes monthly the JOURNAL OF THE AERONAUTICAL SCIENCES and the AERONAUTICAL ENGINEERING REVIEW.

The JOURNAL OF THE AERONAUTICAL SCIENCES prints papers of scientific and technical interest to Institute members and subscribers. In general, it provides an opportunity for specialists to publish articles disclosing new knowledge and new applications in the field of the aeronautical sciences. The JOURNAL restricts itself to the aeronautical aspects of advances in science and engineering, and papers printed have either been submitted directly to the JOURNAL or have been previously presented at a meeting of the Institute.

The AERONAUTICAL ENGINEERING REVIEW keeps members and subscribers informed regarding the contents of new books and current periodicals in the field of aeronautics. It reviews new developments in the aircraft industry and reports on progress from house organs and catalogs published by aircraft and engine manufacturers and other companies engaged in aeronautical activities. It publishes papers on applied engineering and aircraft production. News of Institute activities is published in the REVIEW.

Statements and opinions expressed in the JOURNAL are to be understood as individual expressions of the authors and not those of the Institute.

SUBSCRIPTION RATES

Journal of the Aeronautical Sciences
Published Monthly

United States and Possessions		Foreign Countries Including Canada (American Currency Rates)	
1 Year	$7.00	1 Year	$9.00
Single Copies	0.70	Single Copies	1.00

Aeronautical Engineering Review
Published Monthly

United States and Possessions		Foreign Countries Including Canada (American Currency Rates)	
1 Year	$3.00	1 Year	$3.50
Single Copies	0.30	Single Copies	0.35

Notices of change of address should be sent to the Institute at least 30 days prior to actual change of address.

Manuscripts for publication, proofs, and all correspondence should be addressed to the Editorial Office of the JOURNAL.

Correspondence regarding subscriptions may be addressed to Publication Office, 20th and Northampton Sts., Easton, Pa., or to the Editorial Office of the JOURNAL OF THE AERONAUTICAL SCIENCES, 2 East 64th Street, New York 21, New York.

Copyright, 1947, by the Institute of the Aeronautical Sciences, Inc.

Entered as Second-Class Matter at the Post Office, Easton, Pa., May 1, 1937. Acceptance for mailing at a special rate of Postage provided for in the Act of August 24, 1912. Authorized April 29, 1937.

IN

ARTHUR

P. R. B
J. H. K
JOHN C
BURDET

S. PAUL

BENNET

B. E. A
PETER
REX B.
LAWRE
GEORG
W. A. M

W. M.
WALTE
ERNEST
RALPH
DONAL
R. H. F
JACK F
ROBER

JOHN C.
GRIFFIT
W. A. M
E. U. C
L. C. C

H. H. A
FRANK
SIR GEO
DONALD
HUGH L
W. F. D

E. E. A
HART C
W. A. M
E. L. C
DONALD
SHERMA

JOHN D
E. E. A
HARRY
KARL A
J. L. A
PAUL S
RALPH
P. R. B
WELLW
REX B
G. M.
DON R
HENRY
WILLIA
B. C. I
GEORG
LYMAN
W. G.
WILLI
CHARL
KENNI
CHARL
ALLAN
V. E.
FRANK
CHARL
KARL
EMERS
JOHN
RALPH
LUIS
SMITH
J. P.
WALT
JAMES
C. S.

INSTITUTE of the AERONAUTICAL SCIENCES

President
ARTHUR E. RAYMOND

Vice-Presidents
P. R. BASSETT
J. H. KINDELBERGER
JOHN C. LESLIE
BURDETTE S. WRIGHT

Director
S. PAUL JOHNSTON

Executive Vice-President
BENNETT H. HORCHLER

Past-Presidents
J. C. HUNSAKER
CHARLES L. LAWRANCE
DONALD W. DOUGLAS
GLENN L. MARTIN
CLARK B. MILLIKAN
T. P. WRIGHT
GEORGE W. LEWIS
JAMES H. DOOLITTLE
FRANK W. CALDWELL
HALL L. HIBBARD
HUGH L. DRYDEN
R. H. FLEET
CHARLES H. COLVIN

Secretary
ROBERT R. DEXTER

Treasurer
C. S. JONES

Controller
JOSEPH J. MAITAN

Counsel
ALLAN D. EMIL

COUNCIL

E. E. ALDRIN
PETER ALTMAN
REX B. BEISEL
LAWRENCE D. BELL
GEORGE W. BRADY
W. A. M. BURDEN
CHARLES H. COLVIN
JAMES H. DOOLITTLE
WILLIAM K. EBEL
SHERMAN M. FAIRCHILD
DONALD W. FINLAY
CHARLES FROESCH
LEROY R. GRUMMAN
R. PAUL HARRINGTON
W. WALLACE KELLETT
OTTO E. KIRCHNER
JEROME LEDERER
ROBERT J. MINSHALL
EARL D. OSBORN
ELMER A. SPERRY, JR.
ERNEST G. STOUT
FRED E. WEICK

ADVISORY COMMITTEE

W. M. ALLEN
WALTER BEECH
ERNEST R. BREECH
RALPH S. DAMON
DONALD W. DOUGLAS
R. H. FLEET
JACK FRYE
ROBERT E. GROSS
R. M. HAZEN
H. MANSFIELD HORNER
J. C. HUNSAKER
CROIL HUNTER
TH. VON KÁRMÁN
I. M. LADDON
P. W. LITCHFIELD
F. W. MAGIN
ALFRED MARCHEV
GLENN L. MARTIN
THOMAS A. MORGAN
R. C. MUIR
JOHN K. NORTHROP
W. A. PATTERSON
E. T. PRICE
F. W. REICHELDERFER
LAURANCE S. ROCKEFELLER
FRED H. ROHR
T. CLAUDE RYAN
GUY W. VAUGHAN
EDWARD P. WARNER

HONORARY MEMBERS

JOHN C. ADAMS
GRIFFITH BREWER
W. A. M. BURDEN
E. U. CONDON
L. C. CRAIGIE
IRA C. EAKER
HARRY F. GUGGENHEIM
HENRY G. HOUGHTON
GEORGE C. KENNEY
CURTIS E. LE MAY
GEORGE B. PEGRAM
E. M. POWERS
J. LAURENCE PRITCHARD
ARTHUR W. RADFORD
F. W. REICHELDERFER
L. B. RICHARDSON
H. B. SALLADA
CARL SPAATZ
L. C. STEVENS
NATHAN F. TWINING

HONORARY FELLOWS

H. H. ARNOLD
FRANK W. CALDWELL
SIR GEOFFREY DE HAVILLAND
DONALD W. DOUGLAS
HUGH L. DRYDEN
W. F. DURAND
SIR RICHARD FAIREY
SIR ROY FEDDEN
J. C. HUNSAKER
SIR MELVILL JONES
GEORGE W. LEWIS
GLENN L. MARTIN
GEORGE J. MEAD
SIR FREDERICK HANDLEY PAGE
D. R. PYE
IGOR I. SIKORSKY
G. I. TAYLOR
TH. VON KÁRMÁN
EDWARD P. WARNER
ORVILLE WRIGHT
T. P. WRIGHT

BENEFACTORS

E. E. ALDRIN
HART O. BERG (Deceased)
W. A. M. BURDEN
E. L. CORD
DONALD W. DOUGLAS
SHERMAN M. FAIRCHILD
SIR RICHARD FAIREY
R. H. FLEET
FLORENCE GUGGENHEIM (Deceased)
C. D. HANSCOM
JOHN P. V. HEINMULLER
ALEXANDER KLEMIN
PAUL KOLLSMAN
BELLA C. LANDAUER
WILLIAM LANDAUER
GROVER LOENING
EDMUND C. LYNCH (Deceased)
F. W. MAGIN
GLENN L. MARTIN
GEORGE J. MEAD
S. A. REED (Deceased)
LAURANCE S. ROCKEFELLER
EDWARD P. WARNER

AMERICAN FELLOWS

JOHN D. AKERMAN
E. E. ALDRIN
HARRY G. ARMSTRONG
KARL ARNSTEIN
J. L. ATWOOD
PAUL S. BAKER
RALPH S. BARNABY
P. R. BASSETT
WELLWOOD E. BEALL
REX B. BEISEL
G. M. BELLANCA
DON R. BERLIN
HENRY A. BERLINER
WILLIAM BOLLAY
B. C. BOULTON
GEORGE W. BRADY
LYMAN J. BRIGGS
W. G. BROMBACHER
WILLIAM G. BROWN
CHARLES P. BURGESS
KENNETH CAMPBELL
CHARLES H. CHATFIELD
ALLAN CHILTON
V. E. CLARK
FRANKLIN R. COLLBOHM
CHARLES H. COLVIN
KARL T. COMPTON
EMERSON W. CONLON
JOHN W. CROWLEY, JR.
RALPH S. DAMON
LUIS DE FLOREZ
SMITH J. DE FRANCE
J. P. DEN HARTOG
WALTER S. DIEHL
JAMES H. DOOLITTLE
C. S. DRAPER
IVAN H. DRIGGS
WILLIAM K. EBEL
C. L. EGTVEDT
FREDERIC FLADER
CHARLES FROESCH
JACK FRYE
GARLAND FULTON
LESTER D. GARDNER
RICHARD C. GAZLEY
MICHAEL E. GLUHAREFF
MELVIN N. GOUGH
LEROY R. GRUMMAN
HAROLD R. HARRIS
R. M. HAZEN
ALBERT F. HEGENBERGER
EDWARD H. HEINEMANN
S. D. HERON
HALL L. HIBBARD
L. S. HOBBS
PAUL E. HOVGAARD
WILLIAM HOVGAARD
ROBERT INSLEY
EASTMAN N. JACOBS
CLARENCE L. JOHNSON
S. PAUL JOHNSTON
ALEXANDER KARTVELI
PAUL H. KEMMER
J. H. KINDELBERGER
OTTO E. KIRCHNER
ARTHUR L. KLEIN
ALEXANDER KLEMIN
W. B. KLEMPERER
PAUL KOLLSMAN
OTTO C. KOPPEN
B. V. KORVIN-KROUKOVSKY
S. M. KRAUS
I. M. LADDON
E. S. LAND
CHARLES L. LAWRANCE
JEROME LEDERER
JOHN G. LEE
JOHN C. LESLIE
CHARLES A. LINDBERGH
WILLIAM LITTLEWOOD
GROVER LOENING
ALBERT E. LOMBARD
W. RANDOLPH LOVELACE, II
EUGENE E. LUNDQUIST
R. D. MACCART
JOHN R. MARKHAM
ERLE MARTIN
WM. H. MCAVOY
C. J. MCCARTHY
CLARK B. MILLIKAN
ROBERT J. MINSHALL
JOSEPH S. NEWELL
ALFRED S. NILES
JOHN K. NORTHROP
ARTHUR NUTT
SHATSWELL OBER
ROBERT R. OSBORN
W. BAILEY OSWALD
GEORGE A. PAGE, JR.
F. W. PAWLOWSKI
F. W. PENNOYER, JR.
A. A. PRIESTER
ARTHUR E. RAYMOND
F. W. REICHELDERFER
ELLIOTT G. REID
H. J. E. REID
H. C. RICHARDSON
RUSSELL G. ROBINSON
LEONARD E. ROOT
C. E. ROSENDAHL
ADDISON M. ROTHROCK
WILLIAM T. SCHWENDLER
FRANCIS R. SHANLEY
JAMES M. SHOEMAKER
MAC SHORT
IGOR ALEXIS SIKORSKY
ABE SILVERSTEIN
SELDEN B. SPANGLER
ELMER A. SPERRY, JR.
JOHN STACK
WILLIAM B. STOUT
HARRY A. SUTTON
C. FAYETTE TAYLOR
EDWARD S. TAYLOR
PHILIP B. TAYLOR
TH. THEODORSEN
T. E. TILLINGHAST
S. TIMOSHENKO
L. B. TUCKERMAN
RALPH H. UPSON
J. PARKER VAN ZANDT
J. G. VINCENT
RICHARD VON MISES
FRANK L. WATTENDORF
P. V. H. WEEMS
FRED E. WEICK
R. D. WEYERBACHER
JOHN B. WHEATLEY
ANDREW V. WILLGOOS
DONALD H. WOOD
ROBERT J. WOODS
JOHN E. YOUNGER
ALBERT F. ZAHM
STEPHEN J. ZAND

An Appreciation
To Corporate Members of the Institute of the Aeronautical Sciences

Listed below are the leading aeronautical and industrial companies that make possible the publication of the *Journal of the Aeronautical Sciences*.

They enable the Institute to publish scientific and technical papers in the *Journal* and to devote its pages exclusively to editorial material.

Dues from individual members which would normally be used to publish this scientific and engineering monthly are thus released for additional services to the profession and industry.

The *Aeronautical Engineering Review* and the *Aeronautical Engineering Catalog*, together with the *Journal*, provide a comprehensive technical information service for the benefit of the aircraft and related industries.

Academy of Aeronautics, Inc.
Casey Jones School of Aeronautics
Aero Insurance Underwriters
Aerojet Engineering Corporation
Aeronca Aircraft Corporation
Aeroquip Corporation
Agawam Aircraft Products, Inc.
Airborne Instruments Laboratory, Inc.
Airchox Company Division, Joyce Aviation, Inc.
Aircraft Radio Corporation
Aireon Manufacturing Corporation
AiResearch Manufacturing Company
AiResearch Manufacturing Company of Arizona, Inc.
Airex Manufacturing Company, Inc.
Allis-Chalmers Manufacturing Company
Allison Division, General Motors Corporation
Aluminum Company of America
American Airlines System
American Overseas Airlines, Inc.
American Bosch Corporation
American Phenolic Corporation
Associated Aviation Underwriters
Associated Foundries & Manufacturers, Inc.
Atlas Supply Company
Baker Steel & Tube Company
Beech Aircraft Corporation
Bell Aircraft Corporation
Bendix Aviation Corporation
Bendix Products Division
Bendix Radio Corporation
Eclipse-Pioneer Division
Export Division
Friez Instrument Division
Pacific Division
Scintilla Magneto Company
The BG Corporation
Boeing Aircraft Company
Breeze Corporations, Inc.
Essex Tool & Die Company
Federal Laboratories, Inc.
Cal-Aero Technical Institute, A Division of Grand Central Airport Company
Carrier Corporation
Cessna Aircraft Company
Chandler-Evans Corporation
Chase National Bank of the City of New York
The Cleveland Graphite Bronze Company
The Cleveland Pneumatic Tool Company
Automotive-Aircraft Division
Clifford Manufacturing Company
Consolidated Vultee Aircraft Corporation
Nashville Division
Stinson Aircraft Division
Continental Motors Corporation
Cox and Stevens Aircraft Corporation
Culver Aircraft Corporation
Curtiss-Wright Corporation
Airplane Division
Development Division
Propeller Division
Wright Aeronautical Corporation
Doak Aircraft Company, Inc.
Douglas Aircraft Company, Inc.
El Segundo Plant
Long Beach Plant
The Dow Chemical Company
Dzus Fastener Company, Inc.
Eastern Air Lines, Inc.
Eaton Manufacturing Company
Thomas A. Edison, Incorporated, Instrument Division
Edo Aircraft Corporation
The Electric Auto-Lite Company
Electrol Incorporated
Engineering and Research Corporation
Ethyl Corporation
The Fafnir Bearing Company
Fairchild Camera & Instrument Corporation
Fairchild Aerial Surveys, Inc.
Fairchild Engine and Airplane Corporation
Duramold Division
Fairchild Aircraft Division
Ranger Aircraft Engines Division
Federal Telephone and Radio Corporation

Firestone Aircraft Company
Fletcher Aviation Corporation
General Aviation Equipment Company, Inc.
General Electric Company
General Instrument Corporation
General Motors Corporation
  AC Spark Plug Division
  Aeroproducts Division
  Buick Motor Division
  Cadillac Motor Car Division
  Chevrolet Motor Division
  Delco Products Division
  Delco-Remy Division
  Eastern Aircraft Division
  Fisher Body Division
  Frigidaire Division
  Harrison Radiator Division
  Research Laboratories Division
  Rochester Products Division
The B. F. Goodrich Company
The Goodyear Tire & Rubber Company
Grumman Aircraft Engineering Corporation
W. & L. E. Gurley
Hanna Engineering Works
Haskelite Manufacturing Corporation
Hawaiian Airlines Limited
The Hilliard Corporation
The International Nickel Company
Irving Air Chute Company, Inc.
Jack & Heintz, Inc.
Johns-Manville Sales Corporation
Kaiser Fleetwings, Inc.
Kellett Aircraft Corporation
Kenyon Instrument Company, Inc.
Walter Kidde & Company, Inc.
Kollsman Instrument Division, Square D Company
Langley Corporation
Lavelle Aircraft Corporation
Lear Incorporated
Liberty Aircraft Products Corporation
Link Aviation Devices, Inc.
The Liquidometer Corporation
Lockheed Aircraft Corporation
Longines-Wittnauer Watch Company, Inc.
Magnaflux Corporation
The Marquette Metal Products Company
The Glenn L. Martin Company
The W. L. Maxson Corporation
Warren McArthur Corporation
McDonnell Aircraft Corporation
Menasco Manufacturing Company
Micromatic Hone Corporation
Minneapolis-Honeywell Regulator Company
Moore Drop Forging Company
National City Bank of New York
National Credit Office, Inc.
The New York Air Brake Company
Norma-Hoffmann Bearings Corporation
North American Aviation, Inc.
  North American Aviation, Inc., of Texas
Northrop Aircraft, Inc.
Northwest Airlines, Inc.
Owens-Corning Fiberglas Corporation
Pan American World Airways System
The Parker Appliance Company
Pennsylvania-Central Airlines Corporation
Pesco Products Company Division, Borg-Warner Corporation
Phillips Petroleum Company
Pioneer Parachute Company, Inc.
Piper Aircraft Corporation
Pure Oil Co.
Radioplane Company
Republic Aviation Corporation
J. P. Riddle Company
A. V. Roe Canada Limited
John A. Roebling's Sons Company
Rohr Aircraft Corporation
Roosevelt Field, Inc.
The Ryan Aeronautical Company
Sciaky Brothers
Scott Aviation Corporation
Shell Oil Company, Inc.
Simmonds Aerocessories, Inc.
Skydyne, Inc.
Socony-Vacuum Oil Company
Solar Aircraft Company
Sperry Gyroscope Company, Inc.
Square D Company
Standard Oil Company of California
Standard Oil Company (Indiana)
Standard Oil Company of New Jersey
Swedlow Aeroplastics Corporation
The Texas Company
Thompson Products, Inc.
Tinnerman Products, Inc.
Titeflex, Inc.
Transcontinental & Western Air, Inc.
Union Carbide and Carbon Corporation
  Bakelite Corporation
  Haynes Stellite Company
  Linde Air Products Company
  National Carbon Company
United Aircraft Corporation
  Chance Vought Aircraft Division
  Hamilton Standard Propellers Division
  Pratt & Whitney Aircraft Division
  Pratt & Whitney Aircraft Corporation of Missouri
  Sikorsky Aircraft Division
United Air Lines, Inc.
United States Aviation Underwriters, Inc.
United States Rubber Company
  Dominion Rubber Company, Ltd.
The Variety Aircraft Corporation
Vickers, Inc.
Vidal Corporation
The Waco Aircraft Company
Warner Aircraft Corporation
The Weatherhead Company
Western Air Lines, Inc.
Westinghouse Electric Corporation
Weston Electrical Instrument Corporation
Willys-Overland Motors, Inc., Aircraft Research and Development Division
Wyman-Gordon Company
Young Radiator Company

EDITORIAL COMMITTEE

HUGH L. DRYDEN, *Chairman*

Aerodynamics

William Bollay
Kenneth S. M. Davidson
Walter S. Diehl
Hugh L. Dryden
R. Paul Harrington
P. E. Hemke
Eastman N. Jacobs
Alexander Klemin
W. B. Klemperer
Otto C. Koppen
A. M. Kuethe
John G. Lee
John R. Markham
Clark B. Millikan
Shatswell Ober
W. Bailey Oswald
Manfred Rauscher
Elliott G. Reid
H. J. E. Reid
Benjamin F. Ruffner
G. B. Schubauer
W. R. Sears
Abe Silverstein
R. H. Smith
Th. Theodorsen
M. J. Thompson
Th. von Kármán
Richard von Mises
K. D. Wood

Air Transport

Ralph S. Damon
Charles Froesch
Melvin N. Gough
J. A. Herlihy
William Littlewood
A. A. Priester
Paul E. Richter
N. F. Scudder
T. P. Wright

Aircraft Design

Karl Arnstein
W. E. Beall
Rex B. Beisel
C. P. Burgess
C. H. Chatfield
J. W. Crowley, Jr.
W. K. Ebel
Leroy R. Grumman
Hall L. Hibbard
C. L. Johnson
A. L. Klein
I. M. Laddon
John G. Lee
C. J. McCarthy
William H. Miller
R. H. Prewitt
A. E. Raymond
Igor I. Sikorsky
Th. Troller
R. H. Upson
Fred E. Weick
Robert J. Woods

Radio

C. S. Draper
Lloyd Espenschied
C. G. Fick
Lewis M. Hull
Haraden Pratt
F. X. Rettenmeyer

Physiologic Problems

H. G. Armstrong
Louis H. Bauer
David B. Dill
Eugene Du Bois
W. Randolph Lovelace, II
Ross A. McFarland
A. D. Tuttle

Power Plants and Propellers

M. A. Biot
George W. Brady
Frank W. Caldwell
Ivan H. Driggs
Louis H. Enos
David Gregg
L. S. Hobbs
Albert R. Jacobs
E. E. Johnson
H. M. McCoy
W. C. Nelson
Arthur Nutt
Shatswell Ober
Hans Reissner
David R. Shoults
C. Fayette Taylor
E. S. Taylor
Th. Theodorsen
A. V. Willgoos
D. H. Wood

Structures and Materials

M. A. Biot
W. B. Bleakney
E. W. Conlon
George W. DeBell
J. P. Den Hartog
L. H. Donnell
L. G. Dunn
E. C. Hartmann
N. J. Hoff
W. B. Klemperer
H. L. Langhaar
E. E. Lundquist
C. F. Nagel, Jr.
J. S. Newell
Alfred S. Niles
W. Ramberg
E. Reissner
F. R. Shanley
H. W. Sibert
C. R. Strang
S. Timoshenko
H. S. Tsien
George Tweney
E. E. Weibel
J. E. Younger

Meteorology

C. F. Brooks
D. M. Little
E. J. Minser
Sverre Petterssen
F. W. Reichelderfer
A. F. Spilhaus
P. V. H. Weems
H. C. Willett

Fuels and Oils

D. P. Barnard
A. L. Beall
Luis de Florez
J. H. Doolittle
Graham Edgar
R. T. Goodwin
S. D. Heron
A. M. Rothrock

Instruments

P. R. Bassett
W. G. Brombacher
Charles H. Colvin
C. S. Draper
Lucien L. Friez
Walter McKay
W. A. Reichel
C. F. Savage
A. F. Spilhaus
S. J. Zand

I.A.S. REPRESENTATIVES TO OTHER ORGANIZATIONS

Aircraft Industries Association of America, Inc.—CHARLES MARCUS
American Association for the Advancement of Science—J. C. HUNSAKER
American Society of Mechanical Engineers—JOHN E. YOUNGER
American Standards Association—P. R. BASSETT
Engineering Society of Detroit—DONALD C. HUNT, GEORGE TWENEY
Greater New York Safety Council—WILLIAM LITTLEWOOD
Daniel Guggenheim Medal Board of Award—CHARLES H. COLVIN, GROVER LOENING, LESTER D. GARDNER
Institute of Radio Engineers—L. M. HULL
Manufacturers Aircraft Association—J. T. HARTSON
National Aeronautic Association—WILLIAM R. ENYART
National Fire Protection Association—E. E. ALDRIN
National Research Council Engineering Division—HUGH L. DRYDEN
National Safety Council—JEROME LEDERER
New York Museum of Science and Industry—LESTER D. GARDNER
Society of Automotive Engineers—EDWARD P. WARNER

JOURNAL OF THE AERONAUTICAL SCIENCES

VOLUME 14 JANUARY, 1947 NUMBER 1

A Method for Simplifying the Calculations of the Natural Frequencies for a System Consisting of *n* Rigid Rotating Discs Mounted on an Elastic Shaft*

JOHN L. BOGDANOFF†

Wright Aeronautical Corporation

SUMMARY

A. Stodola[1] has shown how the positive and negative synchronous natural frequencies (N.F.'s) for a system consisting of *n* rigid discs mounted on a rotating elastic shaft can be calculated. (The positive and negative synchronous N.F.'s are defined as the N.F.'s that coincide with or are exactly opposite to, respectively, the rotational speed of the shaft.) The principal assumption used in his method is that the elastic characteristics of the system are symmetrical. This assumption, *combined with a need for only the synchronous N.F.'s*, enabled Stodola to reduce the problem from that of solving for all the roots of an algebraic polynomial (in one unknown) of $8n$ degree to that of obtaining all the roots of a similar polynomial of $2n$ degree.

L. Foppl,[2] using the same procedure as Stodola, obtained the positive and negative synchronous N.F.'s for a rigid disc mounted on a rotating cantilever shaft. In addition, he obtained a fourth degree polynomial (with coefficients that are a function of the disc velocity) whose roots give the N.F.'s of the system. However, this polynomial was not solved explicitly. It was used to obtain limiting expressions for the N.F.'s when the disc angular velocity was large.

In the present paper, the writer discusses a method for finding *all* the N.F.'s for a system consisting of *n* rigid rotating discs mounted on an elastic shaft. With the assumption of elastic symmetry, the problem is *reduced* to finding all the roots of a polynomial of $2n$ degree whose coefficients are functions of the angular velocities of the discs. It is also possible to construct an electronic network and a stationary mechanical model which give *all* and *some*, respectively, of the N.F.'s of the original (symmetric) system. If the system does not possess elastic symmetry, the method reduces the problem to that of finding all the roots of a similar polynomial of $4n$ degree. For this case (unsymmetrical) it is not possible to construct a stationary mechanical model. However, the electronic network can still be made, although it is more complicated than for the symmetric case.

Received June 14, 1946.

* The writer wishes to take this opportunity to thank Prof. E. S. Taylor for his excellent advice given during the preparation of this paper and W. G. Lundquist for permission to publish it.

† Now, Instructor, Civil Engineering Department, Columbia University.

INTRODUCTION

IN THE PAST, the principal source of vibration excitation in a system consisting of *n* rigid rotating discs mounted on an elastic shaft was unbalance in the discs. As a result, the positive and negative synchronous N.F.'s were of primary interest. With the advent of the aircraft propeller-gas turbine combination, additional exciting forces, generated by the propeller, act on the turbine rotating system. These forces can be resolved, by harmonic analysis, into a Fourier series whose terms have periods that are some rational multiple (positive or negative) of one of the disc angular velocities. Therefore, in order to design a system of this type which is free from resonance vibration, it is necessary to know all the natural frequencies of the system as a function of a disc velocity.

If the radii of gyration of each disc are small in comparison with the length of the shaft, the gyroscopic moments may be neglected and each disc may be considered as a point mass. In this case, many methods are available for determining the *n* natural frequencies. Essentially, these methods consist in finding all the roots of a polynomial of *n*th degree, if the system possesses symmetrical elastic properties. However, if the gyroscopic moments of each disc cannot be neglected, the only published procedures known to the writer for finding the N.F.'s of the system involve finding all the roots of a polynomial of $8n$ or $4n$ degrees whose coefficients are functions of the angular velocities of the

L629.051 71099
J82

discs. (The polynomial is of $8n$ degree if the system has unsymmetrical elastic properties and $4n$ degree if these properties are symmetrical.) It is easily seen that in order to find all the N.F.'s, as a function of a disc velocity, for a system with $n \geqslant 3$, a great deal of labor must be expended.

This paper presents a method whereby all the N.F.'s may be obtained by solving for all the roots of a similar polynomial of $4n$ or $2n$ degree (the polynomial is of $4n$ degree for a system with unsymmetrical elastic properties and $2n$ degree if elastic symmetry exists). The first part applies this method to the determination of all the N.F.'s for a system consisting of a single rigid rotating disc mounted on a symmetrical elastic cantilever shaft as a function of the disc angular velocity. The second part of the paper applies this method to the determination of all the N.F.'s for n rigid rotating disc mounted on an elastic shaft as a function of the angular velocity of one of the discs. An Appendix has been included which contains a rigorous analysis of the procedures used in the first and second parts.

NOTATION

Symbol	Unit	Significance
c.g.	....	Center of gravity of disc
l	in.	Length
$M, M_1, M_2, \ldots$	lb.in.$^{-1}$sec.^{2}	Mass
$A, C, A_2, C_2, A_4, C_4, \ldots$	lb.in.sec.^{2}	Mass moment of inertia
$q_{11}, q_{21}, q_{13}, q_{23}, \ldots$	in.	Coordinates of c.g.
$q_{12}, q_{22}, q_{14}, q_{24}, \ldots$	....	Angular coordinates of disc axis
B	lb.in.^{2}	Shaft flexibility
$\omega, \omega_2, \omega_4, \ldots$	rad.sec.$^{-1}$	Angular velocities
$\tau, \tau_1, \tau_2, \ldots$	rad.sec.$^{-1}$	Angular velocities
$\sigma, \sigma', \sigma_1, \sigma_2, \ldots$	rad.sec.$^{-1}$	Angular velocities
e	....	2.718281284
i	....	$\sqrt{-1}$
T, T'	in.lbs.	Kinetic energy
V, V'	in.lbs.	Potential energy
T_0, T_0', T_1	in.lbs.sec.^{2}	Reduced kinetic energy
V_0, V_0'	in.lbs.	Reduced potential energy
m, k, n	....	Real numbers
$\theta_1, \theta_2, \ldots$	in.$^{1/2}$lb.$^{1/2}$	Normal coordinates
j	....	Specific index
r,s	....	Running indexes

1. Rigid Disc on Elastic Cantilever Shaft

Fig. 1 shows a rigid rotating disc, D, mounted on a vertical cantilever shaft. The disc is mounted rigidly on the shaft, and it is assumed that the disc c.g., O', and axis coincide with the elastic axis of the shaft when the system is at rest (as shown in Fig. 1). It is assumed that the cross section of the shaft is uniform along its length, l, and that the principal area moments of inertia of the cross section are equal. ω is the constant angular velocity of the disc. Fig. 2 shows an instantaneous position of the system. The XYZ axes, with origin O at the built-in end of the cantilever, are fixed in space; OZ is vertical. The $X'Y'Z'$ axes, with origin O' at the c.g. of the disc, remain parallel to the XYZ axes during motion. q_{11} and q_{21} are the coordinates of O' projected on the XOY plane; q_1 represents $q_{11} + iq_{21}$. q_{12} and q_{22} are the coordinates of the projection of P'

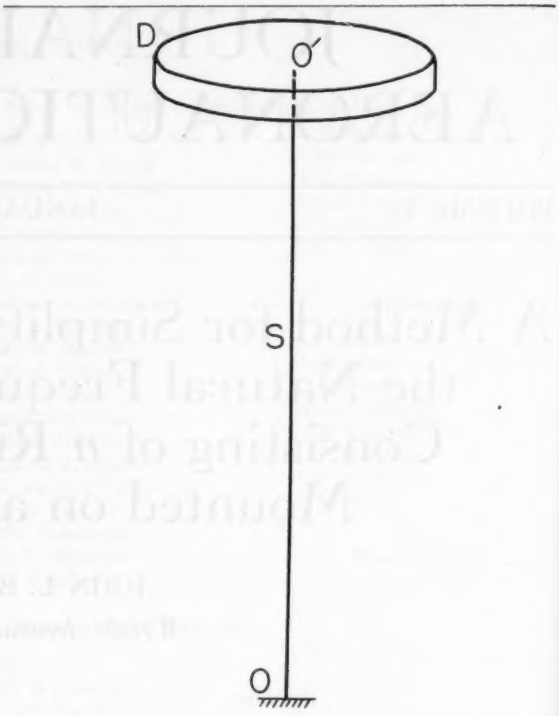

FIG. 1. Rigid rotating disc mounted on an elastic shaft.

on the $X'O'Y'$ plane; q_2 is used to represent $q_{12} + iq_{12}$. (It should be noted that the length of $O'P'$ is taken to be one unit.) q_{11}, q_{21}, and q_{12}, q_{22} are assumed to be small. M is the mass of the disc; C is the moment of inertia about its axis; A is the remaining principal moment of inertia. The shaft is assumed massless and B denotes its flexural rigidity.

The kinetic and potential energies of the system are

$$2T \equiv M(\dot{q}_{11}^2 + \dot{q}_{21}^2) + A(\dot{q}_{12}^2 + \dot{q}_{22}^2) - C\omega(\dot{q}_{12}q_{22} - q_{12}\dot{q}_{22}) + C\omega^2 \quad (1)$$

and

$$2V \equiv \frac{12B}{l^3}(q_{11}^2 + q_{21}^2) - 2\frac{6B}{l^2}(q_{11}q_{12} + q_{21}q_{22}) + \frac{4B}{l}(q_{12}^2 + q_{22}^2) \quad (2)$$

respectively. Lagrange's equations for this case are

$$\left.\begin{aligned} \frac{d}{dt}\left(\frac{\partial T}{\partial \dot{q}_{r1}}\right) - \frac{\partial T}{\partial q_{r1}} &= -\frac{\partial V}{\partial q_{r1}} \\ \frac{d}{dt}\left(\frac{\partial T}{\partial \dot{q}_{r2}}\right) - \frac{\partial T}{\partial q_{r2}} &= -\frac{\partial V}{\partial q_{r2}} \\ \frac{d}{dt}\left(\frac{\partial T}{\partial \omega}\right) &= 0 \end{aligned}\right\} \quad (r = 1, 2) \qquad (a)$$

The equations of motion, obtained by substituting Eqs. (1) and (2) in Eqs. (a), have the following form:

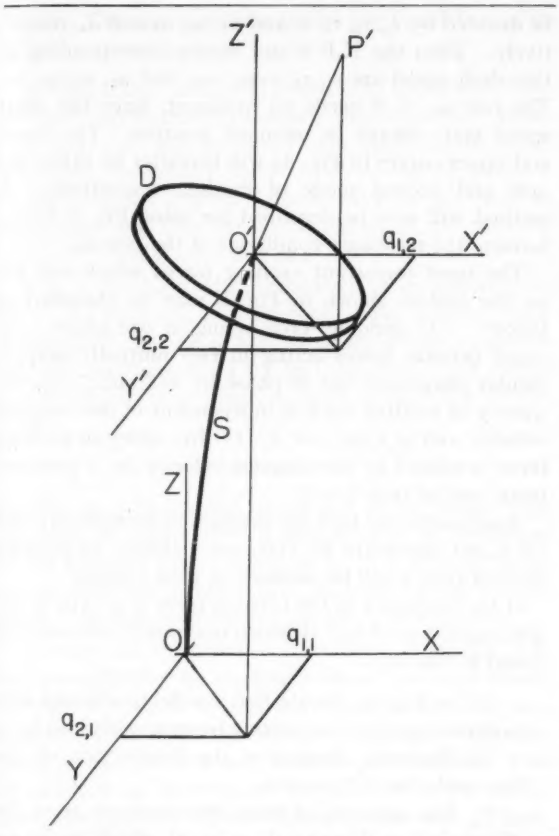

FIG. 2. Instantaneous position of rigid rotating disc mounted on a cantilever shaft.

$$\left.\begin{aligned} M\ddot{q}_{11} &= -\frac{12B}{l^3}q_{11} + \frac{6B}{l^2}q_{12} \\ M\ddot{q}_{21} &= -\frac{12B}{l^3}q_{21} + \frac{6B}{l^2}q_{22} \\ A\ddot{q}_{12} + C\omega\dot{q}_{22} &= \frac{6B}{l^2}q_{11} - \frac{4B}{l}q_{12} \\ A\ddot{q}_{22} - C\omega\dot{q}_{12} &= \frac{6B}{l^2}q_{21} - \frac{4B}{l}q_{22} \\ \frac{d}{dt}\left(C\omega - \frac{C}{2}(q_{12}\dot{q}_{22} - \dot{q}_{12}q_{22})\right) &= 0 \end{aligned}\right\} \quad (3)$$

Examination of the first four equations of Eqs. (3) shows that the first and second and the third and fourth may be combined as

$$\left.\begin{aligned} M\ddot{q}_1 &= -\frac{12B}{l^3}q_1 + \frac{6B}{l^2}q_2 \\ A\ddot{q}_2 - iC\omega\dot{q}_2 &= \frac{6B}{l^2}q_1 - \frac{4B}{l}q_2 \end{aligned}\right\} \quad (4)$$

q_1 and q_2 are vectors in the XOY and $X'O'Y'$ planes, respectively.

The first of Eqs. (4) is the vector form of the linear momentum equation. It shows that the motion is essentially two-dimensional. The second is the vector form for the two components of the moment of momentum equations that are in the $X'O'Y'$ plane. The remainder of the moment of momentum equation is given by:

$$\frac{d}{dt}\left[C\omega - \frac{C}{2}(q_{12}\dot{q}_{22} - q_{12}\dot{q}_{22})\right] = 0 \quad (b)$$

This is the last of Eqs. (3). It shows that the component of the angular momentum vector in the $O'P'$ (or $O'Z'$) direction is constant. It becomes, after carrying out the indicated differentiation,

$$q_{12}\ddot{q}_{22} - q_{12}\ddot{q}_{22} = 0 \quad (5)$$

Eqs. (4) are linear differential equations with constant coefficients. Assume a solution of the form

$$\left.\begin{aligned} q_1 &= q_{10}e^{i\tau t} \\ q_2 &= q_{20}e^{i\tau t} \end{aligned}\right\} \quad (6)$$

Substituting these Eqs. (4),

$$\left.\begin{aligned} -M\tau^2 q_{10} &= -\frac{12B}{l^3}q_{10} + \frac{6B}{l^2}q_{20} \\ -A\tau^2 q_{20} + C\omega\tau q_{20} &= \frac{6B}{l^2}q_{10} - \frac{4B}{l}q_{20} \end{aligned}\right\} \quad (7)$$

The characteristic equation is

$$\begin{vmatrix} \frac{12B}{l^3} - M\tau^2 & -\frac{6B}{l^2} \\ -\frac{6B}{l^2} & \frac{4B}{l} + C\omega\tau - A\tau^2 \end{vmatrix} = 0 \quad (8)$$

It will be shown below that this equation has four real roots (two positive and two negative) for any given value of ω. Therefore, the solutions of Eqs. (4) are periodic.

The N.F.'s for this system are given by the roots of Eq. (8). In expanded form, this equation is

$$\left(4 - \frac{\tau^2}{\alpha^2}\right)\left[2 - \frac{\alpha^2}{\beta^2}\left(\frac{\tau^2}{\alpha^2} - p\frac{\tau\omega}{\alpha^2}\right)\right] - 6 = 0 \quad (9)$$

where $\alpha^2 = 3B/Ml^3$, $\beta^2 = 2B/Al$, $p = C/A$.
The corresponding natural modes can be obtained from either

$$q_{20}/q_{10/1} = {}^1/_2[4 - (\tau^2/\alpha^2)] \quad (10a)$$

or

$$\frac{q_{20}}{q_{10/1}} = 3/\left[2 - \frac{\alpha^2}{\beta^2}\left(\frac{\tau^2}{\alpha^2} - p\frac{\omega\tau}{\alpha^2}\right)\right] \quad (10b)$$

The three parameters, α, α/β, and p, describe the physical characteristics of the system. They have the following meaning:

(1) α is the natural frequency of the system when the disc, D, is assumed to be a point mass.

(2) α/β furnishes the relation between the length of shaft and the radius of gyration of the disc corresponding to the polar moment of inertia C.

(3) p describes the disc form.

α and α/β are both positive and are unrestricted in value. p, however, must satisfy the relation:

$$0 < p \leqslant 2$$

Eq. (6) shows that at a natural frequency a plane through OZ and O' contains $O'P'$. Further, the plane OZO' rotates with constant angular velocity τ about the line OZ. Using these results, it is possible to derive Eqs. (7) by considering the equilibrium of the inertia and elastic forces in, and moments perpendicular to, the plane OZO'. This procedure was followed by Stodola[1] and Foppl,[2] the latter arriving at Eq. (9) for the N.F.'s.

Eq. (9) has four real roots, two positive and two negative, for a fixed but arbitrary value of ω. If these N F.'s, τ, are plotted as the ordinate with ω as the abscissa, four continuous curves are obtained. This process of N.F. determination for a given system having fixed values for p, α^2/β^2 is equivalent to finding all the common values of the following two functions:

$$\left(4 - \frac{\tau^2}{\alpha^2}\right)\left[2 - \frac{\alpha^2}{\beta^2}\left(\frac{\tau^2}{\alpha^2} - p\frac{\omega\tau}{\alpha^2}\right)\right] - 6 = 0 \quad (11)$$

$$\omega/\alpha = \text{constant}$$

where the constant assumes, in turn, all values in the interval $-\infty$ and $+\infty$. Geometrically, this means that the curves in the $(\omega/\alpha) - (\tau/\alpha)$ plane, defined by the first of Eqs. (11), are found by obtaining their intersections with the line ω/α = constant. This line, by sweeping out the entire $(\omega/\alpha) - (\tau/\alpha)$ plane, may be considered as a scanning device. It is obviously immaterial as to just what curve or line is used as the scanning device. The only requirement is that it can be made to pass through every point in the $(\omega/\alpha) - (\tau/\alpha)$ plane. Therefore, replace Eqs. (11) with

$$\left(4 - \frac{\tau^2}{\alpha^2}\right)\left[2 - \frac{\alpha^2}{\beta^2}\left(\frac{\tau^2}{\alpha^2} - p\frac{\omega\tau}{\alpha^2}\right)\right] - 6 = 0 \quad (12)$$

$$\omega/\alpha = m(\tau/\alpha)$$

where m is a real number which varies from $-\infty$ to $+\infty$. If the second of Eqs. (12) is substituted in the first, we obtain

$$\left(4 - \frac{\tau^2}{\alpha^2}\right)\left[2 - \frac{\alpha^2}{\beta^2}(1 - pm)\frac{\tau^2}{\alpha^2}\right] - 6 = 0 \quad (13)$$

Eqs. (13) and (10a), with $\alpha^2/\beta^2 = 1$ and $p = 2$, were used to obtain Figs. 3a and 3b, respectively. Fig. 3a gives the N.F.'s, and Fig. 3b gives the corresponding modes of motion.

Actually, Figs. 3a and 3b are only the upper half of the complete diagram for the N.F.'s and the modes of motion. However, all information can be obtained from these figures in the following manner. Let $\omega_1 \geq 0$ be the angular velocity of the shaft. Find the N.F.'s and modes corresponding to $+\omega_1$, and $-\omega_1$; let these be denoted by τ_1, τ_2, τ_3, τ_4 and α_1, α_2, α_3 and α_4, respectively. Then the N.F.'s and modes corresponding to this shaft speed are τ_1, τ_2, $-\tau_3$, $-\tau_4$ and α_1, α_2, α_3, α_4. The case $\omega_1 < 0$ needs no comment, since the shaft speed may always be assumed positive. The lower and upper curves in Fig. 3a will hereafter be called the first and second mode of motion, respectively. A method will now be described for using Fig. 3 to determine the resonance conditions of the system.

The most important exciting forces which can act on the system shown in Fig. 2 may be classified as follows: (1) periodic force acting in one plane; (2) equal periodic forces acting in two mutually perpendicular planes and out of phase by $\pi/2$ rad.; (3) frequency of exciting force is independent of disc angular velocity and of type 1 or 2; (4) frequency of exciting force is related to disc angular velocity by a constant factor and of type 1 or 2.

Analysis shows[1] that the distinction between (1) and (2) is not important for this case. Hence, an exciting force of type 2 will be assumed in what follows.

If the frequency of the exciting force is of type 3, the disc angular velocities at which resonance will occur are found as follows:

(a) In Fig. 3a, draw a line parallel to abscissa with ordinate equal to the exciting frequency divided by α.

(b) Find the abscissa of the intersection of this line with the N.F. curves.

(c) The abscissa of these intersections gives the dimensionless disc speeds, ω/α, at which resonance will occur.

(d) The mode corresponding to this N.F. and disc speed can be found directly from Fig. 3b.

If the frequency of the exciting force is of type 4, the N.F.'s and corresponding disc speeds may be found as follows:

(a) Assume that the frequency of the exciting force, σ, is related to the angular velocity, ω, of the disc by $\sigma = k_\sigma\,\omega$.

(b) In Fig. 3a, draw line $k_\sigma(\omega/\alpha) = \tau/\alpha$.

(c) Find the abscissa and ordinate of the intersections of this line with the N.F. curves.

(d) The N.F.'s and corresponding disc velocities are given by the ordinate and abscissa, respectively, of these intersections.

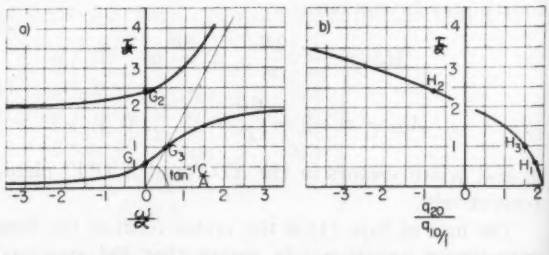

FIG. 3. Natural frequencies and mode of motion for rigid rotating disc mounted on a cantilever.

(e) The corresponding modes are found from Fig. 3b.

A comparison of Eqs. (11) and (13) shows that they are both polynomial of the fourth degree in τ/α. However, Eq. (13) can be solved as a quadratic in τ^2/α^2. Therefore, the labor involved in obtaining all the roots of Eq. (13) (for a given value of m) is at the most no more than half that needed to obtain all the roots of Eq. (11) (for a given value of ω).

If $m \geq A/C$, Eq. (13), considered as an quadratic in τ^2/α^2, will have one negative root. This negative value is discussed because it has no meaning (see Appendix I). It arises because of the fact that two of the curves in the (ω/α)-(τ/α) diagram have asymptotes of the form

$$k(\omega/\alpha) = \tau/\alpha \qquad \text{(c)}$$

In Fig. 3a, which is the upper half of the (ω/α)-(τ/α) diagram, the upper curve is seen to have an asymptote of the form (c) with k equal to 2. A brief description of the behavior of the N.F.'s as ω varies will now be given. In this description q_{10} is assumed constant.

Assume that the disc is not rotating. Then the N.F. and configuration for the first mode of motion is shown on Figs. 3a and 3b by G_{11} and H_1, respectively. As ω increases from zero, the moment applied by the disc to the shaft decreases and the angle q_{20} decreases. This decrease in q_{20} necessitates an increase in the radial force, $M\tau^2 q_{10}$, required to maintain q_{10} constant. Therefore, τ increases. However, as ω increases still further, q_{20} must continue to decrease, and it is obvious that q_{20} must approach zero asymptotically. This means that the radial force, $M\tau^2 q_{10}$, approaches a finite value asymptotically. Therefore, τ cannot exceed a given maximum limit; for this system the limit is 2α. As ω decreases from zero, the disc moment causes q_{20} to increase. The increase in q_{20} necessitates a decrease in the radial force to maintain q_{10} constant. Therefore, τ decreases. As ω approaches minus infinity, q_{20} and τ approach $2(q_{10}/l)$ and 0, respectively.

The N.F. and configuration for the second mode of motion, when ω equals zero, are given in Figs. 3a and 3b by G_2 and H_2, respectively. An increase in ω, from zero, decreases the disc moment. (The disc moment is less than zero when ω equals zero for this mode.) Hence, the radial force necessary to maintain q_{10} fixed increases. Therefore, τ increases. As ω approaches plus infinity, τ also approaches the same value. For extremely large positive values of ω, the disc, in this mode, has the same N.F.'s that this disc would have if it were rotating with the same angular velocity, ω, about a fixed pivot at its c.g. with no restoring moment. As ω decreases from zero, q_{20} gradually increases. Hence, the radial force decreases and τ also decreases. Since q_{20} must approach zero, τ must also approach a fixed value. Of necessity this value of τ is the same as the upper limit for the first mode of motion.

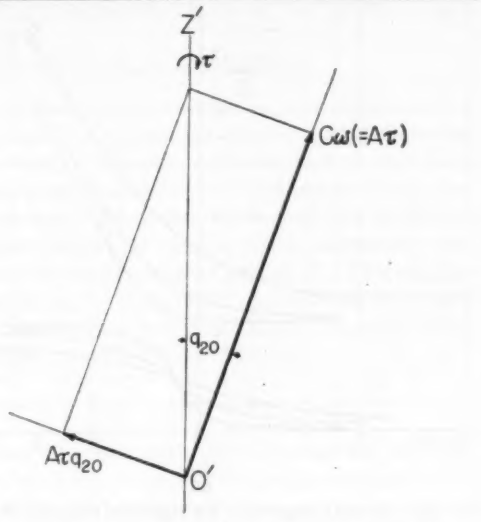

FIG. 4. Angular momentum vectors for a rigid rotating disc mounted on a cantilever.

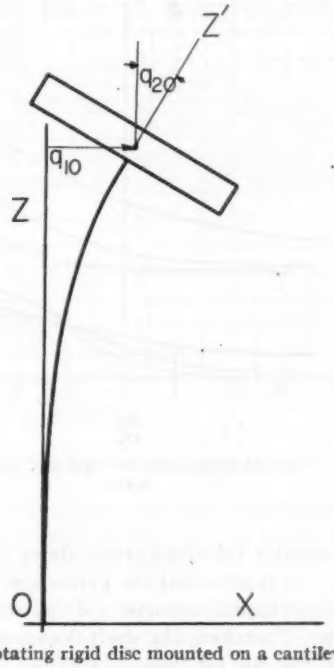

FIG. 5. Nonrotating rigid disc mounted on a cantilever.

At the point G_3 in Fig 3a and H_3 in Fig. 3b, the N.F. and mode for the first mode of motion are $\tau = \alpha$ and $q_{20}/q_{10}/l = 3/2$, respectively; the shaft speed is

$$\omega/\alpha = A/C \qquad (14)$$

This means that at the speed given by Eq. (14) the system in the first mode behaves exactly as if the disc were a point mass. Consider Fig. 4. The plane of the paper is assumed to be the OZO' plane of Fig. 2. The angular momenta of the system corresponding

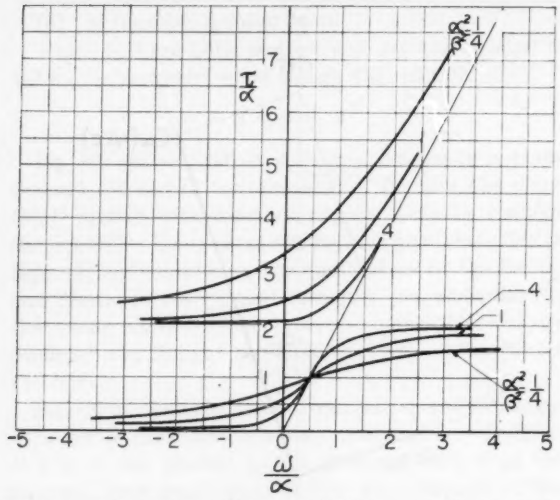

FIG. 6a. Natural frequencies for rigid disc mounted on a cantilever.

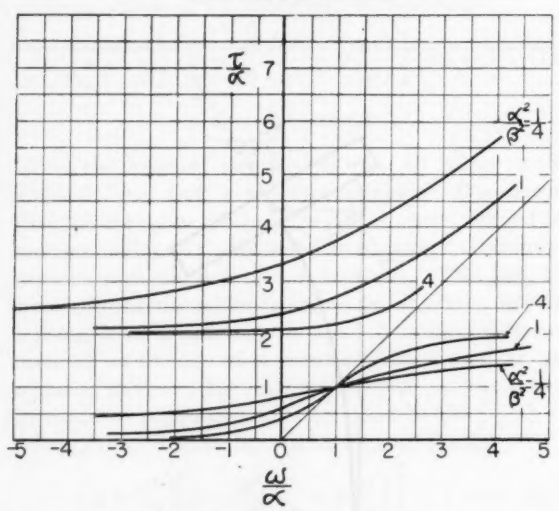

FIG. 6b. Natural frequencies for rigid disc mounted on a cantilever.

to the angular velocjties given above are the marked vectors. It is seen that the gyroscopic moment $C\omega\tau q_{20}$ and angular inertia moment $-A\tau^2 q_{20}$ are just equal and opposite. Therefore, the shaft does not exert any moment on the disc for these conditions.

Consider the system shown in Fig. 5. D is a *nonrotating* rigid disc mounted rigidly on the cantilever shaft OO'. Except for the moments of inertia of D, this system is exactly the same as the one shown in Fig. 2 (i.e., the mass of D', the length OO', the flexural rigidity of the shaft, etc., have the same values as those used previously). Since the disc, D', is not rotating, no value need be assigned to the polar moment of inertia. The moment of inertia of the disc about a line through O' perpendicular to the plane of the figure is assumed to be $(A - mC)$ (where A, m, C have the same

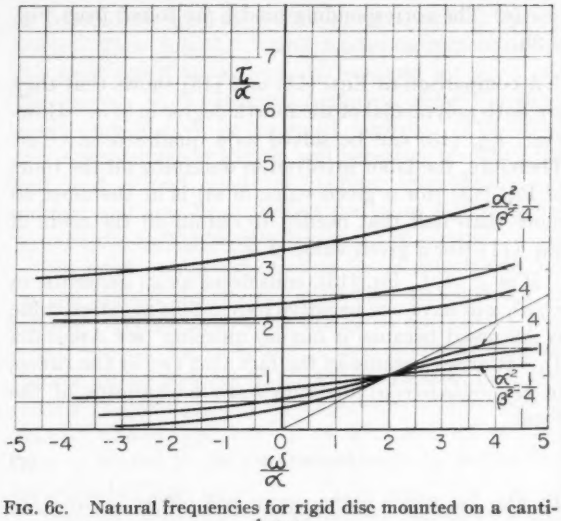

FIG. 6c. Natural frequencies for rigid disc mounted on a cantilever.

value as above). It is assumed that the motion of the system takes place in the plane of the figure. q_{10} represents the maximum linear displacement of the disc from the equilibrium position; q_{20} represents the maximum angular displacement of the disc axis from OZ. The equation of motion for the system are, after assuming small vibrations present:

$$\left.\begin{aligned} -M\tau^2 q_{10} &= -\frac{12B}{l^3}\,q_{10} + \frac{6B}{l^2}\,q_{20} \\ -(A-mC)\tau^2 q_{20} &= \frac{6B}{l^2}\,q_{10} - \frac{4B}{l}\,q_{20} \end{aligned}\right\} \qquad \text{(d)}$$

If the last of Eqs. (12) is substituted in Eqs. (7) the following equations are obtained:

$$\left.\begin{aligned} -M\tau^2 q_{10} &= -\frac{12B}{l^3}\,q_{10} + \frac{6B}{l^2}\,q_{20} \\ -(A-mC)\tau^2 q_{20} &= \frac{6B}{l^2}\,q_{10} - \frac{4B}{l}\,q_{20} \end{aligned}\right\} \qquad (15)$$

It is obvious that Eqs. (15) and (d) are identical. Therefore, the rotating system shown in Fig. 2 may be replaced by the hypothetical *nonrotating* system of Fig. 5. It is interesting to note that the angular moment of inertia of the nonrotating disc becomes negative for $m > A/C$. When this occurs, it is no longer possible to use a real disc.

The above analysis shows that the N.F.'s of the system of Fig. 1 are functions of the three variables ω/α, α^2/β^2, and p. Therefore it is not possible to represent the N.F.'s on any three-dimensional graph. Instead, a *family* of three-dimensional graphs is necessary. Figs. 6a, 6b, and 6c are three graphs of this family. The mode of motion, however, is the same for any N.F. regardless of the values of ω/α, α^2/β^2, and p. Hence, Fig. 3b is complete in itself.

Fig. 6a plots the N.F.'s as a function of ω/α and α^2/β^2; $p = 2$ in this graph. Figs. 6b and 6c do the same

thing except that $p = 1$ and $^1/_2$, respectively. It is clear that Fig. 3a is included in Fig. 6a.

Fig. 6a (as well as Figs. 6b and 6c) shows that as α^2/β^2 decreases the system behaves more nearly like a point mass. As α^2/β^2 increases, however, the system acts more like a disc with fixed c.g. This is as it should be because α/β is a measure of the ratio of the radius of gyration (corresponding to the polar moment of inertia) of the disc to the shaft length.

A comparison of Figs. 6a, 6b, and 6c (for a fixed but arbitrary value of α^2/β^2) shows that as p decreases (from 2) the effect of the angular velocity ω also decreases. Ultimately, the angular velocity is of no importance and may be disregarded. Again this is in accordance with physical intuition.

The common point of the lower set of curves occurring in each of these figures always has the coordinates A/C, 1. As mentioned above, the shaft does not exert any moment on the disc at these values of ω/α, τ/α—i.e., it behaves as a point mass for these conditions.

If a rigid rotating disc is mounted on any other shaft arrangement, a new series of graphs must be made. This is unfortunate but it cannot be avoided.

In conclusion, it must be emphasized that the above graphs can be easily obtained by replacing the variable ω/α with $m(\tau/\alpha)$. This substitution makes it possible to solve the characteristic equation as a quadratic instead of a quartic. The saving of labor entailed in this step is obvious. When the number of discs is equal to, or greater than, 3, the advantages in using this substitution are even greater.

II. n Rigid Rotating Discs on an Elastic Shaft

A. *Elastic System Possesses Symmetry*

Fig. 6 shows a system consisting of n rigid rotating discs $D_1, D_2, \ldots, D_n$ mounted on a vertical elastic shaft S. The shaft is assumed massless, and it may have any bearing arrangement. The bearings may be either flexible or rigid. When the system is at rest (as shown in the figure), each disc c.g. and axis is assumed to coincide with the straight elastic axis of S. The angular velocities $\omega_2, \omega_4, \ldots, \omega_{2n}$ of the discs about their axes are assumed to be related to the angular velocity of the first disc by a constant multiple—i.e.,

$$\omega_r = k_r\omega_2 \qquad (r = 2, 4, \ldots, 2n)$$

If the discs all rotate with the same angular velocity, then they may be considered as rigidly connected to a rotating shaft; otherwise each disc can be considered as centered on a nonrotating shaft by means of a frictionless rigid bearing. A turbogenerator set is an illustration of the former case, while a fan connected to an electric motor by means of a belt or gear drive illustrates the latter. Finally, the system is assumed devoid of all friction.

Let C_{2j}, A_{2j}, M_{2j} represent the polar moment of inertia, diametral moment of inertia, and mass, respectively, of D_j; let $c_{11}, c_{12}, \ldots$ represent the coefficients of elasticity of the assumed symmetrical elastic system. Then the equation from which the N.F.'s of the system can be derived is

$$\begin{vmatrix} c_{11} - M_1\tau^2 & c_{12} & \cdots & c_{1,\,2n} \\ c_{21} & c_{22} - (A_2 - C_2k_2m)\tau^2 & \cdots & c_{2,\,2n} \\ \cdots & \cdots & \cdots & \cdots \\ c_{2n,\,1} & \cdots & & c_{2n,\,2n} - (A_{2n} - C_{2n}k_{2n}m)\tau^2 \end{vmatrix} = 0 \qquad (16)$$

where

$$\omega_r = k_r\omega_2 \qquad (r = 2, 4, \ldots, 2n) \qquad \text{(e)}$$

and

$$\omega_2 = m\tau \qquad \text{(f)}$$

m has the same meaning as in the first section of this paper. The mode of motion for any N.F. can be determined from the linear equations

$$\begin{aligned} &(c_{11} - M_1\tau^2)F_1 + c_{12}F_2 + \cdots + c_{1,\,2n}F_{2n} = 0 \\ &c_{21}F_1 + [c_{22} - (A_2 - C_2k_2m)\tau^2]F_2 + \cdots + c_{2,\,2n}F_{2n} = 0 \\ &\cdots\cdots\cdots\cdots\cdots\cdots\cdots\cdots \\ &c_{2n,\,1}F_1 + c_{2n,\,2}F_2 + \cdots \\ &\qquad + (c_{2n,\,2n} - [A_{2n} - C_{2n}k_{2n}m]\tau^2)F_{2n} = 0 \end{aligned} \qquad (17)$$

Appendix I discusses at length the method used in arriving at Eqs. (16) and (17).

The N.F.'s of the system are best presented in the form of a graph similar to Fig. 3a. A graph of this type may be constructed as follows:

(1) Assume a value for m.

(2) Find the positive roots, τ^2, of Eq. (16) using the m of (1).

(3) Take the positive square roots of the values found in (2). Denote these by $\tau_1, \tau_2, \ldots, \tau_q$.

(4) Using the m of (1), plot the number pairs $(\tau_1 m, \tau_1), (\tau_2 m, \tau_2), \ldots, (\tau_q m, \tau_q)$ with τm as abscissa and τ as ordinate.

(5) Assume a new value for m and begin at (1).

By choosing suitable values for m between $-\infty$ and $+\infty$ and following this procedure, $2n$ curves will be obtained in which the abscissa is the angular velocity of the first disc and the ordinate is the N.F.

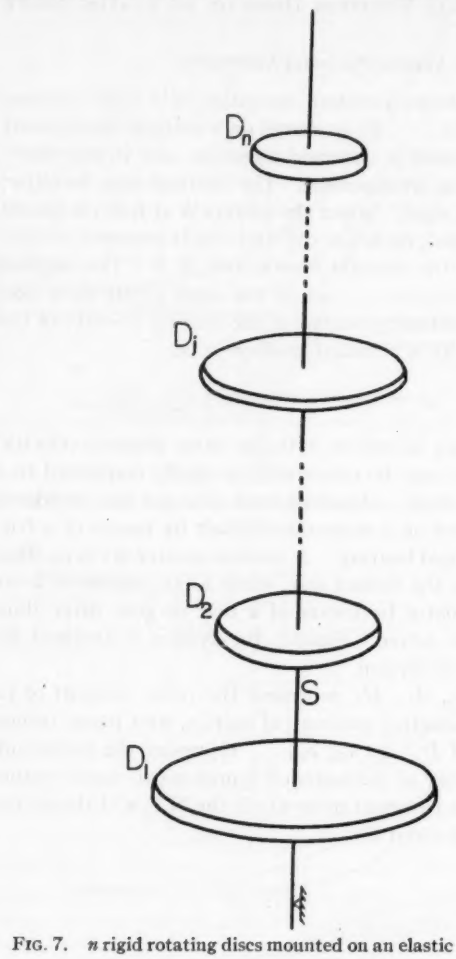

FIG. 7. n rigid rotating discs mounted on an elastic shaft.

The N.F.'s for any given value of ω_2 are obtained in the following manner. Let $\omega_2 = \omega_0$. Find the intersections of the curves with the lines $\omega_2 = \omega_0$ and $\omega_2 = -\omega_0$. Let these intersections be denoted by $\tau_1, \tau_2, \ldots, \tau_{2n}$ and $\tau_1', \tau_2', \ldots, \tau_{2n}'$. Then the N.F.'s are $\tau_1, \tau_2, \ldots, \tau_{2n}, -\tau_1', -\tau_2' \ldots, -\tau_{2n}'$.

The mode of motion for ω_0 and τ_1 (say) is found from Eqs. (17) in the usual manner. However, it is not possible to construct a graph similar to Fig. 3b for this case. The difficulty is due to the complication involved in representing a complete mode as one point on a graph. As a result, the mode is usually found only for a natural frequency that is of particular interest.

In Section I, the important types of exciting forces were classified. Further, a procedure was given there for determining when these exciting forces would be in resonance with the system of that Section. The only modification necessary in that procedure to make it applicable here is to relate the exciting forces to the angular velocity of D_1. If this is done and if a graph of the N.F.'s as a function of the angular velocity of D_1 has been obtained by the above steps (1), (2), (3), (4), and (5), the procedure described in Section I can be used to determine resonance conditions.

The form of Eqs. (17) suggests that a system with nonrotating discs could be devised which would have the same N.F.'s as the original. To do this, the only change necessary in the system shown in Fig. 7 (which has rotating discs) is to alter the value of each disc diametral moment of inertia; the altered values are

$$A_r - mk_rC_r \qquad (r = 2, 4, \ldots, 2n)$$

As long as $A_r/k_rC_r > m$, for $r = 2, 4, \ldots, 2n$, it is at least theoretically possible to construct an equivalent mechanical system with nonrotating discs. If $A_r/k_rC_r < m$ for any value of r, a mechanical construction is not even theoretically possible, because negative or zero moments of inertia cannot be represented by real discs. However, it is possible to construct an electronic circuit that has the equivalent N.F.'s of the original system. The negative moments of inertia are analogous to power input devices.

The system with nonrotating discs mentioned above can be used to calculate the N.F.'s by either Mykelstad's tabular procedure[3] or by Southwell's Relaxation Method.[4] Myklestad's method can be applied in the usual manner, the negative masses causing no difficulty. The Relaxation Method also requires no modification beyond avoiding the negative characteristic values. This can be accomplished by starting each stage of relaxation with an assumed configuration that makes $T_1 > 0$.

B. *Elastic System Unsymmetrical*

The natural frequencies for the system shown in Fig. 6, with unsymmetrical elastic properties, can be determined from the roots of

$$\begin{vmatrix} c_{11} - M_1\tau^2 & 0 & c_{12} & 0 & \cdots \\ 0 & c_{11}' - M_1\tau^2 & 0 & c_{12}' & \cdots \\ c_{21} & 0 & c_{22} - A_2\tau^2 & -C_2k_2m\tau^2 & \cdots \\ 0 & c_{21}' & -C_2k_2m\tau^2 & c_{22}' - A_2\tau^2 & \cdots \\ \cdots & \cdots & \cdots & \cdots & \cdots \end{vmatrix} = 0 \qquad (18)$$

The mode of motion for any N.F. may be found from Eq. (61) in the usual manner. Appendix II contains the derivation of both Eqs. (18) and (61).

Eq. (18) is a polynomial of $4n$ degree in τ^2. It has $4n$ real roots, some positive and some negative. As before, the negative roots have no meaning and may be discarded.

The method described in IIA for plotting the N.F.'s as a function of ω_2 is applicable for this case. Since it can be shown that Eq. (59) has $4n$ positive real roots for any given set of $\omega_2, \omega_4, \ldots, \omega_{2n}$, this graph will contain $4n$ curves. The procedure given in IIA, for determining the N.F.'s for any given set of $\omega_2, \omega_j, \ldots, \omega_{2n}$ and for finding the disc speeds and N.F.'s at which resonance occurs (with different types of exciting forces), can also be applied here without modification. The modes of motion cannot be plotted on a graph because of their complex character. Therefore, it is recommended that the modes be found only for those N.F.'s that are of interest.

The conclusions of Appendix II show that Southwell's Relaxation Method can be used to determine the N.F.'s and normal modes of the system. As before, the negative characteristic values can be avoided by always choosing trial configurations that make

$$M_1(F_{11}^2 + F_{21}^2) + A_2(F_{12}^2 + F_{22}^2) + \ldots\ldots + A_{2n}(F_{1,\,2n} + F_{2,\,2n}^2) - m\sum_{r=2,\,4,\ldots}^{2n} C_r k_r F_{1r} F_{2r} > 0 \quad \text{(g)}$$

Myklestad's tabular procedure can be modified to apply to Eqs. (61). However, the rotating discs cannot be replaced by nonrotating discs as in the case that possessed elastic symmetry.

Appendix I

Fig. 7 shows n rotating rigid discs mounted on a vertical elastic shaft, S. Each disc is mounted rigidly on the shaft, and it is assumed that each disc c.g. and axis coincides with the elastic axis of the shaft when the system is at rest. $\omega_2, \omega_4, \ldots, \omega_{2n}$ are the angular velocities of $D_1, D_2, \ldots, D_n$, respectively, about their axis. Fig. 8 shows the instantaneous position of the disc, D_j. The XYZ axes, with origin at O, are fixed in space; OZ is vertical and it coincides with S when the system is at rest. The $X_j'Y_j'Z_j'$ axes, with origin, O_j', at the c.g. of D_j, remain parallel to the XYZ axes during motion. $q_{1,\,2j-1}$ and $q_{2,\,2j-1}$ are the x and y coordinates of O_j' projected on the XOY plane. $q_{1,\,2j}$ and $q_{2,\,2j}$ are the coordinates of P_j' projected on the $X_j'O_j'Y_j'$ plane, and they are dimensionless. As in the first part of this paper, $O_j'P_j'$ is along the axis of D_j and its length is one unit. $q_{1,\,2j-1}$, $q_{2,\,2j-1}$, $q_{1,\,2j}$, and $q_{2,\,2j}$ are assumed small. With regard to the physical characteristics of D_j, M_{2j-1} is its mass, C_{2j} is its polar moment of inertia, and A_{2j} is the remaining principal moment of inertia. It is assumed that the shaft, S, and its bearings have

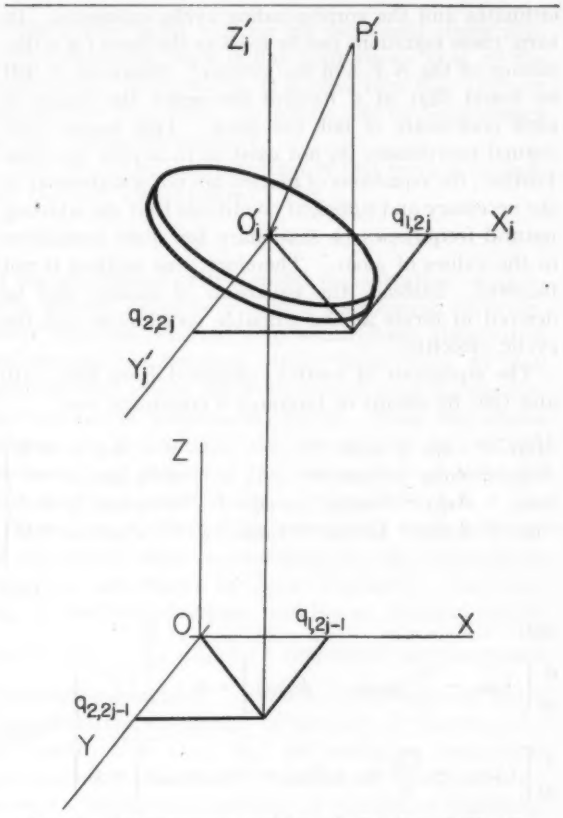

FIG. 8. Instantaneous position of the disc of Fig. 7

equal elastic properties in the XOZ and YOZ planes and that it is massless.

The kinetic and potential energies for this system are:

$$\left.\begin{aligned} 2T \equiv\ & M_1(\dot{q}_{11}^2 + \dot{q}_{21}^2) + A_2(\dot{q}_{12}^2 + \dot{q}_{22}^2) + \ldots \\ & \qquad + A_{2n}(\dot{q}_{1,\,2n} + \dot{q}_{2,\,2n}) \\ & - C_2\omega_2(q_{12}\dot{q}_{22} - \dot{q}_{12}q_{22}) - \ldots \\ & \qquad - C_{2n}\omega_{2n}(q_{1,\,2n}\dot{q}_{2,\,2n} - \dot{q}_{1,\,2n}q_{2,\,2n}) \\ & + C_2\omega_2^2 + \ldots\ldots\ldots\ldots\ldots + C_{2n}\omega_{2n}^2 \end{aligned}\right\} \quad (19)$$

and

$$\left.\begin{aligned} 2V \equiv\ & c_{11}q_{11}^2 + \ldots\ldots\ldots + c_{1,\,2n}q_{1,\,2n}q_{11} \\ & + c_{11}q_{21}^2 + c_{12}q_{22}q_{21} + \ldots + c_{1,\,2n}q_{2,\,2n}q_{21} \\ & + \ldots\ldots\ldots\ldots\ldots\ldots\ldots\ldots \\ & + c_{2n,\,1}q_{11}q_{1,\,2n} + \ldots\ldots\ldots + c_{2n,\,2n}q_{1,\,2n}^2 \\ & + c_{2n,\,1}q_{21}q_{2,\,2n} + \ldots\ldots\ldots + c_{2n,\,2n}q_{2,\,2n}^2 \end{aligned}\right\} \quad (20)$$

respectively. The coefficients c_{rs} are the usual coefficients of elasticity ($c_{rs} = c_{sr}$). T and V are both positive definite quadratic forms in the velocities and displacements, respectively. The form of T and V shows that the system has cyclic coordinates whose velocities are $\omega_2, \omega_4, \ldots, \omega_{2n}$.

The usual procedure at this point is to employ the method of "ignoration of the coordinates"[5] and derive the equations of motion in terms of the palpable co-

ordinates and the corresponding cyclic momenta. In turn, these equations can be used as the basis for a discussion of the N.F.'s of the system.[6] However, it will be found that at a natural frequency the phase of each coordinate is not the same. This means that normal coordinates do not exist as in acyclic systems. Further, the equations of motion are not a statement of the necessary and sufficient conditions that the whirling natural frequencies be stationary for slight variations in the values of mode. Therefore, this method is not followed. Instead, the equations of motion will be derived in terms at the palpable coordinates and the cyclic velocities.

The equations of motion, obtained from Eqs. (19) and (20) by means of Lagrange's equations, are

$$\left.\begin{aligned} &M_1\ddot{q}_{11} + c_{11}q_{11} + c_{12}q_{12} + \ldots\ldots\ldots + c_{1,\,2n}q_{1,\,2n} = 0\\ &M_1\ddot{q}_{21} + c_{11}q_{21} + c_{12}q_{22} + \ldots\ldots\ldots + c_{1,\,2n}q_{2,\,2n} = 0\\ &c_{21}q_{11} + A_2\ddot{q}_{12} + C_2\omega_2\dot{q}_{22} + c_{22}q_{12} + \ldots + c_{2,\,2n}q_{1,\,2n} = 0\\ &c_{21}q_{21} + A_2\ddot{q}_{22} - C_2\omega_2\dot{q}_{12} + c_{22}q_{22} + \ldots + c_{2,\,2n}q_{2,\,n} = 0\\ &\ldots\ldots\ldots\ldots\ldots\ldots\ldots\ldots\ldots\ldots\ldots\ldots\end{aligned}\right\} \tag{21}$$

and

$$\left.\begin{aligned} &\frac{d}{dt}\left[C_2\omega_2 - \frac{C_2}{2}\left(q_{12}\dot{q}_{22} - \dot{q}_{12}q_{22}\right)\right] = 0\\ &\ldots\ldots\ldots\ldots\ldots\ldots\ldots\ldots\ldots\ldots\ldots\ldots\\ &\frac{d}{dt}\left[C_{2n}\omega_{2n} - \frac{C_{2n}}{2}\left(q_{1,\,2n}\dot{q}_{2,\,2n} - \dot{q}_{1,\,2n}q_{2,\,2n}\right)\right] = 0\end{aligned}\right\} \tag{22}$$

It is obvious that if periodic external forces and moments act on the system, the right-hand side of Eqs. (21) and (22) would not be zero. In this discussion, however, all external forces and moments are excluded. The equations of motion given by Eqs. (21) correspond to the palpable coordinates and Eqs. (22) to the cyclic coordinates. Eqs. (22) show that the cyclic momenta of the system are constant.

By means of the substitutions,

$$\left.\begin{aligned} q_{2r-1} &= q_{1,\,2r-1} + iq_{2,\,2r-1}\\ q_{2r} &= q_{1,\,2r} + iq_{2,\,2r}\end{aligned}\right\} \tag{23}$$

the $4n$ Eqs. (21) may be reduced to the $2n$ equations

$$\left.\begin{aligned} &M_1\ddot{q}_1 + c_{11}q_1 + \ldots\ldots\ldots\ldots + c_{1,\,2n}q_{2n} = 0\\ &c_{21}q_1 + A_2\ddot{q}_2 - iC_2\omega_2q_2 + c_{22}\dot{q}_2 + \ldots + c_{2,\,2n}q_{2n} = 0\\ &\ldots\ldots\ldots\ldots\ldots\ldots\ldots\ldots\ldots\ldots\ldots\ldots\\ &c_{2n,\,1}q_1 + \ldots + A_{2n}\ddot{q}_{2n} - iC_{2n}\omega_{2n}\dot{q}_{2n} + c_{2n,\,2n}q_{2n} = 0\end{aligned}\right\} \tag{24}$$

It should be noted that this simplification can be carried out only if the shaft, S, and its bearings have equal elastic properties in the XOZ and YOZ planes. When calculating the N.F.'s of the rotating elements in aircraft reciprocating engines and gas turbines, this condition is usually satisfied. However, there are systems that do not satisfy this condition. This method of analysis does not apply in those cases. Since Eqs. (24) are equivalent to Eqs. (21), the solution of Eqs. (24) and (22) follows.

Eqs. (24) are linear differential equations with constant coefficients. Therefore, assume solutions of the form

$$\left.\begin{aligned} q_1 &= F_1e^{i\tau t}\\ q_2 &= F_2e^{i\tau t}\\ &\ldots\ldots\\ q_{2n} &= F_{2n}e^{i\tau t}\end{aligned}\right\} \tag{25}$$

Substituting Eqs. (25) in Eqs. (24),

$$\left.\begin{aligned} &(c_{11} - M_1\tau^2)F_1 + c_{12}F_2 + \ldots\ldots + c_{1,\,2n}F_{2n} = 0\\ &c_{21}F_1 + (c_{22} + C_2\omega_2\tau - A_2\tau^2)F_2 + \ldots + c_{2,\,2n}F_{2n} = 0\\ &\ldots\ldots\ldots\ldots\ldots\ldots\ldots\ldots\ldots\ldots\ldots\ldots\\ &c_{2n,\,1}F_1 + \ldots + (c_{2n,\,2n} + C_{2n}\omega_{2n}\tau - A_{2n}\tau^2)F_{2n} = 0\end{aligned}\right\} \tag{26}$$

Eliminating the $2n - 1$ ratios $F_1 : F_2 : \ldots : F_{2n}$ from Eqs. (26), the characteristic equation is

$$\Delta(\tau) = 0 \tag{27}$$

where

$$\Delta(\tau) \equiv \begin{vmatrix} c_{11} - M_1\tau^2 & c_{12} & \cdots & c_{1,\,2n}\\ c_{21} & (c_{22} + C_2\omega_2\tau - A_2\tau^2) & \cdots & c_{2,\,2n}\\ \cdots & \cdots & \cdots & \cdots\\ c_{2n,\,1} & \cdots & \cdots & (c_{2n,\,2n} + C_{2n}\omega_{2n}\tau - A_{2n}\tau^2)\end{vmatrix} \tag{28}$$

Eq. (27) is a polynomial of degree $4n$ in τ. If its roots are all real, they determine the N.F.'s of the system. The nature of these roots will now be established.

Let σ be a solution of Eq. (27) and let $F_1, F_2, \ldots, F_{2n}$ be the corresponding variables that satisfy Eqs. (26). Then,

$$2V_0(F) + \left(\sum_{r=2,\,4,\ldots}^{2n} C_r\omega_rF_r^2\right)\sigma - 2T_0(F)\sigma^2 = 0 \tag{29}$$

where

$$2T_0(F) \equiv M_1F_1^2 + A_2F_2^2 + \ldots\ldots\ldots + A_{2n}F_{2n}^2 \tag{30}$$

$$\begin{aligned} 2V_0(F) \equiv\ & c_{11}F_1^2 + c_{12}F_1F_2 + \ldots\ldots + c_{1,\,2n}F_1F_{2n}\\ &+ \ldots\ldots\ldots\ldots\ldots\ldots\ldots\ldots\\ &+ c_{2n,\,1}F_{2n}F_1 + \ldots\ldots\ldots\ldots + c_{2n,\,2n}F_{2n}^2\end{aligned} \tag{31}$$

Both Eqs. (30) and (31) are positive definite quadratic forms. The coefficient of the first degree term in Eq. (29) may be either positive or negative. Eq. (29) shows that, if any of the roots of Eq. (27) are real, they may be either positive or negative. Let σ' be another

root of Eq. (27) and $F_1', F_2', \ldots, F_{2n}'$ the corresponding variables. Then these quantities, together with σ and its F's satisfy

$$\left.\begin{aligned} 2V_0(F,F') + \left(\sum_{2,4}^{2n} \ldots C_r\omega_r F_r F_r'\right)\sigma - 2T_0(F,F')\sigma^2 = 0 \\ 2V_0(F,F') + \left(\sum_{2,4}^{2n} \ldots C_r\omega_r F_r F_r'\right)\sigma' - 2T_0(F,F')\sigma'^{1,2} = 0 \end{aligned}\right\} \tag{32}$$

In these equations

$$\left.\begin{aligned} 2T_0(F,F') &\equiv M_1F_1F_1' + A_2F_2F_2' + \ldots + A_{2n}F_{2n}F_{2n}' \\ 2V_0(F,F') &\equiv c_{11}F_1F_1') + \ldots\ldots\ldots\ldots + c_{1,\,2n}F_{2n}F_1' \\ &+ \ldots\ldots\ldots\ldots\ldots\ldots\ldots\ldots\ldots \\ &+ c_{2n,\,1}F_1F_{2n}' + \ldots\ldots\ldots + c_{2n,\,2n}F_{2n}F_{2n}' \end{aligned}\right\} \tag{33}$$

If σ and σ' are distinct roots of Eq. (27), the following relations are valid:

$$\sigma + \sigma' = \sum_{2,4}^{2n} C_r\omega_r F_r F_r'/2T_0(F,F') \tag{34}$$

$$\sigma\sigma' = V_0(F,F')/T_0(F,F') \tag{35}$$

Assume that Eq. (27) has an imaginary root, and let

$$\left.\begin{aligned} \sigma &= \rho + i\delta, \quad \sigma' = \rho - i\delta \\ F_r &= \mu_r + i\nu_r, \quad F_r' = \mu_r - i\nu_r \end{aligned}\right\} \quad (r = 1, 2, \ldots, 2n) \tag{36}$$

Substituting these relations in Eq. (35),

$$\sigma\sigma' \equiv \rho^2 + \delta^2 = \frac{-V_0(\mu) - V_0(\nu)}{T_0(\mu) + T_0(\nu)} \tag{37}$$

This is impossible since $T_0(\mu)$ and $V_0(\mu)$ are positive definite. Therefore, Eq. (27) has $4n$ real roots, and these roots are continuous functions of the cyclic velocities. This proves that the system shown in Fig. 7 has $4n$ N.F.'s for a fixed but arbitrary set of $\omega_2, \omega_4, \ldots, \omega_{2n}$.

Eq. (29) shows that no roots of Eq. (27) change sign as the cyclic velocities vary. However, when all cyclic velocities are zero, $2n$ of the roots of Eq. (27) are positive and $2n$ are negative. Therefore, $2n$ of the N.F.'s are positive and $2n$ are negative.

Up to this point nothing has been said about Eqs. (22). However, since it has been shown that all the roots of Eq. (27) are real, it is clear that Eqs. (22) are satisfied by Eqs. (25). Therefore, the cyclic momenta of the system are constant.

The geometric interpretation of this method of finding the N.F.'s is as follows. Let

$$k_r = \omega_r/\omega_2 \qquad (r = 2, 4, \ldots, 2n) \tag{38}$$

If the mechanical system under consideration contains only geared connections among its rotating elements, these ratios are constant. In what follows, these ratios will be assumed constant. Using these ratios, we may plot the $4n$ N.F.'s as the ordinate with ω_2 as the abscissa and obtain $4n$ continuous curves. Thus, the above process for determining the $4n$ roots of Eq. (27) is equivalent to obtaining the intersection of these $4n$ curves with the vertical line, ω_2 = constant.

Examination of Eq. (29) shows that the coefficient of the linear term is analogous to the "dissipation function" introduced by Lord Rayleigh.[7] This analogy is algebraic, however, and has no physical significance, for $\left[\sum_{2,4,\ldots}^{2n} C_r\omega_r F_r^2\right]$ represents an *imaginary* "dissipation function." Since a real dissipation function affects the amplitudes of vibration by an exponential factor, it is clear that an imaginary dissipation function must affect only the periods of vibration of the motion. Thus, this concept of imaginary damping could be used to prove that the roots of Eq. (27) are all real. The next step affects the elimination of the linear term in Eq. (29), and introduces the desired hypothetical acyclic system.

Let

$$\omega_2 = m\tau \tag{39}$$

where m is a real number. Substitute these equations in Eqs. (26). This gives

$$\left.\begin{aligned} &(c_{11} - M_1\tau^2)F_1 + C_{12}F_2 + \ldots\ldots\ldots + c_{1,\,2n}F_{2n} = 0 \\ &c_{21}F_1 + [c_{22} - (A_2 - C_2k_2m)\tau^2]F_2 + \ldots + c_{2,\,2n}F_{2n} = 0 \\ &\ldots\ldots\ldots\ldots\ldots\ldots\ldots\ldots\ldots\ldots\ldots\ldots\ldots\ldots \\ &c_{2n,\,1}F_1 + \ldots + [c_{2n,\,2n} - (A_{2n} - C_{2n}k_{2n}m)\tau^2]F_{2n} = 0 \end{aligned}\right\} \tag{40}$$

The characteristic Eq. (27) now becomes

$$\Delta_1(\tau^2) \equiv \begin{vmatrix} c_{11} - M_1\tau^2 & c_{12} & \ldots & c_{1,\,2n} \\ c_{21} & c_{22} - (A_2 - C_2k_2m)\tau^2 & \ldots & c_{2,\,2n} \\ \ldots\ldots & \ldots\ldots & \ldots\ldots & \ldots\ldots \\ c_{2n,\,1} & \ldots & \ldots & c_{2n,\,2n} - (A_{2n} - C_{2n}k_{2n}m)\tau^2 \end{vmatrix} = 0 \tag{41}$$

This equation is a polynomial of degree $2n$ in τ^2. (In what follows, Eq. (41) will be considered *only* as a polynomial of degree $2n$ in τ^2.) The transformation (39) has thus removed all terms of odd degree from the characteristic equation. The nature of the roots, τ^2, in Eq. (41) is the next question.

Let σ^2 be a solution of Eq. (41); let $F_1, F_2, \ldots, F_{2n}$ be the corresponding set of terms which satisfy Eqs.

(40) when σ^2 is substituted for τ^2. Using these values,

$$V_0(F) - T_1(F)\sigma^2 = 0 \tag{42}$$

where

$$2T_1(F) \equiv M_1F_1^2 + (A_2 - C_2k_2m)F_2 + \ldots + (A_{2n} - C_{2n}k_{2n}m)F_{2n} \tag{43}$$

Now $T_1(F)$ is a function of m; in particular, half of its coefficients may be negative or zero. Therefore, $T_1(F)$ may be either positive, negative, or zero. From this it may be concluded that, if $\Delta_1(\tau^2) = 0$ has real roots for τ, they may have any values.

Assume that σ^2 is another root of Eq. (41) distinct from σ^2; let F_1', F_2', ..., F_{2n}' be the corresponding F's. These quantities, in conjunction σ^2, F_1, F_2, ..., F_{2n} and Eqs. (40), permit the formation of

$$\left.\begin{aligned} V_0(F,F') - T_1(F,F')\sigma^2 = 0 \\ V_0(F,F') - T_1(F,F')\sigma'^2 = 0 \end{aligned}\right\} \tag{44}$$

Hence, if σ^2 and σ'^2 are distinct, it may be concluded that

$$V_0(F,F') = 0, \quad T_0(F,F') = 0 \tag{45}$$

In this equation

$$2T_1(F,F') \equiv M_1F_1F_1' + (A_2 - C_2k_2m)F_2F_2' + \ldots + (A_{2n} - C_{2n}k_{2n}m)F_{2n}F_{2n}' \tag{46}$$

These [Eqs. (45)] are the usual orthogonal relations obtained for conservative acyclic systems. They depend only on the symmetry of T_1 and V_0 and not on the signs of the coefficients of these two forms.

If Eq. (41) has imaginary roots, let

$$\left.\begin{aligned} \sigma^2 = \rho + i\delta, \quad \sigma'^2 = \rho - i\delta, \\ F_r = \mu_r + i\nu_r, \quad F_r' = \mu_r + i\nu_r, \end{aligned}\right\} \quad (r = 1, 2, \ldots, 2n) \tag{47}$$

Substituting these relations in Eqs. (45), the following equations result:

$$\left.\begin{aligned} V_0(\mu) + V_0(\nu) = 0 \\ T_1(\mu) + T_1(\nu) = 0 \end{aligned}\right\} \tag{48}$$

The first equation of Eqs. (48) is impossible, since $V_0(F)$ is a positive definite quadratic form in the variables F (or μ). This proves that the characteristic equation, Eq. (41), has no imaginary roots.

Consider the function

$$U = T_1(F)/V_0(F) \tag{49}$$

$V_0(F)$ is a positive definite quadratic form and $T_1(F)$ is a quadratic form whose coefficients are either positive, negative, or zero. Since $V_0(F)$ does not vanish (except when $F_1 = F_2 = \ldots = F_{2n} = 0$), it is obvious that, for at least two sets of $F_1, F_2, \ldots, F_{2n}$, U has a stationary value. If the method of the Calculus is used to search for one of these values, it is seen that Eqs. (40) are the required conditions and that the reciprocal of one of the roots of Eq. (41) is the value in question. Thus U has at least one real stationary value; it may be either positive or negative. Let $F_1, F_2, \ldots, F_{2n}$ be the corresponding set of variables. If the search for stationary values is continued,[6] it can be shown that $2n$ stationary values exist and that these are the reciprocals of the $2n$ real roots of Eq. (41). Therefore, the stationary property of the roots of Eq. (41) has been established.

By means of a linear transformation of the variables, the two forms $T_1(F)$ and $V_0(F)$ may be reduced to

$$\left.\begin{aligned} 2T_1(\theta) \equiv \nu_1^2\theta_1^2 + \ldots\ldots\ldots\ldots + \nu_{2n}^2\theta_{2n} \\ 2V_0(\theta) \equiv \theta_1^2 + \ldots\ldots\ldots\ldots + \theta_{2n} \end{aligned}\right\} \tag{50}$$

This transformation is always possible as long as $V_0(F)$ is positive definite. Hence, normal forms of $T_1(F)$ and $V_0(F)$ exist. In addition, the following relations are valid:

$$\gamma_r = 1/\sigma_r^2 \quad (r = 1, 2, \ldots, 2n) \tag{51}$$

where $\sigma_1^2, \sigma_2^2, \ldots, \sigma_{2n}^2$ are the $2n$ roots of Eq. (41).

A theorem of Algebra[3] states that the number of positive γ_r^2's is equal to the number of positive coefficients in Eq. (43). Thus, by determining the values of

$$A_r - C_rk_rm \qquad (r = 2, 4, \ldots, 2n) \tag{52}$$

we can determine the number of positive γ_r^2's. Inasmuch as Eq. (43) is a function of m only, it is apparent that there can be no less than n and at most $2n$ positive γ_r^2's.

It was shown above that the system under consideration has $4n$ N.F.'s for a given set of ω's. Further, if these N.F.'s are plotted as ordinates with ω_2 as abscissa, $4n$ continuous curves result; $2n$ are on the positive side of the horizontal and $2n$ are on the negative side. The introduction of Eq. (39) thus means that we are determining the intersections of these $4n$ curves with the line

$$\omega_2 = m\tau \tag{53}$$

Thus, the presence of negative roots of τ^2 in Eq. (41) or of negative γ_r^2 has no physical meaning and merely shows that some of the N.F. curves have asymptotes of the form of Eq. (39).* Therefore, the square roots of the positive roots, τ^2, of Eq. (41) are the N.F.'s of the system.

---

* A simple algebraic proof of this can be given as follows: Let σ_1 be a root of Eq. (27) for a given set of ω's.

Then find $m, k_2, k_4 \ldots, k_{2n}$, so that $m = \omega_2/\sigma_1$, and $k_r = \omega_r/\omega_2$ $(r = 2, 4, \ldots, 2n)$. Substitute these relations and $\tau^2 = \sigma_1^2$ in Eq. (41). A comparison shows that Eqs. (27) (with $\tau = \sigma_1$) and (41) are identical. Hence, any one of the $4n$ roots of Eq. (27) is the square root of one of the positive roots of Eq. (41). Let σ_2^2 be one of the positive roots of Eq. (41) for a given set of $m, k_2, \ldots, k_{2n}$.

Find $\omega_2, \omega_4, \ldots, \omega_{2n}$ so that $\omega_2 = \sigma_2 m$, and $\omega_r = k_r\omega_2$ $(r = 4, 6, \ldots, 2n)$. Substitute these relations and $\tau = \sigma_2$ in Eq. (27). It is seen that Eqs. (27) and (41) are identical. Hence, the square root of any of the positive roots of Eq. (41) is also a root of Eq. (27). Therefore, there is a one to one correspondence between the $4n$ roots of Eq. (27) and the square roots of the positive roots of Eq. (41). The negative roots of Eq. (41) (thought of as a polynomial of degree $2n$ in τ^2) have no meaning.

Appendix II

If the system shown in Fig. 6 (and discussed in Appendix I) does not have symmetrical elastic properties the details of Appendix I are changed but the procedure used there remains the same. Therefore, in this section only the details changed by the assumption of unsymmetrical elasticity will be pointed out.

With different elastic properties in the *XOZ* and *YOZ* planes (see Fig. 7), the elastic potential energy becomes

$$\left.\begin{aligned} 2V' \equiv\ & c_{11}q_{11}^2 + c_{12}q_{12}q_{11} + \ldots\ldots + c_{1,2n}q_{1,2n}q_{11} \\ & + c_{11}'q_{21}^2 + c_{12}'q_{22}q_{21} + \ldots\ldots + c_{1,2n}'q_{2,2n}q_{21} \\ & + \ldots\ldots\ldots\ldots\ldots\ldots\ldots\ldots\ldots\ldots \\ & + c_{2n,1}q_{11}q_{1,2n} + \ldots\ldots\ldots\ldots + c_{2n,2n}q_{1,2n}^2 \\ & + c_{2n,1}'q_{21}q_{2,2n} + \ldots\ldots\ldots\ldots + c_{2n,2n}'q_{2,2n} \end{aligned}\right\} \quad (54)$$

The coefficients of elasticity satisfy

$$c_{rs} = c_{sr}, \quad c_{rs}' = c_{sr}'$$

The altered equations of motion are

$$\left.\begin{aligned} & M_1\ddot{q}_{11} + c_{11}q_{11} + c_{12}q_{12} + \ldots\ldots + c_{1,2n}q_{1,2n} = 0 \\ & M_1\ddot{q}_{21} + c_{11}'q_{21} + c_{12}'q_{22} + \ldots\ldots + c_{1,2n}'q_{2,2n} = 0 \\ & c_{11}q_{11} + A_2\ddot{q}_{12} + C_2\omega_2\dot{q}_{22} + c_{22}q_{12} + \ldots\ldots\ldots = 0 \\ & c_{21}'q_{21} + A_2\ddot{q}_{22} - C_2\omega_2\dot{q}_{12} + c_{22}'q_{22} + \ldots\ldots\ldots = 0 \\ & \ldots\ldots\ldots\ldots\ldots\ldots\ldots\ldots\ldots\ldots\ldots\ldots\ldots\ldots \end{aligned}\right\} \quad (55)$$

Eqs. (22) remain the same.

Assume Eqs. (55) have solutions of the form

$$\left.\begin{aligned} q_{11} &= F_{11}\sin\tau t \\ q_{21} &= F_{21}\cos\tau t \\ q_{12} &= F_{12}\sin\tau t \\ q_{22} &= F_{22}\cos\tau t \\ & \ldots\ldots\ldots\ldots \\ & \ldots\ldots\ldots\ldots \end{aligned}\right\} \quad (56)$$

Substituting Eqs. (56) in Eqs. (55),

$$\left.\begin{aligned} & (c_{11} - M_1\tau^2)F_{11} + c_{12}F_{12} + \ldots\ldots\ldots\ldots = 0 \\ & (c_{11}' - M_1\tau^2)F_{21} + c_{12}'F_{22} + \ldots\ldots\ldots\ldots = 0 \\ & c_{21}F_{11} + (c_{22} - A_2\tau^2)F_{12} - C_2\omega_2\tau F_{22} + \ldots\ldots = 0 \\ & c_{21}'F_{21} - C_2\omega_2\tau F_{12} + (c_{22}' - A_2\tau^2)F_{22} + \ldots = 0 \\ & \ldots\ldots\ldots\ldots\ldots\ldots\ldots\ldots\ldots\ldots\ldots\ldots\ldots\ldots \end{aligned}\right\} \quad (57)$$

It is easily seen that Eqs. (56) satisfy Eqs. (22) regardless of the values of $F_{11}, F_{21}, \ldots, F_{2,2n}, \tau$.

Eliminating the $4n - 1$ ratios $F_{11}:F_{21}: \ldots :F_{2,2n}$ from Eqs. (57), the characteristic equation is

$$\Delta'(\tau) = 0 \quad (58)$$

where

$$\begin{vmatrix} c_{11} - M_1\tau^2 & 0 & c_{12} & 0 & \ldots\ldots \\ 0 & c_{11}' - M_1\tau^2 & 0 & c_{12}' & \ldots\ldots \\ c_{21} & 0 & c_{22} - A_2\tau^2 & -C_2\omega_2\tau & \ldots\ldots \\ 0 & c_{21}' & -C_2\omega_2\tau & c_{22}' - A_2\tau^2 & \ldots\ldots \\ \ldots\ldots & \ldots\ldots & \ldots\ldots & \ldots\ldots & \ldots\ldots \end{vmatrix} \quad (59)$$

This equation is a polynomial of $8n$ degree in τ.

It can be shown that Eq. (58) has $8n$ real roots, $4n$ positive and $4n$ negative. Hence, the unsymmetrical system has $4n$ positive and $4n$ negative N.F.'s for any given set of $\omega_2, \omega_4, \ldots, \omega_{2n}$. If all are related to ω_2 by a constant multiple, it is possible to plot a graph similar to Fig. 3a with ω_2 as abscissa and N. F. as ordinate. In this way a graph is obtained with $4n$ curves above the zero ordinate and $4n$ below.

By means of the equations

$$\omega_r = k_r m\tau \qquad (r = 2, 4, \ldots, 2n) \quad (60)$$

a simplification can be made in the above analysis Substituting these equations in Eqs. (57),

$$\left.\begin{aligned} & (c_{11} - M_1\tau^2)F_{11} + c_{12}F_{12} + \ldots + c_{1,2n}F_{1,2n} = 0 \\ & (c_{11}' - M_1\tau^2)F_2 + c_{12}'F_{22} + \ldots + c_{1,2n}'F_{2,2n} = 0 \\ & c_{11}F_{11} + (c_{22} - A_2\tau^2)F_{12} - C_2k_2m\tau^2F_{22} + \ldots\ldots \\ & \qquad + c_{2,2n}F_{1,2n} = 0 \\ & c_{11}'F_{21} + (c_{22}' - A_2\tau^2)F_{22} - C_2k_2m\tau^2F_{12} + \ldots\ldots \\ & \qquad + c_{2,2n}'F_{2,2n} = 0 \\ & \ldots\ldots\ldots\ldots\ldots\ldots\ldots\ldots\ldots\ldots\ldots\ldots\ldots\ldots \end{aligned}\right\} \quad (61)$$

The characteristic equation, for this case, is

$$\Delta_1'(\tau^2) \equiv \begin{vmatrix} c_{11} - M_1\tau^2 & 0 & c_{12} & 0 & \ldots\ldots \\ 0 & c_{11} - M_1\tau^2 & 0 & c_{12}' & \ldots\ldots \\ c_{21} & 0 & c_{22} - A_2\tau^2 & -C_2k_2m\tau^2 & \ldots\ldots \\ 0 & c_{21} & -C_2k_2m\tau^2 & c_{22}' - A_2\tau^2 & \ldots\ldots \\ \ldots\ldots & \ldots\ldots & \ldots\ldots & \ldots\ldots & \ldots\ldots \end{vmatrix} = 0 \quad (62)$$

This equation will be considered as a polynomial of degree $4n$ in τ^2.

It may be shown, by the same procedure that was used in Appendix I, (1) that Eq. (62) has $4n$ real roots;

(2) that some of these roots of (τ^2) may be negative, and (3) that the roots of Eq. (62) are the stationary values of the function

$$U' \equiv \frac{2T_0'(F) - \sum_{2,4,\ldots}^{2n} C_r k_r F_{1,r} F_{2,r}}{2V_0'(F)} \qquad (63)$$

In Eq. (63)

$$2T_0'(F) \equiv M_1(F_{11}^2 + F_{21}^2) + A_2(F_{12}^2 + F_{22}^2) + \ldots\ldots + M_{2n-1}(F_{1,2n-1}^2 + F_{2,2n-1}^2) + A_{2n}(F_{1,2n}^2 + F_{2,2n}^2) \qquad (h)$$

$$2V_0'(F) \equiv \left.\begin{array}{l} c_{11}F_{11}^2 + c_{12}F_{12}F_{11} + \ldots + c_{1,2n}F_{1,2n}F_{11} + \\ c_{11}'F_{21}^2 + c_{12}'F_{22}F_{21} + \ldots + c_{1,2n}'F_{2,2n}F_{21} + \\ \ldots\ldots\ldots\ldots\ldots\ldots\ldots\ldots + \\ c_{2n,1}F_{11}F_{1,2n} + \ldots\ldots + c_{2n,2n}F_{1,2n}^2 + \\ c_{2n,1}'F_{21}F_{2,2n} + \ldots\ldots + c_{2n,2n}'F_{2,2n}^2 \end{array}\right\} \qquad (i)$$

However, it is not possible, in this case, to find a simple method for determining the numbers of negative roots which Eq. (62) possesses for a given set of k_2, k_4, ..., k_{2n}, m. As in Appendix I, the negative roots of Eq. (62) have no meaning and the positive roots determine the N.F.'s.

References

[1] Stodola, A., and Loewenstein, L. C., *Steam and Gas Turbines*, Vol. I, 1st Ed.; McGraw-Hill Book Company, Inc., New York, 1927.

[2] Foppl, Von Ludwig, *Kritische Drehzahlgebiete Der Fliegend Angeardneten Schreibe*, Stephen Timoshenko, 60th Anniversary Volume; McGraw-Hill Book Company, Inc., New York, 1938.

[3] Myklestad, N. O., *Vibration Analysis;* McGraw-Hill Book Company, Inc., New York, 1944.

[4] Southwell, R. V., *Relaxation Methods in Engineering Science*, 1st Ed., Chapt., 7; Oxford University Press, London, 1940.

[5] Lamb, H., *Higher Mechanics*, 2nd Ed., Chapt. 10; Cambridge University Press, London, 1929.

[6] Ibid., Chapt. 11.

[7] Rayleigh, Lord, *Theory of Sound*, Vol. I, 2nd Ed., Chapt. 5; Macmillan Company, London, 1929.

[8] Bocher, M., *Introduction to Higher Algebra*, Chapts. XI and XIII; The Macmillan Company, New York, 1938.

Library Facilities of the Institute of the Aeronautical Sciences

To serve Institute members and others in the aeronautical industry, the Institute of the Aeronautical Sciences offers the facilities of:

The W. A. M. Burden Library
2 East 64th Street
New York 21, N.Y.

The facilities of this library are available for reference study at the Institute.

The Paul Kollsman Lending Library
2 East 64th Street
New York 21, N.Y.

This library loans books without charge to members and others in the United States over eighteen years of age. Full information will be sent on request.

The Pacific Aeronautical Library
6715 Hollywood Boulevard
Los Angeles 28, Calif.

This is a service and reference library for West Coast members and organizations. Full information as to its facilities will be sent on request.

Analytic Definition of a Retractable Landing Gear Axis of Rotation

ROY A. LIMING*

North American Aviation, Inc.

SUMMARY

This paper presents an analytic solution for the problem of determining a skewed axis of rotation for a retractable landing gear whose motion involves a single articulation.

Two simple linear slope equations, developed to define the axis, provide the foundation required for the study of the kinematics system.

The application of this analytic technique reduces the solution of a given problem to a few minutes of mechanical manipulation of a standard calculating machine.

While there are other procedures, both graphical and mathematical, available for obtaining a solution to the problem, the author believes that the method suggested represents the simplest in principle and in practical application to design, as evidenced by the fact that the discussion in this paper represents an abstract of the design procedure used in the North American Aviation Engineering Department with respect to landing gear development in the preliminary as well as the production design stage.

Two examples are worked out in complete detail to show the high-speed inspection character of the analytic approach.

INTRODUCTION

IN THE DEVELOPMENT of a retractable landing gear the designer is usually confronted with the initial problem of establishing an axis of rotation that will in one articulation move the wheel from a given extended to a given retracted position. The discussion that follows is concerned with the general case, in which the plane of symmetry of the wheel is displaced, thereby introducing the familiar problem of the skewed line in space geometry.

The determination of this axis of rotation, a perennial problem child in aircraft design circles, has been the subject of a wide variety of attacks, both graphical and mathematical. A careful survey of such attempts reveals that the mathematical approach has been selected almost invariably as an incidental or subordinate corollary to some particular graphical technique. The special criteria that should properly govern such analysis have been largely ignored, thereby placing the mathematical technique at a disadvantage.

The analytic solution presented in this paper results in the development of two simple linear slope equations defining the axis of rotation. The extreme simplicity of procedure and high speed which characterize the establishment of these slope-intercept equations actually revolutionize design procedure to the extent that all graphical layout intended to define the axis is rendered superfluous.

Received April 11, 1946.

* Head of Engineering-Lofting Mathematics.

DESIGN PROCEDURE

This analytic method is employed directly to define quickly and accurately the axis of rotation as soon as the designer has selected wheel positions, extended and retracted, which represent a reasonably satisfactory design configuration.

The usual design approach is to first establish the extended position of the wheel in the side view. The stowed position is then achieved by selecting the location of the center of the wheel in such a manner as to reach a satisfactory compromise with adjoining structure and the airplane contour. This latter condition may require tilting the wheel axle through one or two angles of inclination, e.g., either in the front or profile view or in both. The tread, variable within specified limits, is selected to fit this general pattern.

The coordinates of the center of the wheel, extended and retracted (see A_E and A_R of Fig. 1), are thus given. Any second point in the rotating system may be employed as a basis for calculation. For maximum convenience, this point may be located a distance of unity along the centerline wheel axle from the wheel center, either inboard or outboard. The coordinates of this point (see B_E and B_R of Fig. 1) may be established immediately in terms of the axle position. The axis of rotation may then be precisely determined with an average expenditure of 10 min. time, using Chart 1 and a standard calculating machine.

Should the axis of rotation thus determined fall in such a position within the airplane as to prevent practical design of a trunnion to support the gear, it becomes necessary to relocate the wheel, usually in the extended position, with respect to the tread and to calculate a new axis position. If the designer, because of the stowage problem, finds his degree of freedom largely restricted to the tread variable, he may request the simultaneous application of the maximum inboard, mean, and maximum outboard positions of the wheel extended. The trend of the rotation axis, subject to the tread variable, may thus be established at once. If no adjustment is necessary, the axis stands precisely defined by the slope-intercept equations obtained by the use of Chart 1. (See Appendix.)

CHART 1
Landing Gear Axis of Rotation. Analytic Calculation Chart

Center of wheel	A_E:	X_1 33.3	Y_1 30	Z_1 −24.9
	A_R:	X_3 0	Y_2 0	Z_3 0
Point on centerline wheel axle	B_E:	X_2 32.3	Y_3 30	Z_2 −24.9
	B_R:	X_4 −0.190067	Y_4 0.254101	Z_4 0.948318
Direction numbers of $\overline{A_E A_R}$: $(X_1 - X_3):(Y_1 - Y_3):(Z_1 - Z_3)$ =		a_1 33.3 :	b_1 30 :	c_1 −24.9
Direction numbers of $\overline{B_E B_R}$: $(X_2 - X_4):(Y_2 - Y_4):(Z_2 - Z_4)$ =		a_2 32.490067 :	b_2 29.745899 :	c_2 −25.848318

Δ	M_1	M_2	p	q	B_1	B_2
$a_1c_2 - a_2c_1$	$\frac{b_2c_1 - b_1c_2}{\Delta}$	$\frac{a_2b_1 - a_1b_2}{\Delta}$	$X_1^2 + Y_1^2 + Z_1^2 - (X_2^2 + Y_2^2 + Z_2^2)$	$X_3^2 + Y_3^2 + Z_3^2 - (X_4^2 + Y_4^2 + Z_4^2)$	$\frac{c_2p - c_1q}{2\Delta}$	$\frac{a_1q - a_2p}{2\Delta}$
−51.746321	−0.672060	0.306040	2,628.9	2,562.3	40.113	0.856
$2\Delta = -103.492642$						

Plan view equation: $X = M_1Y + B_1 : X = \underline{-0.672060Y} + \underline{40.113}$
Side view equation: $Z = M_2Y + B_2 : Z = \underline{0.306040Y} + \underline{0.856}$

CRITERIA CONSIDERED

The following criteria have been established to govern the analytic approach to this problem:

(1) Recognition of analytic techniques as the *natural* mathematical tool for the solution of point-line-plane relationships involved in motion analysis in space.

(2) Employment of a systematic analytic attack to effect a completely simplified solution of the general case.

(3) Elimination of all intermediate steps and formulas between the original basic data and the actual process of calculating the required final data.

(4) Reduction of actual calculation to the most efficient possible mechanical routine.

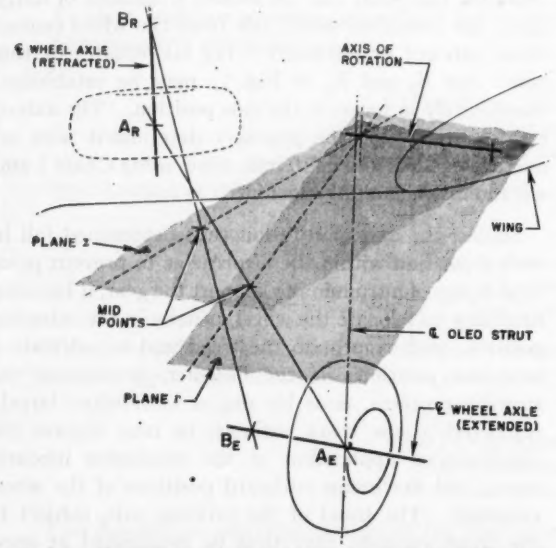

FIG. 1. Perspective view of relevant areas of the wing showing the basic geometric definition of a retractable landing gear axis of rotation. The accompanying discussion analytically reduces the kinematics dimensional specification of this design problem to a simple algebraic routine.

(5) Recognition of the superiority of analytic techniques in the subsequent development of the complete dimensional specification of the landing gear structure and its coordination with the cambered surface of the aircraft.

GEOMETRIC DEFINITION OF THE PROBLEM

Fig. 1 includes relevant plan, profile, and elevation areas of a typical wing combined in convenient perspective form. To establish the geometry of a retractable undercarriage, it is necessary first to define, within the available stowage space, a rotation axis that satisfies the two given positions (extended and retracted) of the wheel.

The wheel is defined geometrically by a straight line representing a segment of its own axis of rotation (the centerline of the axle). The geometric problem consists, then, of bringing this straight line from its extended position in space to its retracted position within the cambered surface of the wing.

The axis of rotation that will permit the achievement of this motion may be defined as a skew line in space, determined by the intersection of two planes normal to, and bisecting, the two lines determined by two positions of any two given points in the rotating system. The basic principle involved is shown in Fig. 2. For the geometric solution of this problem the reader is referred to any standard text in descriptive geometry.

ANALYTIC SOLUTION

The analytic solution is analogous to the geometric definition of the axis. In Fig. 1, the center of the wheel (A) has been chosen as one point, and an arbitrary point (B) conveniently located a distance of unity along the centerline of the axle from point (A) has been chosen as the second of two points defining the position of the wheel, the subscripts (E) and (R) denoting the extended and retracted positions, respectively, of the two points.

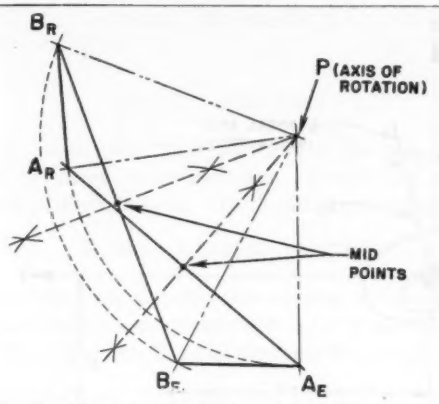

FIG. 2. In this view, the rotation axis is seen as the axis of a cone of projection. The loci of all points of the rotating system are circular arcs in this view and yield the same angular displacement for any given angle of retraction. This view also provides an edge-view of the perpendicular bisector planes of Fig. 1, and supplies from elementary geometry the proof of the method used to define the axis of rotation.

The origin of the coordinate system employed may be taken at any convenient point—e.g., at the conventional fuselage reference system origin, or at some translated point, such as the intersection of a perpendicular through the wheel center with the fuselage plane of symmetry. In the practical example solved in the Appendix, this translated origin is established at the center of the wheel retracted (see point A_R of Fig. 3). The justification for this choice will be obvious to the reader.

In the selected system of coordinates the given points are defined as follows:

Center of wheel

$$A_E\colon\ (X_1,\ Y_1,\ Z_1)$$
$$A_R\colon\ (X_2,\ Y_2,\ Z_2)$$

Point on centerline wheel axle

$$B_E\colon\ (X_3,\ Y_3,\ Z_3)$$
$$B_R\colon\ (X_4,\ Y_4,\ Z_4)$$

The next step is the analytic description of planes perpendicular to lines $\overline{A_EA_R}$ and $\overline{B_EB_R}$ at the respective midpoints of the two lines.

Coordinates of the respective midpoints of the two lines are as follows:

$$\text{Line } \overline{A_EA_R}\colon\ \frac{X_1+X_2}{2},\ \frac{Y_1+Y_2}{2},\ \frac{Z_1+Z_2}{2}$$

$$\text{Line } \overline{B_EB_R}\colon\ \frac{X_3+X_4}{2},\ \frac{Y_3+Y_4}{2},\ \frac{Z_3+Z_4}{2}$$

Direction numbers of the two lines are as follows:

$$\text{Line } \overline{A_EA_R}\colon\ (X_1-X_2):(Y_1-Y_2):(Z_1-Z_2)=a_1:b_1:c_1$$

$$\text{Line } \overline{B_EB_R}\colon\ (X_3-X_4):(Y_3-Y_4):(Z_3-Z_4)=a_2:b_2:c_2$$

Then, from elementary analytic geometry, the equation of the plane perpendicular to line $\overline{A_EA_R}$ at its midpoint (plane Γ of Fig. 1) may be written directly as

$$(X_1-X_2)\left(X-\frac{X_1+X_2}{2}\right)+(Y_1-Y_2)\times\left(Y-\frac{Y_1+Y_2}{2}\right)+(Z_1-Z_2)\left(Z-\frac{Z_1+Z_2}{2}\right)=0 \quad (1)$$

and of the plane perpendicular to line $\overline{B_EB_R}$ at its midpoint (plane Σ of Fig. 1) as

$$(X_3-X_4)\left(X-\frac{X_3+X_4}{2}\right)+(Y_3-Y_4)\times\left(Y-\frac{Y_3+Y_4}{2}\right)+(Z_3-Z_4)\left(Z-\frac{Z_3+Z_4}{2}\right)=0 \quad (2)$$

Eqs. (1) and (2), when transposed, rearranged, and simplified, become

$$a_1X+b_1Y+c_1Z=\frac{(X_1-X_2)(X_1+X_2)}{2}+\frac{(Y_1-Y_2)(Y_1+Y_2)}{2}+\frac{(Z_1-Z_2)(Z_1+Z_2)}{2} \quad (3)$$

$$a_2X+b_2Y+c_2Z=\frac{(X_3-X_4)(X_3+X_4)}{2}+\frac{(Y_3-Y_4)(Y_3+Y_4)}{2}+\frac{(Z_3-Z_4)(Z_3+Z_4)}{2} \quad (4)$$

or, more simply,

$$a_1X+b_1Y+c_1Z=\tfrac{1}{2}(X_1^2+Y_1^2+Z_1^2-Z_2^2-Y_2^2-Z_2^2) \quad (5)$$

$$a_2X+b_2Y+c_2Z=\tfrac{1}{2}(X_3^2+Y_3^2+Z_3^2-X_4^2-Y_4^2-Z_4^2) \quad (6)$$

Eqs. (5) and (6), treated as a simultaneous system, define the line of intersection of the two planes, i.e., the required axis of rotation.

A simpler set of equations is obtained by referring to the *direction number* concept of analytic geometry for more convenient slope-intercept description of the axis. Since the axis appears most closely related to the Y-axis in a position sense, a direction number pattern of the type $M_1:1:M_2$ applies,[1] yielding slope-intercept equations as follows:

$$X=M_1Y+B_1$$
$$Z=M_2Y+B_2$$

To achieve this pattern, Z and X are eliminated, respectively, from the simultaneous system consisting of Eqs. (5) and (6), whence

$$X=\frac{b_2c_1-b_1c_2}{\Delta}Y+\frac{c_2p-c_1q}{2\Delta} \quad (7)$$

$$Z=\frac{a_2b_1-a_1b_2}{\Delta}Y+\frac{a_1q-a_2p}{2\Delta} \quad (8)$$

in which $\Delta=a_1c_2-a_2c_1$.

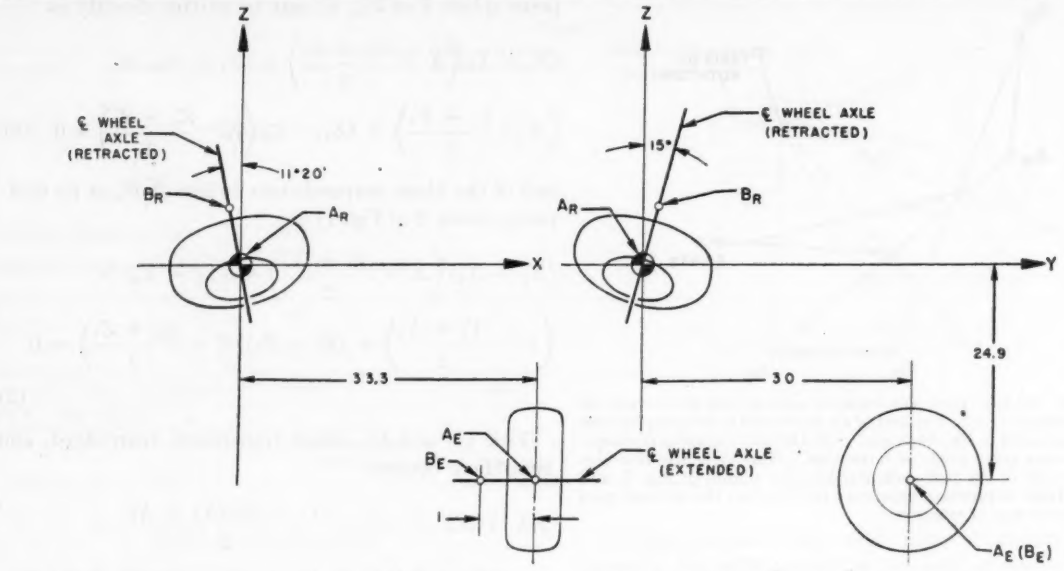

FIG. 3. For illustration convenience, the 1-in. dimension locating the point B_E (or B_R) is applied to exaggerated scale. The designer may desire to apply a slight angle of "toe" to the wheel, thereby modifying the X and Z coordinates of point B_E. Suppose the wheel is rotated counterclockwise (in the front view) about its center (A_E) through an angle α. Then the values $X_3 = X_1 - \cos \alpha$, $Z_3 = Z_1 + \sin \alpha$, used in the chart, will impose this condition upon the kinematics pattern.

$$p = X_1^2 + Y_1^2 + Z_1^2 - (X_2^2 + Y_2^2 + Z_2^2)$$

and

$$q = X_3^2 + Y_3^2 + Z_3^2 - (X_4^2 + Y_4^2 + Z_4^2)$$

CONCLUSIONS

Eqs. (7) and (8) constitute the only working equations[2] required to define absolutely and precisely the axis of rotation. These equations supply immediately the tangent of the angle that the axis of rotation makes with the Y-axis in both the plan and side view, as well as the coordinates (B_1, 0, B_2) of one point on the line. Additional points may be quickly obtained by direct substitution in these linear expressions.

Chart I indicates the small number and complete simplicity of the calculation steps required to secure complete analytic definition of the axis of rotation.

In the example illustrated in Chart 1, based upon an actual design problem, only seven separate calculation steps are required, on a calculator featuring cumulative addition and subtraction of products, to secure the required slopes and intercepts. Only three of these steps are incidental; four out of the seven represent the desired final slope-intercept data defining the axis of rotation.

The mechanical routine of Chart 1 consumes an average of but 10 min. time, a fact easily checked with the data given in the example. Maximum precision may be observed with no additional time required, since it is convenient to use a calculator to the limit of its keyboard, simply by recording more decimal places during the calculation process.

When the four basic points defining the position of the wheel have been set by design, the analytic procedure described above will greatly expedite the preliminary design stage of development, as well as dictate the dimensional specification of the final design, to the complete exclusion of cumbersome, inaccurate graphical procedures.

APPENDIX

The high degree of practicability of the two working equations, Eqs. (7) and (8), is fully demonstrated by the solution given below for the kinematics problem suggested in Fig. 3.

The data shown represent the actual basis for successfully stowing the main wheel of a tricycle gear within the cambered surface of a thin profile, high-speed, laminar-flow wing, the "rigging" of which involved an angle of extreme forward sweep.

Solution: From Fig. 3, the coordinates of points A_E, A_R, and B_E, a point 1 in. inboard along the centerline axle from A_E, may be tabulated directly in the chart.

The coordinates of B_R may be obtained by the following analytic inspection method:

Step 1. Establish from Fig. 3 direction numbers of the centerline axle in the retracted position. If a projection of unity is assumed on the Z-axis, these numbers are

$$-\tan 11^\circ 20' : \tan 15^\circ : 1$$

or

$$-0.200425 : 0.267949 : 1$$

Step 2. Calculate the square root of the sum of the squares of these three numbers. Divide this value into each of the numbers. The resulting quotients are

$$-0.190067 : 0.254101 : 0.948318$$

These values are the direction cosines of the centerline axle retracted; since the point B_R is 1 in. from the origin (A_R), they are likewise the coordinates (X_4, Y_4, Z_4) of the point B_R and are tabulated directly in the chart.

Step 3. Perform the mechanical calculation routine indicated in the chart. (Note that, with A_R as the origin, the expression $X_2^2 + Y_2^2 + Z_2^2$ equals 0 in solving for p; the expression $X_4^2 + Y_4^2 + Z_4^2$ equals 1 in solving for q.)

References

[1] Liming, Roy A., *Practical Analytic Geometry with Applications to Aircraft;* The Macmillan Company, New York, 1944.

[2] Liming, Roy A., *Airfoil Development and Structure Within the Cambered Surface,* Aero Digest, December, 1945; March, April, June, 1946.

Letters to the Editor

Dear Sir:

In the papers "Jet Propulsion and Its Application to High-Speed Aircraft," by D. J. Keirn and D. R. Shoults, JOURNAL OF THE AERONAUTICAL SCIENCES, August, 1946, and "Some Elementary Details of Ramming Intake and Propulsive Jets for Airplanes," by S. A. Moss and W. R. Foote, JOURNAL OF THE AERONAUTICAL SCIENCES, March, 1946, two different interpretations are given for propulsive efficiency although the equations are the same.

In the first paper it is stated that maximum output occurs when $v_i = 2V$, at which point the propulsive efficiency is computed to be 66.7 per cent. Maximum efficiency is stated as occurring when $v_j = V$ where output is zero.

In the second paper one may find a formula for the coefficient of propulsive efficiency which shows that the best speed for an airplane with jet propulsion is infinite.

The question arises whether a definition that gives maximum efficiency when the output is zero or one that permits efficiencies to become greater than 100 per cent is logical from a physical standpoint.

Probably in no other branch of engineering are there so many definitions for one and the same coefficient as there are in this case. It is proposed to present here the derivation of a formula for the propulsive efficiency which is logical from a physical standpoint and is not subject to the criticisms that have been made above.

The general expression for an efficiency is:

$$\eta = \text{output/input} \tag{1}$$

In our case we may state more in detail that η is the ratio of the energy imparted to the body to that of the maximum possible amount of energy available at our disposal in the system considered.

The mass of fuel utilized per second, W_f/g, possesses, just before the combustion process starts, a certain heat content that enables it to propel the jet unit at a momentarily constant forward velocity, V. In the thermal jet, sufficient air pressure must be built up at the entrance to the combustion chamber to force the exhaust jet to discharge to the rear. Assume that the mass of air has a negligible velocity with respect to the propelled unit as it enters the combustion chamber. The heat content, or chemical potential energy, will then be used to accelerate the mass of air and fuel from zero velocity with respect to the propelled unit to the jet exhaust velocity, v_j. Thus

$$L_1 = [(W_a + W_f)/2g]v_j^2 \tag{2}$$

where L_1 is the kinetic energy input to the jet from the chemical potential energy and is dependent on the thermal efficiency conditions whereby the chemical potential energy is converted into kinetic energy of the jet. In our discussion we assume the coefficient of thermal efficiency to be equal to 1.

But the chemical potential energy is not the only energy that the fuel has. Because of the forward velocity of the propelled unit, V, the fuel also contains kinetic energy equal to:

$$L_2 = (W_f/2g)V^2 \tag{3}$$

Thus the maximum energy that can be imparted to the jet unit as input under the most favorable conditions is:

$$\text{Input} = L_1 + L_2 \tag{4}$$

Since output can be expressed as input minus the losses, consideration will now be given to the inherent losses in a jet propulsion unit.

Mention has been made of the necessity of bringing the air to rest at the entrance to the combustion chamber. The work done in compressing this air is chargeable to the thermal efficiency. The kinetic energy of the entering air relative to the propelled body

$$L_3 = (W_a/2g)V^2 \tag{5}$$

is a loss of kinetic energy as far as the propulsive jet is concerned. It is true that it is converted to potential energy in the form of pressure and tends to improve the thermal efficiency of the unit, but from the standpoint of the total balance of kinetic energy it is a loss.

Similarly, the kinetic energy of the jet with respect to the propelled unit differs from the kinetic energy with respect to the ground assumed as the reference system. This reduces the effective output of the jet by the amount:

$$L_4 = [(W_a + W_f)/2g](v_j - V)^2 \tag{6}$$

L_4 is usually called the kinetic energy of the exhaust gases. Expressing the output of the jet as the input minus the losses gives:

$$\text{Output} = L_1 + L_2 - L_3 - L_4 = \left[\left(\frac{W_a + W_f}{g}\right)v_j - \left(\frac{W_a}{g}\right)V\right]V \tag{7}$$

The reactional force of the outflowing gases is equal to:

$$F = \frac{L}{V} = \left(\frac{W_a + W_f}{g}\right)v_j - \left(\frac{W_a}{g}\right)V \tag{8}$$

If the instantaneous coefficient of the propulsive efficiency η_p of a jet propulsion unit is to be defined as output divided by input, we have:

$$\eta_p = \frac{L}{(L_1 + L_2)} = \frac{2[(W_a + W_f)v_j - W_a V]V}{[(W_a + W_f)v_j^2 + W_f V^2]} \tag{9}$$

For W_a = const., W_f = const., v_j = const., we obtain from $(d\eta_p/dV) = 0$,

$$\eta_{pmax.} = (W_a + W_f)/[W_a + (W_a^2 + W_a W_f + W_f^2)^{1/2}] \tag{10}$$

for

$$v_j = [W_a + (W_a^2 + W_a W_f + W_f^2)^{1/2}]V/(W_a + W_f) \tag{11}$$

These formulas may be transformed for two extreme cases:

(a) Pure rocket, i.e., without taking the air from outside:

$$W_a = 0, \quad F = \left(\frac{W_f}{g}\right)v_j, \quad P = \left(\frac{W_f}{g}\right)v_j V \tag{12}$$

$$\eta_p = 2Vv_j/(V^2 + v_j^2) \tag{13}$$

$$\eta_{pmax.} = 1 \text{ for } V = v_j, \quad P_{max.} = \left(\frac{W_f}{g}\right)v_j^2 = (L_1 + L_2) \tag{14}$$

where P denotes the energy output.

(b) Neglect the mass of the fuel:

$$W_f = 0, \quad F = \frac{W_a}{g}(v_j - V), \quad P = \frac{W_a}{g}(v_j - V)V \tag{15}$$

$$\eta_p = 2(v_j - V)V/v_j^2 \tag{16}$$

$$\eta_{pmax.} = 1/2, \text{ for } v_j = 2V \text{ or } V = v_j/2, \quad P_{max.} = \frac{W_a}{g}\left(\frac{v_j}{2}\right)^2 = L_{1/2} \tag{17}$$

The result is that the coefficient of the propulsive efficiency in the case (b) cannot be equal to 1. The coefficient η_p represents well the real conditions. For $V = 0$, $P = \eta_p = 0$ because the body is at rest and one cannot talk about a "propulsive" efficiency. It has a maximum value of 0.5 for $V = v_j/2$ (v_j is assumed to be constant) when P achieves its maximum value. It is equal to zero for $V = v_j$—i.e., where the momentum at the entrance and at the exit is equal.

Similarly, the value of the power P, cannot ever utilize the entire kinetic energy of the jet $(W_a/2g)v_j^2$, since maximum P is equal to $(W_a/g)(v_j/2)^2$.

Let us point out that the above definition of the instantaneous coefficient of the propulsive efficiency represents the useful percentage of the total power without ambiguity. In the papers cited above the coefficient η_p is given identically by the ratio:

$$\eta_p = \frac{(W_a/g)(v_j - V)V}{(W_a/2g)(v_j^2 - V^2)} = \frac{2V}{(v_j + V)} \tag{18}$$

From this identical equation in one paper it is concluded that maximum efficiency occurs when $v_j = V$ where output is zero and that for the maximum output $v_j = 2V$ and $\eta_p = 66.7$ per cent. (Actually, the maximum output is equal to

$$(W_a/g)(v_j/2)^2 = (L_1/2)$$

with $W_f = 0$ in Eq. (1), (2), and η_p is 50 per cent and not 66.7 per cent.) In the other paper, after some transformations, it is concluded that the best speed for an airplane with jet propulsion is infinite and that the propulsive efficiency is equal to 1 when $v_j = V$ and the thrust and the net power used to drive the airplane are both equal to zero. One may ask what this "propulsive" efficiency represents if it is not equal to zero and both the propulsive force and propulsive power are equal to zero. Thus, for the same coefficient that should represent to a certain extent the useful power, we have interpretations that represent anything else but the useful power.

Undoubtedly, the best speed of an airplane occurs when the optimum value of the useful power may be achieved. A simple differentiation of the expression for the useful power (performed by Mr. Keirn and Mr. Shoults) shows that the maximum occurs for $v_j = 2V$. Hence, this is the best speed. The ambiguity in both cited papers has its origin in the fact that all the authors consider the losses only in the form of the energy of jet discharge gases. (The above derivation of the instantaneous coefficient of the propulsive efficiency appeared in the paper "Optimum Height of Flight of Winged Rocket- or Jet-Bomb," by M. Z. Krzywoblocki, *Journal of Applied Physics*, Vol. 16, No. 5, pp. 275–279, May, 1945, and in other magazines.)

M. Z. Krzywoblocki
R. W. McCloy
Associate Professors
Department of Aeronautical Engineering
College of Engineering
University of Illinoi

Dear Sir:

I should like to make a few comments on the paper "On the Steady Flow of a Gas Through a Tube with Heat Exchange or Chemical Reaction" by Paul Chambré and Chia-Chiao Lin which appeared in the *Journal* of October, 1946.

(1) The interesting conclusion is reached that, in the steady, frictionless, nonadiabatic flow of a compressible fluid through a channel of constant cross section, the temperature of the fluid is reduced by the addition of heat to the fluid for Mach Numbers between $1/\sqrt{\gamma}$ and 1. This same result was obtained by the writer some years ago, but it was not published. It was also obtained and published[1] by Dr. Bruce L. Hicks of the Cleveland laboratory of the N.A.C.A.

A slight extension of the analysis and a figure can considerably clarify the physical picture of the phenomenon. Conservation of energy is expressed by Eq. (5) of the reference paper. By the use of Eqs. (1), (4), and (14) and the relation

$$dp/p = (d\rho/\rho) + (dT/T)$$

Eq. (5) can be rewritten as

$$dQ = c_v dT + (c_p - c_v)dT + u du = dU + dW + dE$$

where U = internal energy per unit mass, W = flow work done by unit mass, E = kinetic energy per unit mass, and other symbols are as in the reference paper.

For $dn = 0$, Eq. (22) becomes

$$dT/T = [(1 - \gamma M^2)/(1 - M^2)](dQ/H)$$

or, by use of $H = c_p T$,

$$dH/dQ = (1 - \gamma M^2)/(1 - M^2)$$

It can then easily be shown that

$$dE/dQ = (\gamma - 1)M^2/(1 - M^2) \tag{a}$$

$$dU/dQ = (1/\gamma)[(1 - \gamma M^2)/(1 - M^2)] \tag{b}$$

$$dW/dQ = [(\gamma - 1)/\gamma][(1 - \gamma M^2)/(1 - M^2)] \tag{c}$$

Heat energy that is added to the fluid is therefore divided, in the proportions given by Eqs. (a) to (c), among a change in kinetic energy of directed motion along the pipe, a change in kinetic energy of random motion, and a change in flow work or pumping work. The proportional division of the heat energy among these

(*Continued on page 63*)

Exact and Approximate Solutions of Two-Dimensional Oblique Shock Flow

EDMUND V. LAITONE*

Cornell Aeronautical Laboratory

SUMMARY

This paper contains a simplified presentation of the exact and approximate solutions of supersonic flow over two-dimensional bodies. The data are all presented as a variation with the free stream Mach Number, thereby enhancing their usefulness. An exact solution is given for the maximum flow deflection that can be obtained by means of an oblique shock wave at a given Mach Number. The third and higher terms are presented for the infinite series approximating oblique shock flow. The third term obtained is not the same as that originally given by Busemann in 1935 at the Fifth Volta Congress. The new third term is analyzed to show that under certain conditions an oblique shock flow may be considered isentropic even though the third order of the flow deflection or pressure discontinuity is not negligible. A reliable graphical method is presented whereby the pressure distribution may be quickly and accurately obtained for a two-dimensional body in a supersonic flow field.

INTRODUCTION

THE PERIOD has passed when supersonic flow was merely of theoretical interest to aeronautical engineers. Supersonic wind tunnels are used extensively and designs for supersonic aircraft are being planned.

This paper is a summary of the problems of two-dimensional supersonic flow, an extremely important field, since it can be shown that in some cases the flow over an entire wing in supersonic flight may be considered two dimensional.

All of the computations are based on a γ value of seven-fifths or 1.400. The author's reasons for this selection have been previously stated[1] and are in agreement with the recent evaluations by Keenan and Kaye[2] based on existing spectroscopic data for the constituents of dry air. The thermodynamic derivations are based on the perfect gas relation $p/\rho = RT$ and the assumption that the heat transfer is negligible and the processes are adiabatic. The additional assumptions made in the analysis of shock flow are that the conditions are everywhere uniform ahead of the shock wave, that the equation of conservation of momentum may be directly applied to a stream tube passing through the discontinuity forming the shock wave, and that the loss in kinetic energy through the shock wave appears as heat energy that may be directly measured as an increase in enthalpy. The flow through the shock wave is then an irreversible adiabatic process leading to an increase in entropy.

The standard exact and approximate solutions of two-dimensional supersonic flow problems are extended to larger flow deflections and higher Mach Numbers. The results are made more useful by being presented as a variation with the free stream Mach Number. A graphical method is presented which will quickly and accurately determine the pressure distribution about a two-dimensional body in a supersonic flow field. This method immediately shows whether or not a known solution exists for any portion of the body as long as the surface considered is inclined at less than 15° to the free stream velocity vector. In addition, the method quickly determines a suitable profile shape for any given physically possible pressure distribution.

SYMBOLS

a = local rate of pressure propagation and local velocity of sound = $\sqrt{\gamma p/\rho}$, (ft. per sec.)

C_p = specific heat at constant pressure = 6,007.1, (ft. per sec.)^2/(°F.)

C_v = specific heat at constant volume or constant density = 4,290.8, (ft. per sec.)^2/(°F.)

h = enthalpy = $h_0 + \left(C_vT + \frac{p}{\rho}\right)\Big]_0 = h_0 + (C_pT)\Big]_0 = h_0 + \left(\frac{\gamma}{\gamma - 1}\frac{p}{\rho}\right)\Big]_0$, (ft. per sec.)^2

H = stagnation or total absolute pressure, (lb. per sq.ft.)

M = Mach Number = V/a

$M_{1min.}$ = minimum Mach Number for existence of oblique shock

p = absolute static pressure, (lb. per sq.ft.)

P = pressure coefficient = $(p - p_0)/{}^1\!/_2\rho_0V_0^2$

R = gas constant = $(C_p - C_v)$ = (53.345)(32.174) = 1,716.3, (ft. per sec.)^2/(°F.)

S = entropy = $S_0 + C_v \log\left(\frac{p/\rho^\gamma}{p_0/\rho_0^\gamma}\right)$, $\frac{\text{(ft. per sec.)}^2}{\text{(°F.)}}$

T = absolute Rankine temperature = (°f + 459.69) = (°F.)

u = velocity component normal to shock, (ft. per sec.)

v = velocity component parallel to shock, (ft. per sec.)

V = magnitude of resultant velocity vector, (ft. per sec.)

γ = isentropic gas constant = C_p/C_v = 7/5

θ_s = angle of stream tube deflection or angle of velocity vector behind shock ($\vec{V}_2$) relative to velocity vector upstream of shock ($\vec{V}_1$), rad.

$\theta_{s_{max.}}$ = maximum possible angle of stream tube deflection for a given free stream Mach Number, rad.

Presented at the Aerodynamics Session of the Fourteenth Annual Meeting, I.A.S., New York, January 29–31, 1946.

* Section Head of Flight Research Engineering.

θ_w = angle made by shock wave relative to velocity vector upstream of shock ($\bar{V}_1$), rad.

ρ = mass density = (lb. sec.^{2}/ft.^{4})

Subscripts

0 = free stream conditions at an infinite distance upstream

1 = conditions in uniform parallel flow upstream of shock wave which are equivalent to the free stream conditions at infinity

2 = conditions in uniform parallel flow behind or downstream of shock wave

H = conditions at stagnation point where the velocity is zero

Isentropic Flow

In the first section the equations for isentropic or reversible adiabatic flow will be developed. Although this is an irrotational frictionless flow with no head loss, it is necessary for a study of oblique shock waves since the flow is isentropic on either side of the extremely thin discontinuity sheet defining the shock wave. It will also be shown that even for angles of flow deflection of 15° the flow is approximately isentropic across the shock discontinuity.

The energy equation, neglecting gravity and other extraneous effects, is

$$V^2/2 + h = \text{const.} \tag{1}$$

This expression of constant energy is true for any heat insulated flow; that is, it holds for any adiabatic flow whether it is reversible (isentropic) or irreversible (friction losses) as long as there is no heat transfer to the fluid and the heat produced by any friction losses remains in the fluid.

For a reversible adiabatic or isentropic flow the enthalpy may be simply expressed as

$$h_1 - h_0 = \int_0^1 dp/\rho \tag{2}$$

Then the energy equation for isentropic flow becomes

$$(V_0^2/2) + \int^0 dp/\rho = (V_1^2/2) + \int^1 dp/\rho \tag{3}$$

Because of the fact that the entropy is constant, the pressure and density are explicitly related by

$$p/\rho^\gamma = \text{const.} \tag{4}$$

and, since $p/\rho T$ is constant for a perfect gas, the physical states are related as follows:

$$\frac{p_2}{p_1} = \left(\frac{\rho_2}{\rho_1}\right)^\gamma = \left(\frac{T_2}{T_1}\right)^{\gamma/(\gamma-1)} = \left(\frac{a_2^2}{a_1^2}\right)^{\gamma/(\gamma-1)} \tag{5}$$

Consequently, if only the relations at the end points of an isentropic flow process are desired, Eqs. (3) and (4) may be combined directly in the form

$$\frac{V_0^2}{2} + \frac{\gamma}{\gamma-1}\frac{p_0}{\rho_0} = \frac{V_1^2}{2} + \frac{\gamma}{\gamma-1}\frac{p_1}{\rho_1}$$

Or, more generally, it may be stated that throughout the entire field of isentropic flow

$$\frac{V^2}{2} + \frac{\gamma}{\gamma-1}\frac{p}{\rho} = \text{const.} \tag{6}$$

For zero velocity the stagnation or total pressure H, is obtained, and therefore

$$\frac{V^2}{2} + \frac{\gamma}{\gamma-1}\frac{p}{\rho} = \frac{\gamma}{\gamma-1}\frac{H}{\rho_H} = \frac{V_0^2}{2} + \frac{\gamma}{\gamma-1}\frac{p_0}{\rho_0} \tag{7}$$

where H is constant as long as the flow is isentropic. This may be written as

$$\frac{V^2}{2} + \frac{a^2}{\gamma-1} = \frac{a_H^2}{\gamma-1} = \frac{V_0^2}{2} + \frac{a_0^2}{\gamma-1} \tag{8}$$

Therefore, the Mach Number may be written as

$$M = \frac{V}{a} = \sqrt{\frac{2}{\gamma-1}\left(\frac{a_H^2}{a^2} - 1\right)}$$

or from Eq. (5)

$$M = \sqrt{\frac{2}{\gamma-1}\left[\left(\frac{H}{p}\right)^{(\gamma-1)/\gamma} - 1\right]} = \sqrt{5\left[\left(\frac{H}{p}\right)^{2/7} - 1\right]} \tag{9}$$

Fig. 1 shows the variation of p/H with Mach Number as obtained from Eq. (9).

The following useful relations for the static pressure may be obtained from Eqs. (5) and (7)

$$p = p_0\left[1 - \frac{\gamma-1}{2}M_0^2\left(\frac{V^2}{V_0^2} - 1\right)\right]^{\gamma/(\gamma-1)} =$$

$$H\left[1 - \frac{\gamma-1}{2}\left(\frac{V^2}{a_H^2}\right)\right]^{\gamma/(\gamma-1)} = H\left[1 + \frac{\gamma-1}{2}M^2\right]^{-\gamma/(\gamma-1)}$$

$$= p_0\left(\frac{\rho}{\rho_0}\right)^\gamma = H\left(\frac{\rho}{\rho_H}\right)^\gamma = p_0\left(\frac{T}{T_0}\right)^{\gamma/(\gamma-1)} = H\left(\frac{T}{T_H}\right)^{\gamma/(\gamma-1)} \tag{10}$$

Eqs. (9) and (10) apply to either subsonic or supersonic flow as long as there are no shock waves in the region being considered. For subsonic flow the determination of the local velocity or pressure is difficult since the flow depends not only on the conditions the stream tubes have passed but also upon the conditions everywhere ahead of the stream tubes. This is so because the partial differential equation of subsonic flow is of the elliptic type, which has no real characteristic values. Consequently, the boundary values everywhere in the flow field (including infinity) to some extent influence all the flow. The problem is comparatively simpler for supersonic flow since, in this case, the partial differential equation governing the flow is of the hyperbolic type, which does have real characteristics.[3,4] These characteristics are the Mach lines, which are defined explicitly by the local Mach Number (M) and are straight lines inclined backward at the angle $\sin^{-1}(1/M)$ to the local velocity vector. The velocity component normal to the characteristic or Mach line is always equal to the local speed of sound (α). The physical significance of these charac-

teristics is that all disturbances in the flow field are propagated along them; that is, the characteristics are the envelopes produced by sound waves moving at the local speed of sound. A discontinuity, generally called a limit line, develops whenever these characteristics intersect and most shock waves may be defined as the envelope formed by these intersecting characteristics. In general, nothing occurring downstream of a characteristic can directly influence the flow field upstream of the characteristic.

The remarkable advantage resulting from the existence of these characteristics for isentropic supersonic flow computation is that as long as no discontinuities or shock waves are formed, the pressure and velocity changes depend only upon the angle the stream tube is deflected (θ_s) and the free stream Mach Number (M_0). Consequently, any given solution for the pressure change due to a stream tube deflection at a given free stream Mach Number may be applied to any other isentropic supersonic flow as long as the initial and final angles of flow are known. The simplest solution for isentropic flow is the particular case of free expansion around a sharp corner. Then the rate of expansion is the maximum physically possible and the characteristics or Mach lines become radii originating from the sharp corner;[5] consequently, the velocity component normal to any of these radii is always equal to the local speed of sound, and along a given radius the velocity, pressure, and density are constant.[5] The equation for irrotational supersonic flow expansion ($-\theta_s$) starting from a free stream Mach Number of unity is then

$$-\theta_s = \left[\sqrt{\frac{\gamma+1}{\gamma-1}}\left\{\frac{1}{2}\cos^{-1}\left[(\gamma+1)\left(\frac{p}{H}\right)^{(\gamma-1)/\gamma}-1\right]\right\}-\tan^{-1}\sqrt{\frac{\gamma+1}{\gamma-1}}\tan\left\{\frac{1}{2}\cos^{-1}\left[(\gamma+1)\left(\frac{p}{H}\right)^{(\gamma-1)/\gamma}-1\right]\right\}\right]$$

The values obtained are given in Table 1.

The numerical evaluation for any other supersonic isentropic flow may now be obtained by reading θ_s as the difference in Table 1 from the θ_s value corresponding to the given free stream Mach Number. A compression would correspond to a positive flow deflection ($+\theta_s$) while an expansion corresponds to a negative flow deflection ($-\theta_s$). In applying the solution to a given surface, however, there are three conditions that can invalidate the results. Since the isentropic expansion given in Table 1 is the most rapid physically possible, the flow would leave a given surface and continue exactly as in Table 1 as a free expansion if the magnitude of the negative surface deflection were greater than the corresponding value given in Table 1. The other two limitations are for supersonic compression. The flow must not become subsonic from too great a compression. The rate of surface deflection must not be large enough to make the characteristics intersect so near to the surface that the resultant shock wave would affect the surface pressures.[5]

TABLE 1
Values for Isentropic Expansion Around a Sharp Corner
Two-Dimensional Flow
$\gamma = 7/5$

P/H	$-\theta_s°$	M
0.5283	0	1
0.5	0.437	1.046
0.45	1.986	1.132
0.4	4.139	1.223
0.35	6.789	1.322
0.3	9.935	1.433
0.2724	11.87	1.500
0.25	13.65	1.559
0.2026	17.81	1.700
0.2	18.06	1.709
0.15	23.49	1.897
0.12	27.44	2.040
0.1	30.53	2.157
0.08	34.28	2.300
0.06	38.75	2.484
0.05	41.45	2.601
0.04	44.62	2.746
0.03	48.50	2.935
0.02722	49.75	3.000
0.02	53.61	3.208
0.015	57.00	3.406
0.01	61.49	3.693
0.005	68.45	4.210
0.001	81.77	5.566
0.0005	86.51	6.234
2.356×10^{-4}	102.32	10
1.278×10^{-4}	121.23	30
2.790×10^{-11}	127.59	100
0	130.45	∞

When the values in Table 1 are plotted in the manner shown in Fig. 1, all three of the previous objections are automatically considered for any given problem. For example, the θ_s scale is also shown in Fig. 1 for any isentropic flow starting from a free stream Mach Number of 1.5. Then if the negative surface deflection for free expansion is greater than 118.6° the Mach Number becomes infinite, showing that the flow has left the surface and has continued as a free expansion. If the positive surface deflection is greater than 11.87° then the Mach Number becomes less than unity, showing that the solution is invalid.

So far the solution is exact for any flow expansion and for extremely small flow compressions. The solution is also exact for the particular case of large flow compressions where the characteristics or Mach lines do not intersect. However, it will be shown later that even when the Mach lines do intersect and form shock waves, Fig. 1 still gives a good approximation to the flow pressures for positive surface changes of less than 15° since the flow is still approximately isentropic. If shock waves are then admitted to the solution another difficulty arises. If $+\theta_s$ is greater than $\theta_{s_{max.}}$ (Appendix I), there is a standing shock wave upstream of the surface producing mixed subsonic and supersonic flow behind the shock wave and over the surface. However, in Appendix I it is shown that for

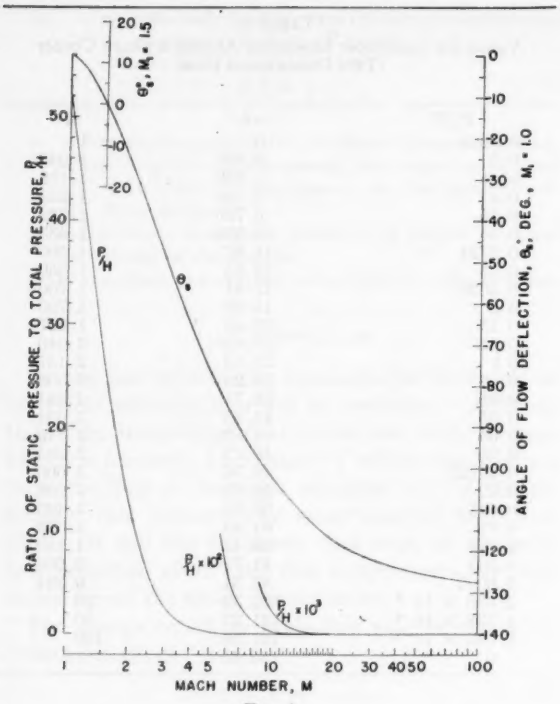
RATIO OF STATIC PRESSURE TO TOTAL PRESSURE, $\frac{p}{H}$
ANGLE OF FLOW DEFLECTION, θ_s°, DEG., $M_1 = 1.0$
θ_s°, $M_1 = 1.5$
$\frac{p}{H}$
θ_s
$\frac{p}{H} \times 10^2$
$\frac{p}{H} \times 10^3$
MACH NUMBER, M

FIG. 1.

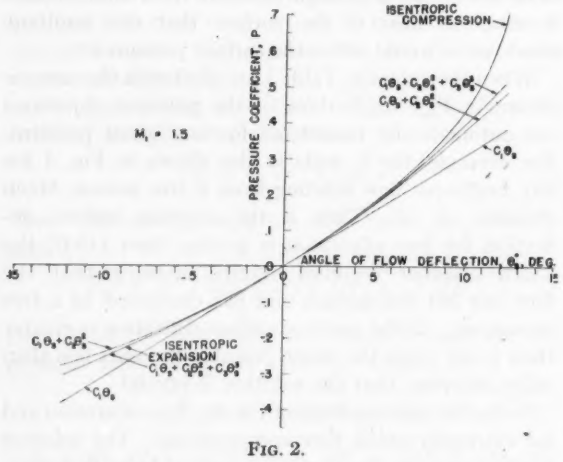

FIG. 2.

any $+\theta_s^\circ$ less than 15° the use of Fig. 1 will automatically yield a subsonic Mach Number if the standing wave exists in front of the surface. Consequently, Fig. 1 not only provides an extremely rapid solution for supersonic flow problems now solved by existing methods but it is also remarkably reliable.

The pressure change for a given flow deflection may be obtained from Fig. 1 by

$$\frac{p_2}{p_1} = \frac{p_2/H}{p_1/H}$$

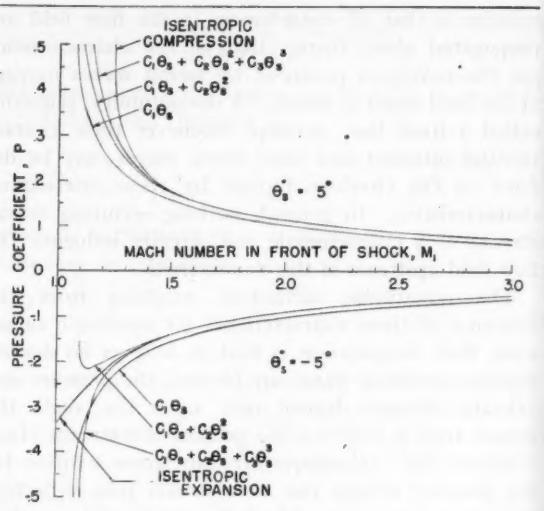

FIG. 3.

and the pressure coefficient P may be computed as

$$P = \frac{p_2 - p_1}{{}^1/_2\rho_1 V_1^2} = \frac{1}{(\gamma/2)M_1^2}\left(\frac{p_2}{p_1} - 1\right) \qquad (11)$$

or for isentropic flow

$$P = \frac{1}{(\gamma/2)M_1^2}\left(\left\{\frac{1 + [(\gamma-1)/2]M_1^2}{1 + [(\gamma-1)/2]M_2^2}\right\}^{\gamma/(\gamma-1)} - 1\right)$$

Fig. 2 shows the variation of the pressure coefficient with a given stream tube deflection starting from a free stream Mach Number of 1.5. Fig. 3 shows the effect of the initial free stream Mach Number on the pressure coefficient produced by a stream tube deflection of 5°.

The approximation to the isentropic solution as found by Busemann[6] yields

$$P = C_1\theta_s + C_2\theta_s^2 + C_3\theta_s^3 + \ldots\ldots \qquad (12)$$

where

$$C_1 = \frac{2}{(M_1^2 - 1)^{1/2}},\quad C_2 = \frac{[(\gamma+1)/2]M_1^4 - 2M_1^2 + 2}{(M_1^2 - 1)^2}$$

$$C_3 = \frac{1}{(M_1^2 - 1)^{7/2}}\left[\frac{(\gamma+1)}{4}M_1^8 - \frac{(-2\gamma^2 + 7\gamma + 5)}{4}M_1^6 + \frac{(4\gamma^4 - 28\gamma^3 + 109\gamma^2 + 230\gamma + 105)}{48(\gamma+1)}M_1^4 - 2M_1^2 + \frac{4}{3}\right]$$

and the pressure coefficients obtained from these terms are also shown in Figs. 2 and 3.

The first term $C_1\theta_s$ is simply the tangent to the isentropic solution and is the linear approximation. The addition of the second term $C_2\theta_s^2$ takes into account the curvature of the isentropic solution, and

yields the parabolic approximation. The addition of the third term $C_0\theta_s^3$ considers the rate of change of curvature of the isentropic solution and for $M > 1.3$ gives a good approximation even for large $-\theta_s$ values (isentropic expansion) and gives a good approximation for $+\theta_s$ (isentropic compression) up to about 5°. These approximations are extremely useful for analytical solutions. For small surface deflections, general conclusions for supersonic airfoils have been obtained by formally integrating the expression obtained from the first two terms over the airfoil surface.[4–6]

Oblique Shock Waves

The equations for two-dimensional supersonic oblique and normal shock flow will now be developed. These relations were discovered by Rankine, Hugoniot, and Meyer, and although they are available in many standard references[3–5] they will be presented here in a form more suitable for actual numerical computations.

Fig. 4 shows the oblique shock wave discontinuity with an abrupt change in pressure and velocity. The conditions of uniform parallel flow prevail on each side of the discontinuity sheet or shock wave. Although the previous characteristic solution for isentropic supersonic flow could exist for any positive or negative θ_s, the oblique shock wave exists only for a finite positive θ_s; that is, only for an abrupt flow compression accompanied by an increase in entropy.[5]

The momentum equation applied to the flow normal to the discontinuity yields

$$\rho_1 u_1^2 + p_1 = \rho_2 u_2^2 + p_2 \tag{13}$$

The continuity equation for the flow normal to the discontinuity is

$$\rho_1 u_1 = \rho_2 u_2 \tag{14}$$

The momentum equation for the flow tangential to the discontinuity is

$$(\rho_1 u_1) v_1 = (\rho_2 u_2) v_2$$

and comparison with Eq. (14) shows that necessarily

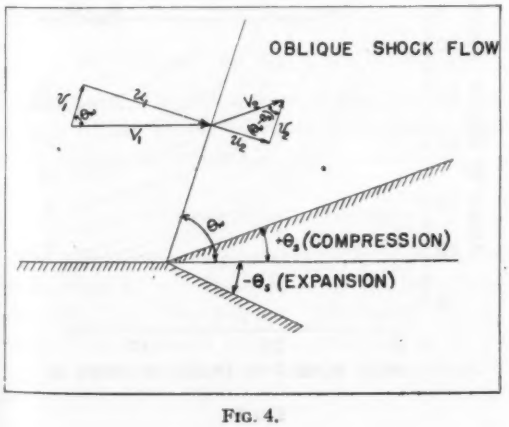

Fig. 4.

$$v_1 = v_2 = v \tag{15}$$

The energy equation, Eq. (1), becomes

$$\frac{u_1^2 + v^2}{2} + h_1 = h_H = \frac{u_2^2 + v^2}{2} + h_2 \tag{16}$$

or

$$(u_1^2/2) + h_1 = (u_2^2/2) + h_2 \tag{17}$$

In addition, for any perfect gas

$$\frac{p}{\rho}\Big]_1^2 = RT\Big]_1^2 = (\gamma - 1)C_v T\Big]_1^2 = \left(\frac{\gamma - 1}{\gamma}\right)C_p T\Big]_1^2 = \left(\frac{\gamma - 1}{\gamma}\right)h\Big]_1^2$$

Therefore, Eqs. (16) and (17) become

$$\frac{V_1^2}{2} + \frac{\gamma}{\gamma - 1}\frac{p_1}{\rho_1} = \frac{\gamma}{\gamma - 1}\frac{H_1}{\rho_{H1}} = C_p T_H = \frac{\gamma}{\gamma - 1}\frac{H_2}{\rho_{H2}} = \frac{V_2^2}{2} + \frac{\gamma}{\gamma - 1}\frac{p_2}{\rho_2} \tag{18}$$

$$\frac{u_1^2}{2} + \frac{\gamma}{\gamma - 1}\frac{p_1}{\rho_1} = \frac{u_2^2}{2} + \frac{\gamma}{\gamma - 1}\frac{p_2}{\rho_2} \tag{19}$$

Eq. (18) shows that the stagnation temperature (T_H) must be the same on both sides of the discontinuity. It is interesting to note that Eq. (18) is identical in form to Eq. (7). However, it will be shown that the following inequalities are associated with Eq. (18)

$$\left(\frac{p_2}{\rho_2^\gamma}\right) > \left(\frac{p_1}{\rho_1^\gamma}\right), \quad H_2 < H_1$$

while for Eq. (7) these quantities must both be equal in order that Eq. (5) may be used. This means that for isentropic flow, the pressure or density is determined explicitly from Eqs. (5) and (7), while some additional relation between the pressure and density is required for the adiabatic flow process before Eq. (18) can provide a complete solution.

For example, if we take an adiabatic flow with a head loss but with the additional restriction that the local static pressure (p_2) has returned to the original free stream static pressure (p_0) then

$$p_2 = p_0, \quad \frac{\rho_0}{\rho_2} = \frac{T_2}{T_0} = \frac{a_2^2}{a_0^2}$$

Also, Eq. (18) may be written identical to Eq. (8) as

$$\frac{V_0^2}{2} + \frac{a_0^2}{\gamma - 1} = \frac{a_H^2}{\gamma - 1} = \frac{V_2^2}{2} + \frac{a_2^2}{\gamma - 1}$$

Consequently, for $p_2 = p_0$ and $H_2 \neq H_0$

$$\frac{a_2^2}{a_0^2} = \frac{\rho_0}{\rho_2} = \left[1 - \frac{\gamma - 1}{2}M_0^2\left(\frac{V_2^2}{V_0^2} - 1\right)\right] = \left\{\frac{1 + [(\gamma - 1)/2]M_0^2}{1 + [(\gamma - 1)/2]M_2^2}\right\}$$

From Eq. (10) an analogous expression for isentropic flow with

$$p_2 \neq p_0,\ H_2 = H_0$$

may be written as

$$\left(\frac{p_0}{p_2}\right)^{1/\gamma} = \left(\frac{a_0^2}{a_2^2}\right)^{1/(\gamma-1)} = \frac{\rho_0}{\rho_2} = \left[1 - \frac{\gamma-1}{2} M_0^2 \left(\frac{V_2^2}{V_0^2} - 1\right)\right]^{-1/(\gamma-1)} = \left\{\frac{1 + [(\gamma-1)/2]M_0^2}{1 + [(\gamma-1)/2]M_2^2}\right\}^{-1/(\gamma-1)}$$

Of course, the latter relations for isentropic flow all reduce to unity when $p_2 = p_0$. The comparison simply serves to emphasize that Eqs. (3) and (5) must be used only for isentropic flow.

For adiabatic shock flow with a head loss and entropy increase, the pressure and density relation may be obtained directly from Eqs. (13), (14), and (19) by eliminating u_1 and u_2

$$\left.\begin{aligned} \frac{\rho_2}{\rho_1} &= \frac{[(\gamma+1)/(\gamma-1)](p_2/p_1) + 1}{[(\gamma+1)/(\gamma-1)] + (p_2/p_1)} = \frac{6(p_2/p_1)+1}{6 + (p_2/p_1)} \\ \frac{p_2}{p_1} &= \frac{[(\gamma+1)/(\gamma-1)](\rho_2/\rho_1) - 1}{[(\gamma+1)/(\gamma-1)] - (\rho_2/\rho_1)} = \frac{6(\rho_2/\rho_1) - 1}{6 - (\rho_2/\rho_1)} \end{aligned}\right\} \quad (20)$$

The isentropic flow equation, Eq. (4), is compared with the shock flow equation, Eq. (20), in Fig. 5.

From Fig. 4 and Eqs. (14) and (15)

$$\frac{\tan\theta_w}{\tan(\theta_w - \theta_s)} = \frac{u_1/v_1}{u_2/v_2} = \frac{u_1}{u_2} = \frac{\rho_2}{\rho_1} \quad (21)$$

Therefore

$$\left(1 - \frac{\rho_1}{\rho_2}\right) = \frac{\sin\theta_s}{\sin\theta_w \cos(\theta_w - \theta_s)}, \left(\frac{\rho_2}{\rho_1} - 1\right) = \frac{\sin\theta_s}{\cos\theta_w \sin(\theta_w - \theta_s)} \quad (22)$$

Also from Fig. 4

$$\left.\begin{aligned} u_1 &= V_1 \sin\theta_w = a_1 M_1 \sin\theta_w \\ u_2 &= V_2 \sin(\theta_w - \theta_s) = a_2 M_2 \sin(\theta_w - \theta_s) \end{aligned}\right\} \quad (23)$$

The pressure discontinuity may now be evaluated by combining Eqs. (13) and (14) in the following manner:

$$p_2 - p_1 = \rho_1 u_1^2 \left(1 - \frac{\rho_1}{\rho_2}\right) = \rho_2 u_2^2 \left(\frac{\rho_2}{\rho_1} - 1\right) \quad (24)$$

Then Eqs. (22) and (23) may be used to eliminate u_1 and ρ_2 from Eq. (24)

$$p_2 - p_1 = \rho_1 V_1^2 \frac{\sin\theta_w \sin\theta_s}{\cos(\theta_w - \theta_s)} = \frac{\rho_1 V_1^2}{1 + \cot\theta_w \cot\theta_s} \quad (25)$$

The velocity discontinuity may also be obtained by combining Eqs. (20) and (24)

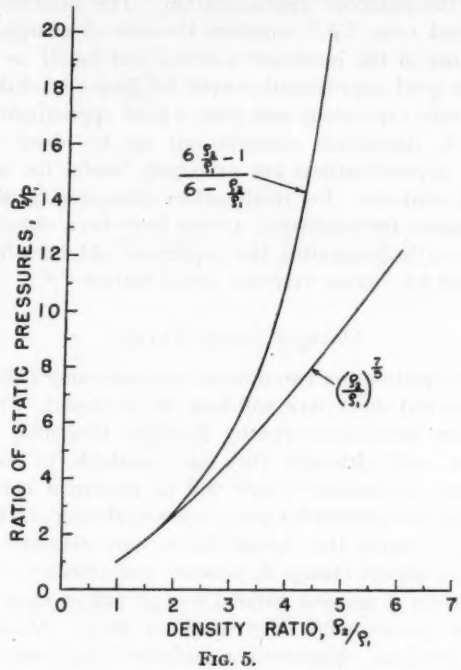

FIG. 5.

$$\left.\begin{aligned} u_1^2 &= \frac{p_2 - p_1}{\rho_1[1 - (\rho_1/\rho_2)]} = \frac{(\gamma-1)p_1 + (\gamma+1)p_2}{2\rho_1} \\ u_2^2 &= \frac{p_2 - p_1}{\rho_2[(\rho_2/\rho_1) - 1]} = \frac{(\gamma+1)p_1 + (\gamma-1)p_2}{2\rho_2} \end{aligned}\right\} \quad (26)$$

Then, introducing Eq. (23)

$$\left.\begin{aligned} M_1^2 \sin^2\theta_w &= \frac{u_1^2}{a_1^2} = \frac{\gamma+1}{2\gamma}\left(\frac{p_2}{p_1}\right) + \frac{\gamma-1}{2\gamma} \\ M_2^2 \sin^2(\theta_w - \theta_s) &= \frac{u_2^2}{a_2^2} = \frac{\gamma+1}{2\gamma}\left(\frac{p_1}{p_2}\right) + \frac{\gamma-1}{2\gamma} \end{aligned}\right\} \quad (27)$$

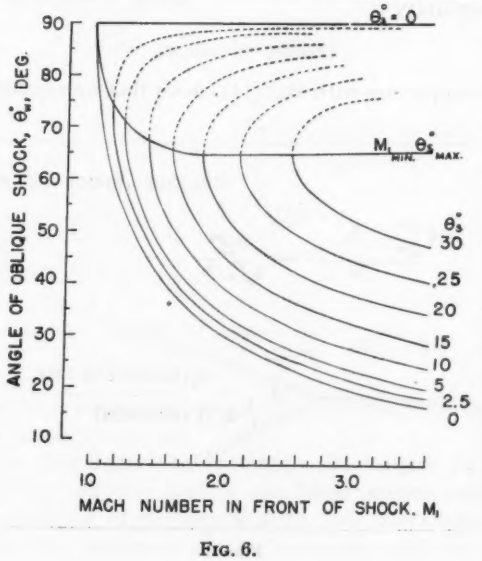

FIG. 6.

Another useful relation for M_1 in terms of only θ_w and θ_s may be obtained by writing Eq. (26) as

$$u_1^2 = \frac{\gamma p_1}{\rho_1} + \frac{\gamma + 1}{2}\left(\frac{p_2 - p_1}{\rho_1}\right)$$

and the desired equation is obtained by substituting Eqs. (23) and (25)

$$\frac{1}{M_1^2} = \sin^2\theta_w - \frac{\gamma + 1}{2}\frac{\sin\theta_w \sin\theta_s}{\cos(\theta_w - \theta_s)} \tag{28}$$

Expressions for the stagnation pressure (H) on either side of the discontinuity may be obtained from Eqs. (9) and (27)

$$\left.\begin{aligned}\left(\frac{H_1}{p_1}\right)^{(\gamma-1)/\gamma} &= 1 + \frac{\gamma - 1}{2}M_1^2 = 1 + \frac{(\gamma^2 - 1)}{4\gamma \sin^2\theta_w}\left(\frac{p_2}{p_1} + \frac{\gamma - 1}{\gamma + 1}\right)\\ \left(\frac{H_2}{p_2}\right)^{(\gamma-1)/\gamma} &= 1 + \frac{\gamma - 1}{2}M_2^2 = 1 + \frac{(\gamma^2 - 1)}{4\gamma \sin^2(\theta_w - \theta_s)}\left(\frac{p_1}{p_2} + \frac{\gamma - 1}{\gamma + 1}\right)\end{aligned}\right\} \tag{29}$$

Although the discontinuity in entropy across the shock wave is associated with an irreversible flow process, its magnitude may be evaluated by integrating any reversible process between the two states since entropy is a thermodynamic property that is independent of the process and is only a function of the initial and final physical states.

$$S_2 - S_1 = \int_1^2 C_v \frac{dT}{T} + \int_1^2 \frac{p\,d(1/\rho)}{T} = C_v\left[\log\left(\frac{p_2}{p_1}\right)\left(\frac{\rho_1}{\rho_2}\right) + (\gamma - 1)\log\left(\frac{\rho_1}{\rho_2}\right)\right] = C_v \log\left[\frac{(p_2/\rho_2^\gamma)}{(p_1/\rho_1^\gamma)}\right] \tag{30}$$

For any isolated system the entropy must either remain constant or increase and the entropy can remain constant only for a reversible adiabatic, therefore

$$(p_2/\rho_2^\gamma) > (p_1/\rho_1^\gamma)$$

and from Eqs. (20), (27), and (29)

$$p_2 > p_1,\ \rho_2 > \rho_1,\ M_2 < M_1,\ H_2 < H_1$$

Consequently, the shock wave defined by these equations is an irreversible adiabatic compression resulting in an increase in entropy.

Normal Shock Waves

The preceding equations also apply to normal shock waves when $\theta_w = \pi/2$ and $\theta_s = 0$. In order to apply Eqs. (13), (14), (16), (18), and (20) directly to a normal shock, it is necessary only to note that $u = V$ and $v = 0$; consequently, the relations for a normal shock are

$$\frac{2}{\gamma - 1}\left[\left(\frac{H_1}{p_1}\right)^{(\gamma-1)/\gamma} - 1\right] = M_1^2 = \frac{\gamma + 1}{2\gamma}\frac{p_2}{p_1} + \frac{\gamma - 1}{2\gamma}$$

and

$$\frac{2}{\gamma - 1}\left[\left(\frac{H_2}{p_2}\right)^{(\gamma-1)/\gamma} - 1\right] = M_2^2 = \frac{\gamma + 1}{2\gamma}\frac{p_1}{p_2} + \frac{\gamma - 1}{2\gamma}$$

or in terms of M_1

$$\frac{p_2}{p_1} = \frac{\gamma M_1^2 - [(\gamma - 1)/2]}{(\gamma + 1)/2}$$

$$\frac{\rho_2}{\rho_1} = \frac{(\gamma + 1)/2}{(1/M_1^2) + [(\gamma - 1)/2]} = \frac{V_1}{V_2}$$

$$M_2^2 = \frac{1 + [(\gamma - 1)/2]M_1^2}{\gamma M_1^2 - [(\gamma - 1)/2]} = \frac{(T_H/T_1)}{(p_2/p_1)[(\gamma + 1)/2]}$$

$$H_1/p_1 = \{1 + [(\gamma - 1)/2]M_1^2\}^{\gamma/(\gamma-1)}$$

$$\frac{H_2}{p_2} = \left[\frac{(\gamma + 1)^2}{4\gamma}\left(\frac{2\gamma M_1^2}{2\gamma M_1^2 - \gamma + 1}\right)\right]^{\gamma/(\gamma-1)}$$

Discussion of Shock Wave Equations

If the oblique shock wave relations for a constant free stream Mach Number (M_1) and a varying flow deflection (θ_s) are desired, then the equations and graphs introduced by Taylor and Maccoll[5] give a convenient solution. However, the following presentation is more useful, especially if the oblique shock wave relations are required for a given angle of flow deflection as would normally be required for a given wedge or airfoil profile.

Taking γ as 7/5 the equations for oblique shock flow become

$$\frac{\rho_2}{\rho_1} = \frac{\tan\theta_w}{\tan(\theta_w - \theta_s)},\quad \frac{p_2}{p_1} = \frac{6(\rho_2/\rho_1) - 1}{6 - (\rho_2/\rho_1)}$$

$$M_1^2 = \frac{[(6/7)(p_2/p_1)] + (1/7)}{\sin^2\theta_w},\quad M_2^2 = \frac{[(6/7)/(p_2/p_1)] + (1/7)}{\sin^2(\theta_w - \theta_s)}$$

$$\frac{H_2}{H_1} = \frac{p_2}{p_1}\left[\frac{1 + (M_2^2/5)}{1 + (M_1^2/5)}\right]^{7/2} = \frac{p_2}{p_1}\left(\frac{T_1}{T_2}\right)^{7/2}$$

The curves presented in Figs. 6 to 10 were obtained for constant values of θ_s by assuming values of θ_w between 0 and $\pi/2$. Also included in the figures are the limiting cases of the oblique shock; that is, the normal shock wave ($\theta_w = \pi/2,\ \theta_s = 0$)

$$\frac{p_2}{p_1} = 1/6(7M_1^2 - 1),\quad \frac{\rho_2}{\rho_1} = \frac{6(p_2/p_1) + 1}{6 + (p_2/p_1)}$$

$$M_2^2 = \frac{[6/(p_2/p_1) + 1]}{7},\quad \frac{H_2}{H_1} = \frac{p_2}{p_1}\left\{\frac{6 + [1/(p_2/p_1)]}{6 + (p_2/p_1)}\right\}^{7/2}$$

and the Mach wave ($\theta_w = \sin^{-1}(1/M_1),\ \theta_s = 0$)

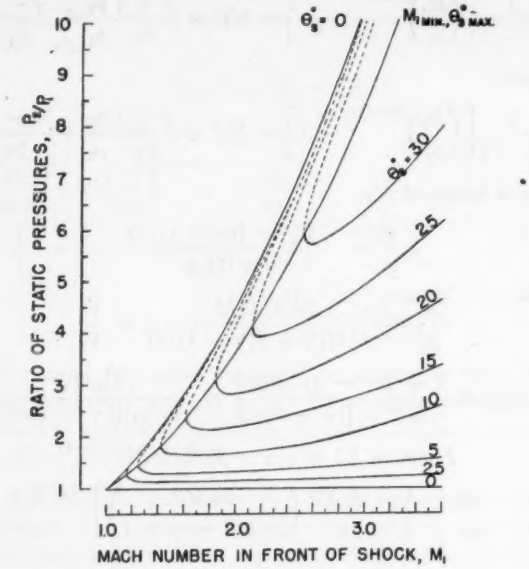

FIG. 7.

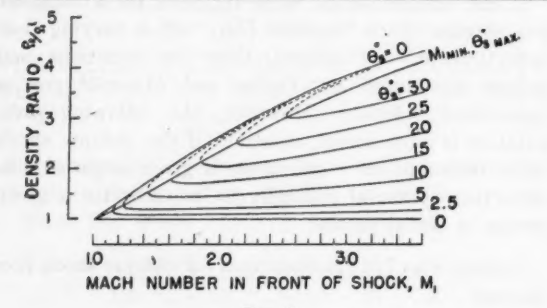

FIG. 8.

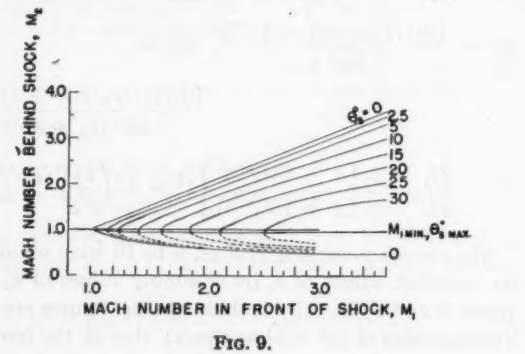

FIG. 9.

$$p_2/p_1 = \rho_2/\rho_1 = M_2/M_1 = H_2/H_1 = 1$$

The normal shock and the Mach wave lines form an envelope for the oblique shock waves as θ_s approaches zero as a limit. Figs. 6 to 10 are equivalent to the Busemann shock polars[3,4] but are more suitable for numerical computation.

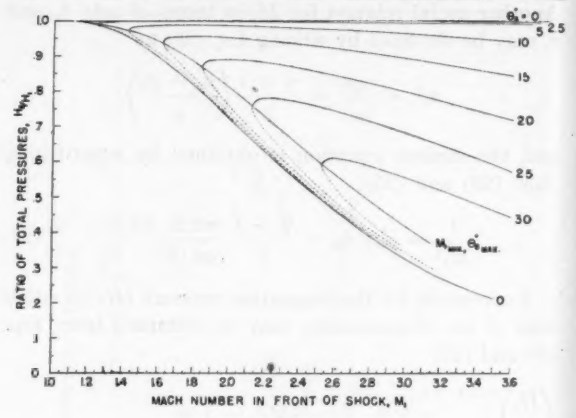

FIG. 10.

It is important to note in Figs. 6 to 10 that there is a minimum free stream Mach Number ($M_{1min.}$) below which an oblique shock wave solution does not exist for a given θ_s, and when this minimum Mach Number is exceeded there are two possible oblique shock wave solutions for each M_1. The solution for $M_{1min.}$ for the existence of an oblique shock with a given stream deflection is obviously identical to the solution of the maximum flow deflection ($\theta_{s_{max.}}$) possible at a given free stream Mach Number. The exact solution of this problem is given in Appendix I and Table 2. The numerical values from Table 2 are also included in Figs. 6 to 10 and form a line dividing the oblique shock flow solution into two parts. The solid line portion, although it has a smaller entropy increase, is still the more dynamically stable oblique shock wave[7] and is the one always found in practice.[5]

Fig. 9 shows that M_2, the Mach Number behind the normal shock wave, is always subsonic, and the same is true for the flow near $M_{1min.}$ for an oblique shock. However, for the oblique shock M_2 is only slightly less than unity, and as $M_{1min.}$ is exceeded the

TABLE 2

Values of the Minimum Mach Number and Maximum Flow Deflection
Two-Dimensional Flow
$\gamma = 7/5$

$\theta_{s_{max.}}$	$M_{1_{min.}}$	M_2	p_2/p_1	ρ_2/ρ_1	H_2/H_1	$\theta_w°$
0	1	1	1	1	1	90
0.5	1.046	0.9855	1.074	1.053	0.9999	80.28
1	1.075	0.9775	1.122	1.086	0.9998	77.93
2	1.122	0.9660	1.205	1.142	0.9994	75.12
2.5	1.143	0.9614	1.243	1.168	0.9990	74.12
5	1.240	0.9438	1.432	1.291	0.9952	70.82
10	1.421	0.9251	1.843	1.537	0.9717	67.45
15	1.614	0.9188	2.360	1.813	0.9385	65.73
20	1.84	0.9201	3.073	2.142	0.8695	64.90
25	2.125	0.9281	4.133	2.546	0.7581	64.62
27	2.265	0.9328	4.722	2.736	0.6989	64.63
30	2.519	0.9408	5.895	3.058	0.5908	64.80
35	3.144	0.9566	9.370	3.723	0.3705	65.40
40	4.446	0.9764	19.179	4.610	0.1306	66.33
45	14.10	0.9977	198.2	5.829	0.00943	67.62
45.584	∞	1	∞	6	0	67.792

abrupt decrease in Mach Number becomes less and the flow remains supersonic throughout. Figs. 6 to 10 all show that once $M_{1min.}$ has been exceeded the relations for the oblique shock wave tend to form a family of curves parallel to the simple isentropic Mach wave relation, especially for small θ_s. It should be possible to determine simple approximate relations for oblique shock waves; for example, a family of parallel straight lines would approximate the relation between M_2 and M_1 (Fig. 9) for a rather wide range of M_1 and θ_s.

At present there is no known general flow solution downstream of the shock wave if the flow near the surface has become subsonic. This is so because, as previously mentioned, the resulting subsonic flow by itself is rather difficult to solve since there are no real characteristics, while the actual mixed field of subsonic and supersonic flow is even more complicated.

For M_1 less than $M_{1min.}$ there is a standing shock wave upstream that is entirely detached from the two-dimensional body. For a region near the nose of the body the flow is subsonic with an ordinary stagnation point somewhere on the nose of the body. No solution has yet been presented for the pressures over the body in this type of flow but Crocco[11] has found a relation for the amount of rotation in each stream tube behind the shock wave, and the author, in a paper not yet published, has obtained an approximate solution for the distance from the standing shock wave to the stagnation point on the body. Of course, a body having a finite thickness at the nose or having a semi-wedge angle greater than 45.58° will always have a detached standing shock wave at ordinary Mach Numbers. Only a true wedge having θ_s less than $\theta_{s_{max.}}$ will allow an ideal attached oblique shock wave to exist for a finite free stream Mach Number.

If M_1 is only slightly greater than $M_{1min.}$ the shock wave will be attached to the nose of the wedge but the flow behind the shock wave will still be subsonic over a portion of the wedge and no general solution can be obtained. The shock wave will not be a plane discontinuity sheet but will be curved near the wedge and gradually will become a plane parallel to the free stream Mach lines at some distance from the body. The flow through the outer portion of the shock wave will pass through unaltered and of course be supersonic as well as isentropic.

However even if the flow is supersonic everywhere behind the oblique shock, a true plane oblique shock can exist only for a finite distance from a finite body. Only an infinite wedge can have an oblique shock wave producing uniform parallel flow everywhere behind the shock wave. The infinite wedge and its infinite oblique shock wave must of necessity also have an infinite drag since the entropy discontinuity, although it may be small, still acts over an infinite surface. A Mach wave can extend to infinity since it is an infinitesimal disturbance which has no discontinuity; however, a shock wave always has a finite discontinuity. A finite body, of course, cannot have an infinite drag, so the oblique shock of a finite body cannot extend to infinity. This may also be found to be true from the physical consideration of the Mach lines formed by the changes in the body's surface behind the nose wedge. These Mach lines interfere with the oblique shock at some finite distance from the body. The Mach lines form an envelope which causes the oblique shock wave to curve and continually reduces the pressure and resulting entropy discontinuity until at some finite distance from the body the oblique shock has been transformed into a Mach wave and the flow is then unaltered in passing through it.

Since the stagnation enthalpy (h_H) is constant through a shock wave, Eq. (16), Crocco[11] has shown that the flow rotation in any stream tube behind a shock wave is proportional to the static pressure (p_2). Consequently, the flow immediately behind a shock wave is irrotational (velocity potential exists) only if the flow is uniform and parallel. Only an infinite wedge satisfies this condition exactly. However, for all practical purposes the oblique shock existing at the nose of any body having a sharp leading edge whose θ_s is less than $\theta_{s_{max.}}$ satisfies these conditions. The oblique shock will remain plane far enough from the body that the flow may be considered everywhere irrotational behind the shock if the flow is everywhere supersonic. Therefore, a velocity potential exists between shock waves and it is valid to use the isentropic solution of Fig. 1 for any flow expansion.

Approximate Solution of Oblique Shock Flow

Fig. 10 shows that the head loss is almost negligible for flow deflections less than 5° and is fairly small even for larger flow deflections at some Mach Numbers. This is an indication that the flow is approximately isentropic for small flow deflections. That this is so was first proved by Busemann[3] who found that

$$S_2 - S_1 = f(\theta_w)\theta_s^3 + 0(\theta_s^4)$$

However, Figs. 5, 7, and 10 indicate that even a fairly large θ_s may possibly produce an oblique shock across which the flow is approximately isentropic if the pressure or density change is small. In this case the two curves in Fig. 5 can be shown to be identical to the second order because the first and second derivatives of Eqs. (6) and (20) have the same limit as M_1 approaches unity ($\rho_2 \to \rho_1$, $p_2 \to p_1$). For example, Eq. (26) can be written as

$$u_1 = \sqrt{\frac{\rho_2}{\rho_1}\left(\frac{p_2 - p_1}{\rho_2 - \rho_1}\right)}, \quad u_2 = \sqrt{\frac{\rho_1}{\rho_2}\left(\frac{p_2 - p_1}{\rho_2 - \rho_1}\right)}$$

or

$$\left(\frac{p_2 - p_1}{\rho_2 - \rho_1}\right) = \gamma\left(\frac{p_2 + p_1}{\rho_2 + \rho_1}\right) = u_1 u_2 = a_{(M=1)}^2$$

Then, when M_1 approaches unity as a limit the above

equations for an oblique shock becomes identical to the isentropic equations

$$dp/d\rho = \gamma(p/\rho) = a^2$$

The curves in Fig. 5 diverge with a large pressure or density increase because the third and higher derivatives at an M_1 of unity are not identical. It is seen that if $\rho_2/\rho_1 < 1.60$ or $p_2/p_1 < 1.95$, then the oblique shock flow Eq. (20) is represented within 1 per cent by the isentropic flow Eq. (6). Figs. 7 and 8 show that for Mach Numbers less than 2.71 a flow deflection of 10° will be within this range, while for smaller flow deflections that Mach Number range within which the flow is approximately isentropic is greatly increased. Fig. 10 shows that for this range the total pressure loss due to the shock will be less than 3 per cent.

The preceding conclusions may also be justified by combining Eqs. (20) and (30) to show that for an oblique shock

$$S_2 - S_1 = C_v \sum_{n=1}^{\infty} \frac{(-1)^n}{n}\left[\left(\frac{1-\gamma}{2}\right)^n + \gamma - \left(\frac{1+\gamma}{2}\right)^n\right]\left(\frac{\rho_2}{\rho_1} - 1\right)^n =$$

$$\left(\frac{\gamma^3-\gamma}{12}\right)\left[\left(\frac{\rho_2}{\rho_1} - 1\right)^3 - \frac{3}{2}\left(\frac{\rho_2}{\rho_1} - 1\right)^4 + \frac{3}{20}(\gamma^2+11)\left(\frac{\rho_2}{\rho_1} - 1\right)^5 - \cdots\right] =$$

$$C_v\left(\frac{\gamma^3-\gamma}{12\gamma^3}\right)\left[\left(\frac{p_2}{p_1} - 1\right)^3 - \frac{3}{2}\left(\frac{p_2}{p_1} - 1\right)^4 + \frac{3}{20}\left(\frac{1}{\gamma^2} + 11\right)\left(\frac{p_2}{p_1} - 1\right)^5 - \cdots\right] =$$

$$C_v\left(\frac{\gamma^3-\gamma}{12\sin^3\theta_w\cos^3\theta_w}\right)\left[\theta_s^3 - \left(\frac{3-6\cos^2\theta_w}{2\sin\theta_w\cos\theta_w}\right)\theta_s^4 + \cdots\right] \quad (31)$$

so that if the third order of density, pressure, or flow deflection increment is negligible the oblique shock flow is approximately isentropic. Then if the conditions of negligible entropy change are satisfied, Fig. 1 or Table 1 may be used for the oblique shock flow computation. This is a great simplification since Fig. 1 then provides a solution for all supersonic flow problems in this range. In addition, the conditions that the flow must everywhere be supersonic and that the minimum Mach Number must be exceeded before an oblique shock can exist are automatically satisfied since in Appendix I it is shown that Fig. 1 fails to provide a solution whenever these conditions exist for any $+\theta_s$ less than 15°.

For normal shock

$$[(p_2/p_1) - 1] = [2\gamma/(\gamma+1)](M_1^2 - 1)$$

therefore

$$S_2 - S_1 = C_v[2\gamma(\gamma-1)/3(\gamma+1)^2](M_1^2-1)^3 + 0(M_1^2-1)^4$$

Consequently, even a normal shock is approximately isentropic for Mach Numbers near unity. Figs. 7 and 8 show that the normal shock can be approximated by isentropic compression within 1 per cent for Mach Numbers less than 1.35. Fig. 10 shows a 3.03 per cent total pressure loss through the normal shock at $M_1 = 1.35$.

In Appendix II an infinite series expansion is found for the pressure increase through an oblique shock wave for a given positive flow deflection ($+\theta_s$)

$$P = \sum_{n=1}^{\infty} b_n\theta_s^n \quad (32)$$

where

$$b_1 = 2/(M_1^2-1)^{1/2},\ b_2 = \{[(\gamma+1)/2]M_1^4 - 2M_1^2 + 2\}/(M_1^2-1)^2$$

$$b_3 = \frac{1}{(M_1^2-1)^{7/2}}\left[\frac{(\gamma+1)^2}{16}M_1^8 - \frac{(-3\gamma^2+12\gamma+7)}{12}M_1^6 + \frac{3(\gamma+1)}{2}M_1^4 - 2M_1^2 + \frac{4}{3}\right]$$

$$b_4 = \frac{1}{(M_1^2-1)^5}\left[\frac{(3\gamma^3-3\gamma^2-7\gamma-1)}{24}M_1^{10} + \frac{(3\gamma^3-3\gamma^2+33\gamma+7)}{24}M_1^8 + \frac{(3\gamma^2-9\gamma-2)}{2}M_1^6 + \frac{(8\gamma+2)}{3}M_1^4 - \frac{2}{3}M_1^2 + \frac{2}{3}\right]$$

The expressions for b_1 to b_6 are derived in Appendix II; the values of b_1 to b_4 for various Mach Numbers are given in Table 3 and presented in Fig. 11. It is seen that C_1 and C_2 of Eq. (12) are identical to b_1 and b_2 of Eq. (32); C_3, however, is not identical to b_3, therefore the variation of C_3 with Mach Number is also shown in Fig. 11.

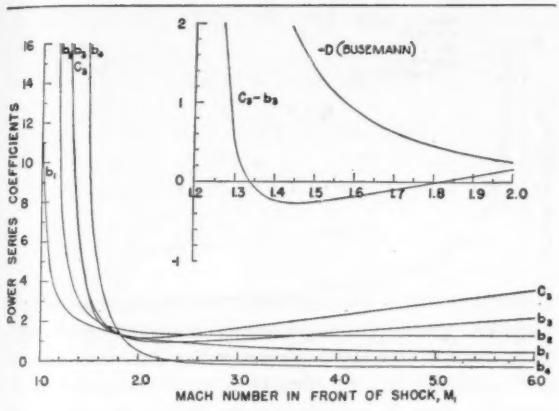

FIG. 11.

The first two terms of Eq. (12), or Eq. (32), give the two approximations for oblique shock and supersonic isentropic flow which have been used in practice.[5] The first term ($b_1\theta_s$ or $C_1\theta_s$) gives the linear or Ackeret[8] approximation while the addition of the second term ($b_2\theta_s^2$ or $C_2\theta_s^2$) gives the parabolic or Busemann[9] approximation. The additional term $C_3\theta_s^3$ giving the third approximation to isentropic flow is taken as given by Busemann[6] but the author believes that the term $(C_3 - D)\theta_s^3$ giving the third approximation to the oblique shock flow as derived by Busemann[6] is incorrect and the expression derived in Appendix II, $b_3\theta_s^3$ is the correct third order term.

Fig. 11 shows that for Mach Numbers less than 1.3 the values for b_1, b_2, b_3 and C_3 tend to approach infinity rapidly as M_1 approaches unity; consequently, the power series representation by Eqs. (12) or (32) is not good for Mach Numbers less than 1.3.

In Fig. 11 it is seen that b_3 and C_3 are of approximately the same magnitude and that for Mach Numbers greater than 1.82, b_3 is less than C_3. This shows that, contrary to Busemann,[6] the oblique shock wave, at least for small flow deflections, produces a smaller pressure increase than does an isentropic compression for all free stream Mach Numbers greater than 1.82. In addition, the b_4 term becomes negative for all Mach Numbers greater than 2.4, indicating that for larger flow deflections at high Mach Numbers the oblique shock produces a much smaller pressure increase than does an isentropic compression for the same flow deflection. This result should be expected since the increase in entropy due to the oblique shock is at the expense of the kinetic energy which is converted into heat energy (an increase in enthalpy). Consequently, for a given speed the pressure change should be less as the entropy increases. However, Fig. 11 shows that b_3 is slightly greater than C_3 in the Mach Number range of 1.34 to 1.82. Therefore, for a given free stream Mach Number in this range and for a given small positive flow deflection, the oblique shock produces a slightly greater pressure increase than does an isentropic compression. This apparently anomalous condition can exist because at a given free stream Mach Number the pressure increase in Eq. (32) depends only on the flow deflection. Figs. 7 and 8 show that for this Mach Number range the pressure or density discontinuity is actually a minimum for any given small flow deflection. That is, for a given θ_s the resulting p_2/p_1 or ρ_2/ρ_1 is a minimum and is closest to that for a Mach wave; consequently, from Eq. (31) the entropy discontinuity is actually a minimum in this Mach Number range. In addition, the data for Fig. 10 definitely showed that for any given small θ_s the value of H_2/H_1 was nearer to unity for Mach Numbers in the range of 1.34 to 1.82.

It is rather interesting to digress for a moment and note that for an airfoil in subsonic flight the local Mach Number range in which the compressibility shock[10] occurs is generally 1.4 to 1.5. This is the Mach Number range wherein b_3 is approximately 9 per cent more positive than C_3. Consequently, in this local supersonic Mach Number range for a given pressure increase the required positive flow deflection is slightly less for an oblique shock than for an isentropic compression. Now the positive flow deflection on the rearward portion of an airfoil section could be produced only by a boundary layer separation or thickening. Therefore, if the boundary layer can easily leave the surface, the required compression for a return to subsonic flow could occur by means of a relatively large boundary layer separation accompanied by an isentropic compression and Mach Number decrease outside the boundary layer[10] (the boundary layer flow is, of course, subsonic and nonisentropic) until finally the boundary layer will no longer thicken. The final flow compression to a subsonic Mach Number can then be accomplished by a normal shock wave. However, if the boundary layer cannot easily separate from the surface, then the flow compression and resultant subsonic Mach Number could be obtained directly by an

TABLE 3
Values of Coefficients for Power Series Approximations
$\gamma = 7/5$

M	$b_1 = C_1$	$b_2 = c_2$	b_3	C_3	b_4
1.1	4.364	30.32	544.4	646.3	1299.
1.2	3.015	8.307	53.22	59.05	516.3
1.3	2.408	4.300	14.53	14.94	77.49
1.4	2.048	2.919	6.128	5.885	22.51
1.5	1.789	2.288	3.331	3.059	8.965
1.6	1.601	1.950	2.153	1.961	4.293
1.8	1.336	1.618	1.280	1.262	1.339
2.0	1.155	1.467	1.019	1.140	0.4711
2.2	1.021	1.386	0.9394	1.174	0.1274
2.4	0.9167	1.337	0.9356	1.263	−0.0468
2.6	0.8333	1.306	0.9654	1.374	−0.1319
2.8	0.7647	1.284	1.013	1.494	−0.1540
3	0.7071	1.269	1.069	1.619	−0.2248
4	0.5164	1.232	1.405	2.252	−0.2928
5	0.4082	1.219	1.764	2.879	−0.3221
6	0.3381	1.212	2.127	3.498	−0.3340
8	0.2520	1.207	2.852	4.720	−0.3470
10	0.2010	1.204	3.578	5.937	−0.3471
100	0.02000	1.200	37.28	59.99	−0.350
Large M	$2/M$	1.2	$0.36M$	$0.6M$	−0.352

oblique shock accompanied by a relatively small separation of the boundary layer. Figs. 6 and 10 show that for a given pressure increase an oblique shock, although requiring a higher local Mach Number, has less total pressure loss than a normal shock. Consequently, unless the Mach Number is very nearly unity before the normal shock occurs, the total drag, including the effect of the relatively thicker boundary layer, will probably be greater with the combination of isentropic compression followed by a normal shock than it would be with the oblique shock alone. If the boundary layer cannot separate at all, the flow compression can be accomplished only by means of a large normal shock which would probably produce the greatest drag on the airfoil. However, the resultant drag, including the effect of the boundary layer separation, would probably be approximately of the same magnitude for all three cases and the type of flow would depend upon the boundary layer Reynolds Number.

Since $b_3 = C_3$ at Mach Numbers of 1.34 and 1.82, the oblique shock flow may be considered approximately isentropic to the third order of flow deflection for Mach Numbers in this range. Fig. 12 for a Mach

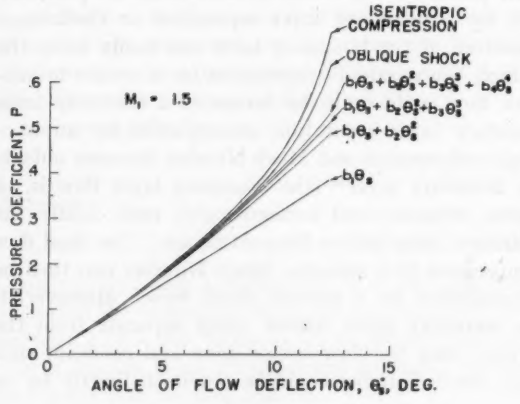

FIG. 12.

Number of 1.5 shows that even near $\theta_{s_{max.}}$ the pressure coefficient produced by an oblique shock is only 8 per cent less than that produced by isentropic compression. It is also seen that the fourth order approximation from Eq. (32) is only 2 per cent less than the pressure coefficient produced by an oblique shock flow deflection of almost 10°. Fig. 13 for a flow deflection of 5° shows that the oblique shock and isentropic compression are in close agreement, and for Mach Numbers greater than 1.3 all the approximations of Eq. (32) higher than the first order give results practically identical to that of the oblique shock.

Fig. 14 shows that even for a $+\theta_s$° value of 15° the isentropic compression will give a good numerical approximation for oblique shock flow for $M_1 < 10$. The power series approximation from Eq. (32) also

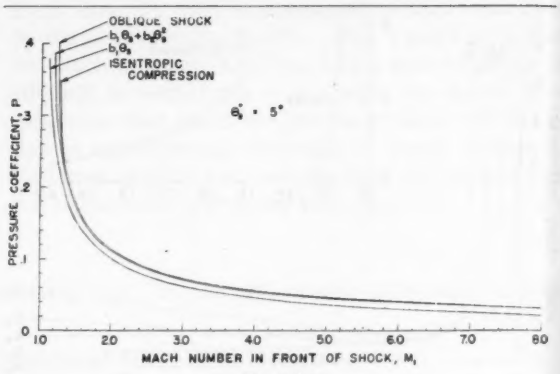

FIG. 13.

is good for Mach Numbers sufficiently greater than $M_{1_{min.}}$. However, for Mach Numbers above 10 the third and higher orders of the power series representation diverge rapidly from the oblique shock values. This occurs because the third and higher order odd terms of Eq. (32) have no limit as M_1 increases, as may be seen from Eq. (32) where for extremely large M_1

$$P \approx \frac{2}{M}\theta_s + \left(\frac{\gamma+1}{2}\right)\theta_s^2 + \frac{(\gamma+1)^2}{16}M\theta_s^3 + \left(\frac{3\gamma^3 - 3\gamma^2 - 7\gamma - 1}{24}\right)\theta_s^4 + \cdots\cdots$$

This shows that as long as θ_s is finite, regardless of how small it may be, the third order term will increase without a limit as the Mach Number increases. Therefore, Eq. (32), Eq. (12), or similar expansion in terms of θ_s cannot be used to investigate the flow at extremely large Mach Numbers.

Approximate Relations for Extremely Large Mach Numbers

Simple relations for the limiting values for an oblique shock as M_1 increases without limit may be obtained

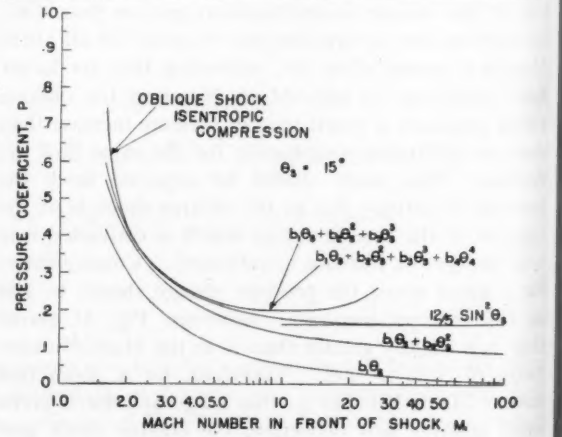

FIG. 14.

from Eqs. (20), (21), (24), and (27).

$$\left.\begin{aligned} \frac{P_2}{p_1} &\to (2\gamma/\gamma+1)\sin^2\theta_w(M_1^2) \\ M_2^2 &\to (\gamma-1)/2\gamma\sin^2(\theta_w-\theta_s) \\ \frac{\rho_2}{\rho_1} &= \frac{\tan\theta_w}{\tan(\theta_w-\theta_s)} \to \frac{\gamma+1}{\gamma-1} \\ \frac{p_2-p_1}{{}^1/_2\rho_1 V_1^2} &\to \frac{4}{\gamma+1}\sin^2\theta_w \end{aligned}\right\} \quad (33)$$

However, as M_1 increases without limit it is obvious that the physical limitations of the theory are eventually exceeded. The so-called "exact" oblique shock flow equations were developed on the premise of no heat transfer (with the exception of any occurring internally within the infinitesimal discontinuity sheet forming the shock wave). For large M_1 the resulting compression produces an extremely large temperature rise which would invalidate the supposition of no heat conduction or radiation. A better approximation for large M_1 would then be obtained by either assuming an isothermal process (equivalent to $\gamma = 1$) or assuming that $\theta_w \to \theta_s$. Either condition applied to Eqs. (20), (21), (24), and (27) yields the following approximation for large M_1 and finite θ_s which agree with those given by Epstein[7]

$$\left.\begin{aligned} &\theta_w \to \theta_s,\ \gamma = 1,\ M_2^2 \to 0 \\ \frac{\rho_2}{\rho_1} &= \frac{p_2}{p_1} \to \sin^2\theta_w(M_1^2) \to \sin^2\theta_s\,(M_1^2) \\ &\frac{p_2-p_1}{{}^1/_2\rho_1 V_1^2} \to 2\sin^2\theta_w \to 2\sin^2\theta_s \end{aligned}\right\} \quad (34)$$

However, for infinitesimal θ_s the process may still be assumed an irreversible adiabatic with no heat transfer. In this case, Eq. (28) or Fig. 6 shows that θ_w becomes extremely small for small θ_s; therefore, Eq. (21) for large M_1 becomes

$$\frac{\theta_w}{\theta_w-\theta_s} \approx \frac{\rho_2}{\rho_1} \to \frac{\gamma+1}{\gamma-1}$$

or

$$\sin\theta_w \approx \theta_w \to [(\gamma+1)/2]\theta_s$$

and from Eq. (33)

$$\left.\begin{aligned} p_2/p_1 &\to [\gamma(\gamma+1)/2]\theta_s^2 M_1^2 \\ M_2^2 &\to 2/\gamma(\gamma-1)\theta_s^2 \\ \frac{\rho_2}{\rho_1} &\to \frac{\gamma+1}{\gamma-1},\ \theta_w \to \left(\frac{\gamma+1}{2}\right)\theta_s \\ [(p_2-p_1)/{}^1/_2\rho_1 V_1^2] &\to (\gamma+1)\theta_s^2 \end{aligned}\right\} \quad (35)$$

It is seen that for $\theta_s \to 0$ and for $\gamma = 1$ Eqs. (33), (34), and (35) give the same limit for the pressure coefficient P, namely:

$$P = [(p_2-p_1)/{}^1/_2\rho_1 V_1^2] \to 2\theta_s^2$$

as M_1 becomes extremely large.

In Fig. 14 the approximate relation for large M_1 is taken as

$$P = (\gamma+1)\sin^2\theta_s = (12/5)\sin^2\theta_s \quad (36)$$

It is seen that this value closely approximates the "exact" oblique shock flow relation for $M_1 > 15$.

It is interesting to note that for extremely high Mach Numbers Eq. (34) shows that the entire area affected by the oblique shock becomes only a thin film near the surface ($\theta_w \to \theta_s$). Consequently, all the front surfaces of the body are exposed directly to M_1 and V_1, and Eq. (34) may therefore be applied to all the front surfaces facing the stream. The pressure may be taken as zero for all the back faces and Eq. (34) then provides a complete pressure distribution for any two- or even three-dimensional body at extremely high Mach Numbers.[7]

Pressure Distribution on Two-Dimensional Bodies

In supersonic flow the study of a two-dimensional body is even more important than in subsonic flow since the flow over any rectangular wing may be considered everywhere two dimensional except at the wing tips. This is obvious because of the existence of the real characteristics in supersonic flow and the fact that nothing occurring downstream of a characteristic can directly affect the flow upstream from it. If the wing tip plan form is cut off along a Mach line then even the flow over the wing tip is two dimensional.[8] In addition, the flows over the upper and lower surfaces are now independent of each other because the conditions at the trailing edge can no longer directly affect the supersonic flow over the body.

It is again worth while to emphasize that only the supersonic isentropic flow defined by Eqs. (3) and (5) is everywhere irrotational with a continuous velocity potential. The shock flow-defined by Eqs. (18) and (20) must always have a discontinuous drop in velocity potential at the plane discontinuity sheet defining the shock wave. The flow between shock waves can be irrotational with a continuous velocity potential only if the shock wave extends to infinity. However, for all practical purposes the shock wave for a finite body generally extends far enough from the body so that a continuous velocity potential may be assumed to exist in between the shock waves. This does show, however, that an exact rigorous solution is not yet available even when viscosity effects are neglected; consequently, the simplest approximate solution will probably be satisfactory within certain limits. The final criterion should, of course, be predicated on experimental verification.

The following will attempt to provide a guide to the application of the solutions presented in this paper.

(1) $\theta_{s_{max.}}{}^\circ > |\theta_s{}^\circ| < 2^\circ,\ 1.1 < M_1 < 15$

The Ackeret or linear approximation

$$P = C_1\theta_s = b_1\theta_s = \frac{2}{\sqrt{M_1^2 - 1}}\theta_s$$

will be satisfactory. This approximation is independent of the nature of the gas or the thermodynamic process and may be directly integrated to yield extremely simple expressions for the forces on an airfoil.[5]

(2) $\qquad \theta_{s_{max.}}{}^\circ > |\theta_s{}^\circ| < 5^\circ,\ 1.3 < M_1 < 15$

The Busemann or parabolic approximation

$$P = C_1\theta_s + C_2\theta_s{}^2 = b_1\theta_s + b_2\theta_s{}^2 =$$

$$\frac{2}{\sqrt{M_1^2 - 1}}\theta_s + \left\{\frac{[(\gamma + 1)/2]M_1^4 - 2M_1^2 + 2}{(M_1^2 - 1)^2}\right\}\theta_s{}^2$$

will be satisfactory. This second order approximation now depends upon the nature of the gas but is still independent of any entropy increase (irreversibility). This expression has also been formally integrated over the airfoil surface to show the dependence of the forces on the surface slopes.[4, 6]

(3) $\qquad |\theta_{s_{max.}}{}^\circ| > \theta_s{}^\circ < +15^\circ,\ M_1 < 10$

In this case the third approximation given by the first three terms of Eqs. (12) and (32) may be used. This approximation now contains the effect due to the irreversible entropy increase caused by an oblique shock and is tedious to integrate formally. This has been done by Busemann[4, 6] for a circular arc profile. It may be seen that the value given by Busemann for $D = (C_3 - b_3)$ is incorrect as shown in Fig. 11 and the value of D should be taken from Eqs. (12) and (32). In addition, it is shown in Fig. 14 that the third and higher order approximations given by Eqs. (12) and (32) are invalid for $M_1 > 10$, or $M_1 < 1.3$.

However, it has been shown that the flow approximation given by Table 1 or Fig. 1 may be used for numerical evaluation of all the compression and expansion flow over the body as long as $M_1 < 10$, $\theta_s{}^\circ < 15^\circ$. As previously pointed out, the use of Fig. 1 automatically satisfies the conditions required for the existence of the solution.

(4) $\qquad |\theta_{s_{max.}}{}^\circ| > \theta_s{}^\circ > +15^\circ$

Fig. 7 should be used to determine the pressure increase through all shock compressions where $\theta_s{}^\circ > 15^\circ$, while Fig. 1 may be used for the regions of flow expansion and also for flow compressions where $\theta_s{}^\circ < 15^\circ$. In this case the existence of the assumed shock wave and of supersonic flow throughout must always be checked from Table 2 and Fig. 9 although the use of Fig. 1 or Fig. 7 would automatically eliminate the need for Table 2.

For cases (1), (2), and even (3) the flow is approximately isentropic, therefore the pressure changes are reversible. Consequently, the pressure will always be the same when the surface slope (θ_s) is the same. For example, whenever θ_s becomes zero, $p_2 = p_1$. However, for case (4) the process is now irreversible, and the pressure behind an oblique shock will be determined by Fig. 7 and cannot return to the corresponding value. For example, when θ_s again becomes zero behind a shock, $p_2 > p_1$.

(5) $\qquad M_1 > 15$

For large M_1 use Eq. (36) for flow compression and Fig. 1 for flow expansion. Then with extremely large M_1 use Eq. (34) for flow compression and for flow expansion obtain a solution similar to Fig. 1 by utilizing the isothermal supersonic flow around a sharp corner.[7] If the Mach Number is extremely large, then Eq. (34) may be used directly to obtain the entire pressure distribution for any two- or even three-dimensional body.[7]

Case (3) is the most important one for practical supersonic airfoil design. For the design of airfoils with sharp leading edges the use of Table 1 or Fig. 1 may be greatly simplified if the variation of p/H_1 with θ_s is directly shown as in Fig. 15 and the pressure coefficient is taken as p/H_1 rather than P. Then the movable θ_s scale may simply have its zero value shifted to the value corresponding to the free stream Mach Number (M_1) and the pressure coefficient (p/H_1) is then read directly from Fig. 15 for the given surface slope. The inverse problem of determining the profile

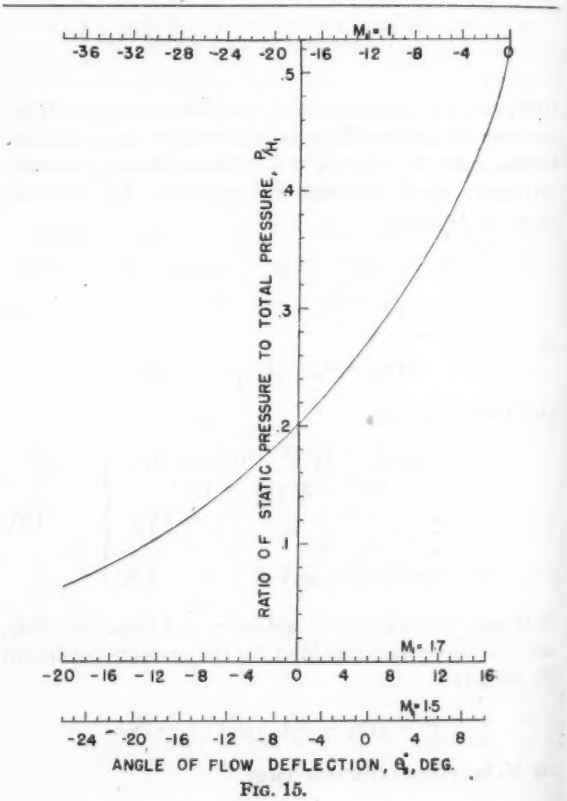
M₁= 1
-36 -32 -28 -24 -20 -16 -12 -8 -4 0
.5
.4
.3
.2
.1
RATIO OF STATIC PRESSURE TO TOTAL PRESSURE, p/H₁
M₁= 1.7
-20 -16 -12 -8 -4 0 4 8 12 16
M₁= 1.5
-24 -20 -16 -12 -8 -4 0 4 8
ANGLE OF FLOW DEFLECTION, θ, DEG.

FIG. 15.

that will produce any given physically possible pressure, distribution is also determined directly from Fig. 15. The scale for θ_s in Fig. 15 either may be made movable or the difference in θ_s required to shift the scale to a new M_1 may be algebraically added to the given surface slope. The position of the θ_s scale is shown in Fig. 15 for an M_1 of 1.5 and 1.7.

For supersonic pressure distributions it is probably better to use the pressure coefficient p/H_1 rather than P. The pressure summation to determine the resultant forces can be easily accomplished; for example,

$$H_1 = \{1 + [(\gamma - 1)/2]M_1^2\}^{\gamma/(\gamma-1)}\, p_1 = \{1 + [(\gamma - 1)/2]M_1^2\}^{\gamma/(\gamma-1)}\left[\frac{{}^1/_2\rho_1 V_1^2}{(\gamma/2)M_1^2}\right]$$

therefore,

$$C_L = \frac{H_1}{{}^1/_2\rho_1 V_1^2}\oint\left(\frac{p}{H_1}\right)d\left(\frac{x}{c}\right) = \frac{\{1 + [(\gamma - 1)/2]M_1^2\}^{\gamma/(\gamma-1)}}{(\gamma/2)M_1^2}\oint\left(\frac{p}{H_1}\right)d\left(\frac{x}{c}\right)$$

Also from Eq. (11)

$$P = \frac{1}{(\gamma/2)M_1^2}\left(\left(\frac{p}{H_1}\right)\{1 + [(\gamma - 1)/2]M_1^2\}^{\gamma/(\gamma-1)} - 1\right)$$

The main advantage of the pressure coefficient P over p/H_1 is that a zero value of P shows the location of free stream values on the airfoil surface. However, in the type of supersonic flow assumed in Fig. 1 or Fig. 15 ($\theta_s° < 15°$) the free stream conditions are always found whenever the airfoil surface has a θ_s value of zero and are therefore already known. In addition, the local Mach Number over the airfoil surface is directly related to p/H_1 by Eq. (9) or Fig. 1.

Fig. 16 shows the pressure distribution obtained from Fig. 15 for the Stanton[8, 9] Biconvex Circular Arc profile for a free stream Mach Number of 1.7. The p/H_1 value for the oblique shock at the sharp nose

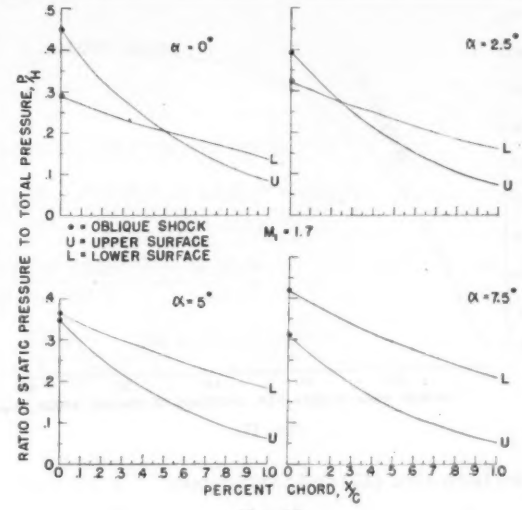

FIG. 16.

($x/c = 0$) is obtained from Fig. 7 and also shown in Fig. 16. The p/H_1 values in Fig. 15 are in good agreement with the ${}^1/_2P$ values given by Hooker[9] except for $\alpha = 0°$. Then the value at the nose ($x/c = 0$, $\theta_s° = 16°$) as given by Hooker is much greater than that produced by an oblique shock. However, Fig. 15 shows that even for this θ_s value of 16° the p/H_1 given by Fig. 14 is practically the same as for an oblique shock. Consequently, the values given by Fig. 14 should have even better agreement with the experimental values than those given by Hooker. When Fig. 1 or Fig. 14 is used for $\theta_s° > 15°$ the result should be checked by Fig. 7 for the p_2/p_1 value and by Fig. 9 to be certain that $M_2 > 1$. After the pressure forces on the airfoil itself have been obtained, the velocity and pressure in the wake may be approximated by utilizing Fig. 10 to obtain the total pressure loss through the oblique shocks. However, it must be noted that the boundary layer viscosity effects have been entirely neglected.

Appendix I

MAXIMUM FLOW DEFLECTION

If the maximum flow deflection ($\theta_{s_{max.}}$) for a given free stream Mach Number (M_1 = const.) is desired, then Eq. (28) may be differentiated with respect to θ_w considering M_1 a constant and $d\theta_s/d\theta_w = 0$.

$$\sin 2\theta_w - \frac{\gamma + 1}{2}\sin\theta_s\left[\frac{\cos\theta_w\cos(\theta_w - \theta_s) + \sin\theta_w\sin(\theta_w - \theta_s)}{\cos^2(\theta_w - \theta_s)}\right] = 0 \qquad (37)$$

However, this is identical to the relation that would be obtained if the minimum free stream Mach Number ($M_{1_{min.}}$) for the existence of an oblique shock for a given positive surface deflection (θ_s = const.) were required. Since for $M_{1_{min.}}$, $1/M_1^2$ is a maximum, Eq. (28) yields

$$\partial(1/M_1^2)/\partial\theta_w = (\partial/\partial\theta_w)\{\sin^2\theta_w - [(\gamma + 1)/2][\sin\theta_w\sin\theta_s/\cos(\theta_w - \theta_s)]\} = 0 \qquad (38)$$

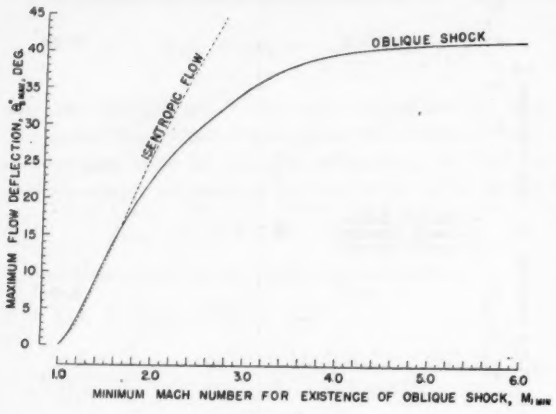
OBLIQUE SHOCK
ISENTROPIC FLOW
MAXIMUM FLOW DEFLECTION, $\theta_{s_{max.}}$, DEG.
MINIMUM MACH NUMBER FOR EXISTENCE OF OBLIQUE SHOCK, $M_{1_{min.}}$

FIG. 17.

Then both Eqs. (37) and (38) become

$$\left[\sin 2\theta_w - \frac{\gamma+1}{4}\frac{\sin 2\theta_s}{\cos^2(\theta_w - \theta_s)}\right] = 0 \qquad (39)$$

Eqs. (28) and (39) are then solved in the form

$$\left.\begin{aligned} \sin 2\theta_w \cos^2(\theta_w - \theta_{s_{max.}}) &= {}^3/_5 \sin 2\theta_{s_{max.}} \\ \frac{1}{M_{1_{min.}}^2} &= \sin^2\theta_w - \frac{6}{5}\frac{\sin\theta_w \sin\theta_{s_{max.}}}{\cos(\theta_w - \theta_{s_{max.}})} \end{aligned}\right\} \qquad (40)$$

and the values are given in Table 2 and Fig. 17. It is obvious physically that the solution of $M_{1_{min.}}$ and $\theta_{s_{max.}}$ are equivalent when it is noted that Fig. 6 may be obtained directly from Eq. (28).

An approximation to this exact solution was given by Busemann[6] as

$$\theta_{s_{max.}} \approx \frac{(4/3)^{3/2}}{\gamma+1}\frac{(M_{1_{min.}}^2 - 1)^{3/2}}{M_{1_{min.}}^2} = 0.321\frac{(M_{1_{min.}}^2 - 1)^{3/2}}{M_{1_{min.}}^2}$$

This approximates Table 2 for θ_s values less than 20°. However, a more useful approximation may be obtained by observing in Table 2 that M_2 is only slightly less than unity for small θ_s. Consequently, the values of Table 1 approximate those of Table 2 for small θ_s, since Table 1 indicates the isentropic flow compression that would be required to reduce the Mach Number to exactly unity. Fig. 17 shows that the $\theta_{s_{max.}}$ obtained from the isentropic flow approximation (Table 1) agrees fairly well with the exact solution (Table 2) up to a $\theta_{s_{max.}}$ of 20°. For $\theta_{s_{max.}}$ less than 15° the isentropic compression is a desirable conservative approximation. Fig. 9 immediately shows that the isentropic approximation is actually a better criterion for $\theta_{s_{max.}}$ or $M_{1_{min.}}$ in supersonic flow computations with $\theta_s < 15°$. In Fig. 9 it is seen that for M_1 near $M_{1_{min.}}$ the flow behind the shock is still subsonic ($M_2 < 1$); consequently, the oblique shock flow solution is no longer valid behind the shock. The use of Table 1 or Fig. 1 for $\theta_{s_{max.}}$ or $M_{1_{min.}}$ eliminates this difficulty by automatically keeping M_2 greater than unity.

The approximate relation

$$\theta_w \approx \pi/4 + \theta_{s_{max.}}/2$$

as given by Epstein[7] may be obtained as an exact value for the limit of Eq. (40) as M_1 approaches infinity. When $M_1 \to \infty$, Eq. (40) becomes

$$\frac{\sin 2\theta_{s_{max.}}}{\sin\theta_{s_{max.}}} = 2\frac{\sin 2\theta_w}{\sin\theta_w}\cos(\theta_w - \theta_s)$$

or

$$\tan\theta_{s_{max.}} = -\cot 2\theta_w$$

therefore

$$\theta_w = \pi/4 + \theta_{s_{max.}}/2 \qquad (41)$$

However, as shown in Table 2, this relation is not even a rough approximation when $M_1 < 4$. As a matter of fact, Eq. (41) is not even physically justified for extremely large M_1 since it was previously pointed out that the "exact" oblique shock flow equations are invalid for large M_1 because the heat transfer accompanying the extremely high temperatures produced by the shock is not considered in the theory. Actually, for large M_1 it would probably be best to use the relation Eq. (35)

$$\theta_w \to [(\gamma+1)/2]\theta_{s_{max.}}$$

and as a limit Eq. (34) yields

$$\lim_{M_1\to\infty} \theta_w \to \theta_s$$

Appendix II

Power Series Approximation for an Oblique Shock

The pressure coefficient (P) may be obtained from Eq. (25) as

$$P = (p_2 - p_1)/{}^1/_2\rho_1 V_1^2 = 2/[1 + (\cot\theta_w/\tan\theta_s)] \qquad (25')$$

Then from Eq. (27)

$$\sin^2\theta_w = \{[(\gamma+1)/4]M_1^2 P + 1\}/M_1^2$$

or

$$\cot^2\theta_w = \{(M_1^2 - 1) - [(\gamma+1)/4]M_1^2 P\}/\{[(\gamma+1)/4]M_1^2 P + 1\}$$

Therefore, assuming P is small and expanding in powers of P:

$$\cot \theta_w = \sum_{n=1}^{\infty} a_n P^{n-1} \tag{42}$$

where

$$a_1 = (M_1^2 - 1)^{1/2},\ a_2 = -[(\gamma + 1)/2^3]\,[M_1^4/(M_1^2 - 1)^{1/2}]$$

$$a_3 = \frac{(\gamma + 1)^2}{2^7}\,\frac{(3M_1^8 - 4M_1^6)}{(M_1^2 - 1)^{3/2}},\ a_4 = -\frac{(\gamma + 1)^3}{2^{10}}\,\frac{(5M_1^{12} - 12M_1^{10} + 8M_1^8)}{(M_1^2 - 1)^{5/2}}$$

$$a_5 = \frac{(\gamma + 1)^4}{2^{15}}\,\frac{(35M_1^{16} - 120M_1^{14} + 144M_1^{12} - 64M_1^{10})}{(M_1^2 - 1)^{7/2}}$$

$$a_6 = -\frac{(\gamma + 1)^5}{2^{17}}\,\frac{(63M_1^{20} - 280M_1^{18} + 480M_1^{16} - 384M_1^{14} + 128M_1^{12})}{(M_1^2 - 1)^{9/2}}$$

Then, assuming θ_s is also small

$$\tan \theta_s = \theta_s + (\theta_s^3/3) + (2\theta_s^5/15) + \ldots\ldots$$

and combining this with Eqs. (25′) and (42) gives

$$P = \sum_{n=1}^{\infty} b_n \theta_s^n \tag{43}$$

where

$$b_1 = 2/a_1,\ b_2 = -(b_1/a_1)(1 + a_2 b_1)$$

$$b_3 = -(1/a_1)(b_2 + 2a_2 b_1 b_2 + a_3 b_1^3 - {}^2/_3)$$

$$b_4 = -(1/a_1)[{}^1/_3 b_1 + b_3 + a_2(2b_1 b_3 + b_2^2) + 3a_3 b_1^2 b_2 + a_4 b_1^4]$$

$$b_5 = -(1/a_1)[{}^1/_3 b_2 + b_4 + 2a_2(b_1 b_4 + b_2 b_3) + 3a_3 b_1(b_1 b_3 + b_2^2) + 4a_4 b_1^3 b_2 + a_5 b_1^5 - (4/15)]$$

$$b_6 = -(1/a_1)[(2/15)b_1 + {}^1/_3 b_3 + b_5 + a_2(2b_1 b_5 + 2b_2 b_4 + b_3^2) + a_3(6b_1 b_2 b_3 + b_2^3 + 3b_1^2 b_4) + a_4 b_1^2(4b_1 b_3 + 6b_2^2) + 5a_5 b_1^4 b_2 + a_6 b_1^6]$$

The coefficients b_1 to b_6 could be computed for any M_1 directly from Eqs. (42) and (43). However, the coefficients b_1 to b_4 may be more conveniently written by combining Eqs. (42) and (43) to the form given in Eq. (32).

It is also useful to write Eq. (43) in the form

$$\theta_s = \left[\left(\frac{1}{b_1}\right)P - \left(\frac{b_2}{b_1^3}\right)P^2 + \left(\frac{2b_2^2 - b_1 b_3}{b_1^5}\right)P^3 + \left(\frac{5b_1 b_2 b_3 - b_1^2 b_4 - 5b_2^3}{b_1^7}\right)P^4 + \ldots\ldots\right] \tag{44}$$

or from Eq. (32)

$$\theta_s = \frac{(M_1^2 - 1)^{1/2}}{2}P - \frac{\{[(\gamma + 1)/4]M_1^4 - M_1^2 + 1\}}{4(M_1^2 - 1)^{1/2}}P^2 + \ldots\ldots$$

Eq. (44) may be used to determine the angle of stream tube deflection if the local pressure coefficient P is known.

Similarly, Eq. (42) may be transformed to an expression that would determine the local pressure coefficient if M_1 and θ_w are measured,

$$P = \left[\frac{1}{a_2}(\cot \theta_w - \sqrt{M_1^2 - 1}) - \frac{a_3}{a_2^3}(\cot \theta_w - \sqrt{M_1^2 - 1})^2 + \left(\frac{2a_3^2 - a_2 a_4}{a_2^5}\right)(\cot \theta_w - \sqrt{M_1^2 - 1})^3 + \ldots\ldots\right] \tag{45}$$

REFERENCES

[1] Laitone, Edmund V., *Letter to the Editor*, Journal of the Aeronautical Sciences, Vol. 12, No. 2, p. 220, April, 1945.

[2] Keenan, Joseph H., and Kaye, Joseph, *Thermodynamic Properties of Air*, pp. 36, 58; John Wiley & Sons, Inc., New York, 1945.

[3] Busemann, A., *Gasdynamik, Handbuch der Experimentalphysik*, Vol. 4, pp. 418–444; Wien-Harms, 1931.

[4] Sauer, Robert, *Theoretische Einführung in die Gasdynamik*, Springer-Verlag, Berlin, 1943.

(*Continued on page 58*)

The Bending of Rotor Blades*

ALEXANDER H. FLAX†

Piasecki Helicopter Corporation

Introduction

The problem of determining bending moments in rotor blades is a fundamental one in the design of rotating wing aircraft. Several methods for solving the problem have been proposed, both empirical and theoretical. In general, the theoretical methods have been so involved that most blade designers have had to take recourse to empirical or semiempirical methods. Recently, Owen[1] has shown that, in several cases for which he obtained more or less precise solutions of the differential equation for blade bending, Cierva's empirical formula[13] gave excellent agreement with the "exact" solutions for the bending moment. Owen's method is not, however, adaptable to the practical case of a blade of varying section. This has made it extremely worth while to determine the assumptions and limitations inherent in Cierva's formula, in order that it may be used with confidence in its range of applicability.

It will be the purpose of this paper to review the fundamental equations that govern blade bending; to indicate several possible methods of solution, together with the simplifying assumptions necessary for each; and to discuss the analytical basis for various approximate and empirical methods, particularly Cierva's formula. Finally, an extension to hinged rotor blades of the Stuart-Myklestad tabular method of propeller blade stress analysis[9, 10] will be made, together with some notes on numerical calculation.

The question of aerodynamic loading on the blade will not be discussed here, since it has been treated in considerable detail in a number of other papers.[5, 6]

Symbols

EI = bending stiffness

L = differential operator

$$\frac{d^2}{dr^2}\left(EI\frac{d^2}{dr^2}\right) - Q_r\frac{d^2}{dr^2} + \frac{pd}{dr}$$

M = moment on blade

m = mass per unit length

p = axial loading (centrifugal force) per unit length

Q_r = total centrifugal force acting on the cross-sectional area at r

r = radial distance from center of rotation to point on blade

S = shear on blade

t = transverse loading per unit length on blade

t_1 = transverse aerodynamic loading per unit length on blade

t_2 = inertia loading per unit length on blade

w = rate of change of beam shear dS/dr

y = blade bending deflection measured from line through hinge inclined at angle β

z = blade deflection measured from plane of rotation

β = blade flapping angle

ψ = blade azimuth angle measured from most downwind position

The Fundamental Equations for Blade Bending

The fundamental equations of blade bending may be derived by a consideration of Fig. 1. Here the blade resultant tranverse load per unit length is represented by t and the axial centrifugal load is represented by p. In general, t will be a function of r and ψ, while p will be a function of r only, for small displacements of the blade. The moment on a section through the blade at radius r is:

$$M = \int_r^R t(r_1 - r)dr_1 - \int_r^R p[(r_1 - r)\beta + (y_1 - y)]dr_1 \quad (1)$$

In accordance with usual beam theory, $M = EI(d^2y/dr^2)$, or

$$EI\frac{d^2y}{dr^2} = \int_r^R t(r_1 - r)dr_1 - \int_r^R p[(r_1 - r)\beta + (y_1 - y)]dr_1 \quad (2)$$

Differentiating Eq. (2) twice with respect to r,

$$\frac{d^2}{dr^2}\left(EI\frac{d^2y}{dr^2}\right) = t - p\beta - p\frac{dy}{dr} + \frac{d^2y}{dr^2}\int_r^R p\,dr_1 \quad (3)$$

This same equation may also be derived by consideration of the rate of change of shear on a differential length of blade, as shown in Fig. 2.

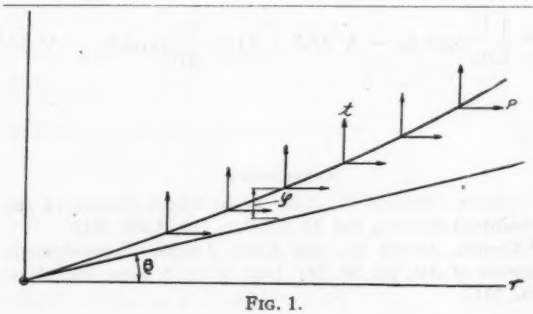

Fig. 1.

Received May 14, 1946.

* Acknowledgment is due to Miss Ida Leane Warren for her assistance in performing most of the numerical computations, in investigation of numerical methods, and in checking some of the mathematical development.

† Now, Assistant Head, Structures Department, Cornell Aeronautical Laboratory.

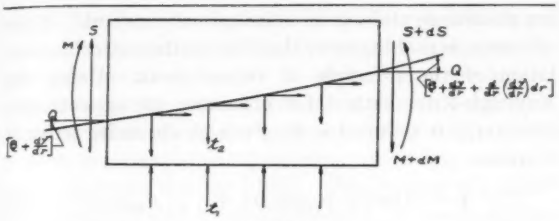

FIG. 2.

The transverse loading t is composed of two parts: one, t_1, the aerodynamic surface forces, and the other, t_2, the body forces, due to weight and inertia. Thus:

$$t = t_1 - m\left(g + r\frac{d^2\beta}{dt^2} + \frac{d^2y}{dt^2}\right) \qquad (4)$$

For blades of the type generally used in flapping rotors, the weight term, mg, is negligible in comparison with the aerodynamic and inertia loadings. The inertia term $m(d^2y/dt^2)$ is in most cases small compared to $mr \times (d^2\beta/dt^2)$ unless the periodic aerodynamic forces are in resonance with one of the natural bending frequencies of the rotating blade. In this connection, it must be noted that the aerodynamic loading, t_1, will also be altered somewhat by the deflection of the blade. At any section, the blade will have an additional transverse velocity dy/dt, which will change the local angle of attack and, hence, the aerodynamic loads. From the standpoint of resonance, this additional aerodynamic load will constitute a damping force. For most rotors conforming to current design practice, however, it appears that y is small and resonance in the flapping plane does not occur, at least below blade stall. Measurements on the British C 30 autogyro[2] have confirmed this.

Hufton, Nutt, Bigg, and Beavan[2] have included the effect of the d^2y/dt^2 term in an analysis of the C 30 rotor, but it does not appear to be important. In the analysis discussed in this paper, unless otherwise noted, the effect of blade flexibility on the aerodynamic and inertia loadings will be assumed to be neglected. In short, the transverse loading, t_1, will be that calculated for a hinged rigid blade.

The effects of torsional flexibility also appear to have been neglected in most blade bending analyses and will not be treated here. The influence of such torsional flexibility on blade loads, treated as a problem separate and distinct from the blade bending, may be found in papers by Wheatley[3] and Beavan and Lock.[4]

In the solutions to the blade bending problem of Owen,[1] Hufton, et al.,[2] and Cierva,[13] it is also assumed that the value of β is that obtained for a rigid blade, which again merely amounts to assuming that y is small compared to βr over most of the blade. In the Stuart-Myklestad[9, 10] method, it is not necessary to make this assumption. This matter is, however, worthy of some further discussion, since it suggests a means of simplifying the differential equation of the problem.

The value of β is determined from the condition that, for a hinged blade, the moments about the hinge must be zero. Writing the moment at the root from Eq. (1) ($r = 0$),

$$M = \int_0^R tr_1\,dr_1 - \int_0^R p\,(r_1\beta + y_1)dr_1 = 0 \qquad (5)$$

For a rigid blade $y_1 = 0$ or

$$\int_0^R tr_1\,dr_1 - \beta\int_0^R pr_1\,dr_1 = 0 \qquad (6)$$

It may readily be shown that the omission of the y_1 term in Eq. (5) is equivalent of the omission of the dy/dr term in Eq. (3). In the solutions of Owen, Hufton, et al., and Cierva, the value of β isdetermined on the basis of a rigid blade [Eq. (6)], but the dy/dr term is retained in Eq. (3). The dy/dr term is usually small compared to β (about 5 per cent maximum in a typical problem) so that it makes little difference in the solution. When β is computed from Eq. (6), there appears to be little theoretical justification for either procedure. It will later be found convenient for certain analyses to neglect the dy/dr term.

The basic equation to be solved in the theory of blade bending has been developed as

$$\frac{d^2}{dr^2}\left(EI\frac{d^2y}{dr^2}\right) - Q_r\frac{d^2y}{dr^2} + p\frac{dy}{dr} = t - p\beta \qquad (7)$$

where $Q_r = \int_r^R p\,dr_1$ is the total centrifugal force at any section. A mathematical solution of this equation for the general case where Q_r, EI, and p are arbitrary functions of r is extremely difficult; in fact, no such solution appears to have been attained even for the particular case of constant EI and mass distribution. Hufton, et al.,[2] have pointed out the slowness of convergence of a series solution. Various approximate methods of analysis, most of them laborous, have been proposed. It is next proposed to review a number of these methods, together with their basic assumptions and limitations.

VARIOUS METHODS OF SOLUTION

Collocation

Hufton, et al.,[2] have employed the method of collocation in the solution of the problem. Basically, this method assumes that the solution is given by the *finite* series of n terms.

$$y = A_1\phi_1(r) + A_2\phi_2(r) + \ldots A_n\phi_n(r) \qquad (8)$$

where the ϕ's are arbitrary functions of r except that they satisfy the boundary conditions and where the A's are undetermined constants. Values of $\phi_n(r)$ satisfying the boundary conditions may readily be formulated for most physical problems as algebraic poly-

nomials or trigonometric series. This expression for y is then substituted back into the differential Eq. (7), leading to an algebraic equation with the nA's as unknowns. Then n values of r corresponding to n arbitrary points on the blade are substituted successively into the equation leading to n equations in the n unknowns. It is thus assumed that the differential equation is satisfied at the boundaries and at the n arbitrarily chosen points on the blade. The degree of approximation is improved as more terms in the series are chosen. Following this procedure, one is left with the unpleasant task of solving a considerable number of simultaneous equations.

In the solution by Hufton, et al., the terms in dy/dr and d^2y/dt^2 are retained in the equation, but β is assumed to be the value obtained from the rigid blade equations.

Type Solutions

Owen[1] has solved the problem for a blade of constant EI and mass distribution by an essentially inverse method. Here a moment curve of some plausible shape is assumed, and the loading that produces such a moment is determined. Mathematically, this is a much simpler problem, and Owen has determined related loadings for a large class of useful moment curves, which he has named "type solutions." The procedure in solving a given problem is to find a type loading curve, or a linear combination of such curves, which represents a satisfactory approximation to the given loading. The moments will then be given by the corresponding type moment curve or linear combination of such curves.

The method is extremely useful for studying qualitative effects of changes in stiffness and blade weight for blades of constant section, but it is not at all suited for application to blades with arbitrary distribution of mass and stiffness such as frequently arise in helicopter practice.

Energy Solutions

The method of virtual work may be applied to the problem. It can be shown by Euler's equations of the Calculus of Variations that the exact solution of the differential Eq. (7) is given by the function y, which annuls the first order variation of the integral expression

$$I = \int_0^R \frac{EI}{2}\left(\frac{d^2y}{dr^2}\right)^2 dr + \int_0^R \frac{Q_r}{2}\left(\frac{dy}{dr}\right)^2 dr - \int_0^R t'y\, dr \quad (9)$$

where $t' = t - p\beta$. This may be expressed as

$$\delta I = 0 \quad (10)$$

when the variation is expressed by $y' = y + \epsilon\eta(r)$, where $\eta(r)$ is an arbitrary function satisfying the boundary conditions and ϵ is an infinitesimal constant. This, of course, is nothing more than the mathematical formulation of the principle of virtual work. Using the Rayleigh-Ritz method for obtaining an approximate solution, y is assumed to be given by the finite series of n terms

$$y = A_1\phi_1(r) + A_2\phi_2(r) + \ldots A_n\phi_n(r) \quad (11)$$

where the ϕ's are arbitrary functions satisfying the boundary conditions and the A's are constants to be determined. Eq. (10) is then replaced by the condition

$$\sum_{m=1}^{m=n} \frac{\partial}{\partial A_m}\left[\int_0^R \frac{EI}{2}\left(\frac{d^2y}{dr^2}\right)^2 dr + \int_0^R \frac{Q_r}{2}\left(\frac{dy}{dr}\right)^2 \times dr - \int_0^R t'y\, dr\right]\delta A_m = 0 \quad (12)$$

Upon substitution of Eq. (11) for y in Eq. (12), n simultaneous algebraic equations in the nA's result.

Galerkin's Method

Galerkin's method[7] is a generalization of the virtual work—Rayleigh-Ritz method for solving the differential equations of mechanics. Galerkin's method is, however, applicable to differential equations, whether they arise from mechanics or not. Let us write Eq. (7) in the form

$$L(y) - t' = 0 \quad (13)$$

where L is the differential operator

$$\frac{d^2}{dr^2}\left(EI\frac{d^2}{dr^2}\right) - Q_r\frac{d^2}{dr^2} + p\frac{d}{dr}$$

If an approximation for y other than the true solution is used, Eq. (13) will not be satisfied for all values of r. Instead,

$$L(y) - t' = \epsilon \quad (14)$$

where ϵ is the error of the approximation. The best approximate solution is obviously the one that makes the square of the error, integrated over the blade span, a minimum or

$$\int_0^R \left[L(y) - t'\right]^2 dr = \int_0^R \epsilon^2\, dr = \text{minimum} \quad (15)$$

If the finite series of Eq. (11) is substituted for y, this condition may be expressed as

$$\sum_{m=1}^{m=n} \frac{\partial}{\partial A_m}\left[\int_0^R \left\{L(y) - t'\right\}^2\right]\delta A_m = 0 \quad (16)$$

This again leads to n simultaneous equations for the n unknown A's.

Hohenemser's Method

Hohenemser[8] has applied what is basically Galerkin's method to the solution of the blade bending problem,

except that he converted the differential equation to an equivalent integral equation before proceeding with the minimization of the error. In Hohenemser's solution, only a single term is used for the unknown parameter of the problem, instead of a series similar to Eq. (11), so that, in general, close approximation is not to be expected over much of the blade. For the case of a blade of constant EI and mass distribution, Hohenemser has obtained the approximate solution

$$M = M_{RG}/[1 + 0.052(Q_0R^2/EI)] \tag{17}$$

where M_{RG} is the moment on a rigid blade. This solution has been obtained for constant, linear, and parabolic distributions of air load on the blade, without much change of the constant 0.052. It should be remarked here, that Hohenemser does not assume β to be the value for the rigid blade but rather determines its value for the flexible blade.

Successive Approximations

A method of successive approximations may be used to solve the integro-differential equation, Eq. (2), employing either analytical or numerical procedures. Denoting the successive values of y as, $y^{(0)}$, $y^{(1)}$, $y^{(2)}$, $\ldots y^{(n)}$, the following set of equations may be written

$$EI\frac{d^2y^{(0)}}{dr^2} = \int_r^R t(r_1 - r)dr_1 - \int_r^R p[(r_1 - r)\beta]dr_1$$

$$EI\frac{d^2y^{(1)}}{dr^2} = \int_r^R t(r_1 - r)dr_1 - \int_r^R p[(r_1 - r) \times \beta + (y_1^{(0)} - y^{(0)})]dr$$

$$\cdots\cdots\cdots\cdots\cdots\cdots\cdots\cdots\cdots\cdots$$

$$\cdots\cdots\cdots\cdots\cdots\cdots\cdots\cdots\cdots\cdots$$

$$EI\frac{d^2y^{(n)}}{dr^2} = \int_r^R t(r_1 - r)dr_1 - \int_r^R p[(r_1 - r) \times \beta + (y_1^{(n-1)} - y^{(n-1)})]dr_1 \tag{18}$$

Thus each succesive value of y may be obtained by direct integration. The process is continued until a satisfactory degree of agreement between $y^{(n-1)}$ and $y^{(n)}$ is obtained. Convergence will be rather slow because the moment relieving effect of the centrifugal tension, which is neglected in the determination of $y^{(0)}$, plays so large a part in the final result.

Cierva's Method

Cierva's method[13] was presented without proof as a rapid engineering method for obtaining rotor blade bending moments. The method is simple in application and consists of obtaining the bending moment for loads on a rigid but hinged blade, M_R, and the bending moment on a blade that is bent to the curvature it would have if only the centrifugal force resisted bending, M_f. M_R is readily obtained from Eq. (1) by setting y equal to zero. M_f is obtained by the following procedure. EI is set equal to zero in Eq. (7).

$$-Q_r\frac{d^2y}{dr^2} + p\frac{dy}{dr} = t - p\beta \tag{19}$$

This is equivalent to

$$(d/dr)[-Q_r(dy/dr)] = t - p\beta$$

or integrating,

$$Q_r(dy/dr) = \int_r^R (t - p\beta)dr \tag{20}$$

The integral on the left-hand side of Eq. (20) is the shear on a rigid blade as obtained from conventional beam theory. This may be denoted as S_r. Then

$$dy/dr = S_r/Q_r \tag{21}$$

The value of dy/dr is easily obtained, since both S_r and Q_r are basic quantities used in blade analysis. The value of M_f is obtained as

$$M_f = EI\frac{d^2y}{dr^2} = EI\frac{d}{dr}\left(\frac{S_r}{Q_r}\right) \tag{22}$$

The differentiation of (S_r/Q_r) is usually done graphically. Having the values of M_R and M_f Cierva gives the following formula for the bending moment on the blade:

$$M = M_RM_f/(M_R + M_f) \tag{23}$$

The Stuart-Myklestad Method

A tabular numerical method for propeller blade stress analysis has been presented by Stuart.[9] The method as presented originally required several repeated trials. Myklestad,[10] however, has shown how the procedure may be modified so that the necessity for repeated trials may be eliminated. This method, although intended for application to propellers, is directly applicable to blades having fixed root ends. It may be extended to blades having hinged ends without much difficulty.

In carrying out an analysis by this method, the blade is first divided into numbered stations at interval Δr apart. Midway between these stations are lettered stations as shown in Fig. 3. Then, from beam theory, to a degree of approximation which improves as Δr is made smaller:

$$\left(\frac{dz}{dr}\right)_b = \left(\frac{dz}{dr}\right)_a + \Delta r\left(\frac{M}{EI}\right)_1 \tag{24}$$

and

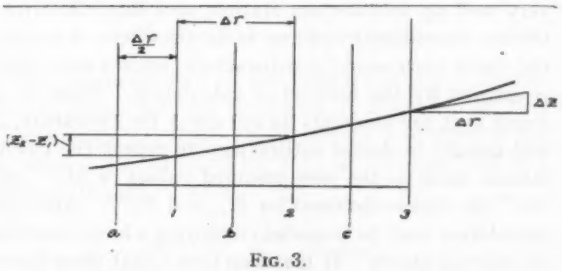

FIG. 3.

$$z_2 - z_1 = \Delta r(dz/dr)_b \tag{25}$$

Finally, the difference in moment between two stations is

$$M_2 = M_1 + \Delta r S_b + (z_2 - z_1)Q_b \tag{26}$$

The calculations may conveniently be set up in the tabular form given by Stuart. Dealing first with a fixed end blade, the moment at all points on the blade may be determined if the root end moment is known. This, of course, is not the case. The tip moment, however, mus be zero, and any value of root moment other than the correct one will not give this result. In the Myklestad method, an arbitrary value of root moment, $M_0^{(1)}$, is assumed, and the calculations of Eqs. (24) to (26) are made with the air-load shears acting on the blade; the resulting tip moment is called $M_T^{(1)}$. Then a second arbitrary moment, $M_0^{(2)}$, is assumed at the root, and the calculation is repeated without any shears acting on the blade; the resulting tip moment is called $M_T^{(2)}$. The moment, M_F, at any point on the fixed end blade is then given as

$$M_F = M^{(1)} - (M_T^{(1)}/M_T^{(2)})M^{(2)}$$

To take care of a blade hinged at the root, a unit value of dz/dr or coning angle is assumed at the root; no air-load shear is assumed to be acting; and a third set of moments on the blade, $M^{(3)}$, is obtained with the arbitrary root moment, $M_0^{(3)}$, and the arbitrary tip moment, $M_T^{(3)}$. Since the tip moment must be zero in this case too,

$$M^{(4)} = M^{(3)} - (M_T^{(3)}/M_T^{(2)})M^{(2)}$$

where $M^{(4)}$ is the moment at any point because of the unit coning angle at the root. Now the moments on a hinged blade may be obtained from the condition that the value of root moment must be zero, which gives

$$M_H = M_F - (M_{F_0}/M_0^{(4)})M^{(4)}$$

In making the calculations by means of this method, it is necessary to use a considerable number of significant figures and to retain the same number of decimal places throughout the calculation. Five decimal places have been found to be satisfactory in a number of cases. In any particular solution, it appears to be desirable to run a check table on the final solution wherein the moments obtained are checked against blade curvature. Often it has been found that the values of moment check very well up to a certain station, and then the errors become increasingly large up to the tip where, of course, the check must again be satisfactory, since a zero value is assured by the method of calculation. When it is found that the moments do not check the curvature, it will usually be found satisfactory to repeat the calculations using as the new assumed values of $M_0^{(1)}$ and $M_0^{(3)}$ the values obtained for M_{F_0} and $M_0^{(4)}$. Also, the calculation may be repeated employing a larger number of decimal places. It has been found that these latter procedures are more likely to be required with step tapered spars than with spars having no sudden changes of section.

Solution of the Bending Problem for a Special Case

For the special case where the ratio of centrifugal force to bending stiffness is constant, it is possible to obtain a simple solution for the bending equation. This case is of considerable interest for two reasons: First, it is a better approximation to actual conditions for a modern blade with step tapered spar than the common assumption of constant section; second, it provides a valuable insight into the theoretical basis for Cievra's method, as will be shown later.

If the dy/dr term is omitted from Eq. (7), (a step that is justified in the earlier part of this paper) and if $t - p\beta$ is replaced by $w(r)$, there is obtained:

$$\frac{d^2}{dr^2}\left(EI\frac{d^2y}{dr^2}\right) - Q_r\frac{d^2y}{dr^2} = w(r) \tag{30}$$

From fundamental beam theory,

$$M = EI(d^2y/dr^2)$$

which when substituted in Eq. (30) leads to

$$d^2M/dr^2 - (Q_r/EI_r)M = w(r) \tag{31}$$

Let Q_r/EI_r be some constant, say k^2; then,

$$d^2M/dr^2 - k^2M = w(r) \tag{32}$$

The boundary conditions to be satisfied are

$$M = 0 \quad \text{at } r = 0$$

$$M = 0 \quad \text{at } r = R$$

The loading $w(r)$ is arbitrary, but it is always zero at the root and at the tip, so that it may be represented by the following Fourier series:

$$w(r) = \sum_{n=1}^{\infty} A_n \sin(n\pi r/R) \tag{33}$$

where

$$A_n = \frac{2}{R}\int_0^R (w)r \sin\frac{n\pi r}{R}\,dr \tag{34}$$

in accordance with Fourier's Theorem.[14] A particular solution of Eq. (32) in operator form is

$$M = \frac{1}{D^2 - k^2}\sum_{n=1}^{\infty} A_n \sin\frac{n\pi r}{R} \tag{35}$$

This is easily solved to give

$$M = \sum_{n=1}^{\infty} -\frac{A_n}{(n\pi/R)^2 + k^2}\sin\frac{n\pi r}{R} \tag{36}$$

The complete solution to Eq. (32) is

$$M = A \cosh kr + B \sinh kr + \sum_{n=1}^{\infty} \frac{-A_n}{(n\pi/R)^2 + k^2} \times \sin (n\pi r/R) \quad (37)$$

By consideration of the boundary conditions, it is found that $A = B = 0$ or

$$M = \sum_{n=1}^{\infty} \frac{-A_n}{(n\pi/R)^2 + k^2} \sin \frac{n\pi r}{R} \quad (38)$$

The bending moment on a rigid blade may be obtained from Eq. (32) by setting $k = 0$, which leads to:

$$M_R = -\sum_{n=1}^{\infty} \frac{A_n}{(n\pi/R)^2} \sin \frac{n\pi r}{R} + C_1 r + C_2 \quad (39)$$

From the boundary conditions $C_1 = C_2 = 0$, and

$$M_R = -\sum_{n=1}^{\infty} \frac{A_n}{(n\pi/R)^2} \sin (n\pi r/R) \quad (40)$$

The bending moment on an entirely flexible blade, M_f, as described by Cierva may be obtained from Eqs. (30) and (22).

$$M_f = EI(d^2y/dr^2) = -EI(w(r)/Q_r)$$

or

$$M_f = -w(r)/k^2 \quad (41)$$

Using the Fourier series for $w(r)$,

$$M_f = -\sum_{n=1}^{\infty} (A_n/k^2) \sin (n\pi r/R) \quad (42)$$

Applying Cierva's formula,

$$M = \frac{\sum_{n=1}^{\infty} \frac{A_n}{(n\pi/R)^2} \sin \frac{n\pi r}{R} \sum_{n=1}^{\infty} \frac{A_n}{k^2} \sin \frac{n\pi r}{R}}{\sum_{n=1}^{\infty} \left[\frac{A_n}{(n\pi/R)^2} + \frac{A_n}{k^2} \right] \sin \frac{n\pi r}{R}} \quad (43)$$

This formula will be exactly equivalent to the "exact" solution Eq. (38) if the loading is given by a single harmonic of the Fourier series, or if Cierva's method is applied separately to the moments resulting from each harmonic loading term, and the results added. In this connection it should be noted that for conditions that lead to maximum blade moments (aerodynamic and centrifugal components) the loading curve does not differ too greatly from a sinusoidal shape over the first half of the blade.

Eq. (38) provides a fairly simple solution to the bending problem for the blade of constant Q_r/EI_r or for blades that approximate this. The Fourier loading coefficients A_n are not difficult to obtain using Eq. (34), if only a few terms are used, and, if greater accuracy is desired, more terms may readily be obtained by some numerical scheme such as Runge's method. The main value of this solution, however, lies in the insight into Cievra's method which it provides.

Analytical Basis for Cierva's Method

In order to provide a sound basis for the general comprehension and application of Cierva's method, the establishment of a theoretical basis for it seems essential. The results obtained for the blade of constant Q_r/EI_r may, in fact, be generalized so that no limitation need be placed on either Q_r or EI_r except that they remain bounded and piecewise smooth functions, which is more a mathematical, than a practical, restriction.

Suppose the variations in EI_r and Q_r are given as

$$\left.\begin{aligned} EI_r &= EI_0\, m(r) \\ Q_r &= Q_0 n(r) \end{aligned}\right\} \quad (43)$$

Then

$$\frac{Q_r}{EI_r} = \frac{Q_0}{EI_0} \frac{n(r)}{m(r)} = \mu q(r) \quad (43a)$$

Eq. (31) for blade bending may then be written

$$(d^2M/dr^2) - \mu q(r) M = w(r) \quad (44)$$

This is still subject to the boundary conditions

$$M(0) = 0$$
$$M(R) = 0$$

Now consider the equation

$$(d^2M/dr^2) + \mu q(r)\, M = 0 \quad (45)$$

This equation for the specified boundary conditions can only have a solution for certain values of M, say $\lambda_1, \lambda_2 \lambda_3, \ldots \lambda_n$ as is demonstrated in Courant-Hilbert.[11] These values of u are called characteristic or "eigen" values. To each characteristic value λ_n corresponds a characteristic function ϕ_n which satisfies the equation.

In the special case previously solved, where q is a constant, it may readily be seen that $\lambda_n = (n\pi/R)^2$ and

$$\phi_n = \sin n\pi_r/R$$

It can be demonstrated[11] that an equation of type similar to Eq. (45) will have an infinite denumerable number of λ's. Also, the system of functions ϕ_n will be orthogonal—i.e.,

$$\int_0^R q(r)\phi_n\phi_m dr = 0 \quad (m \neq n) \quad (46)$$

The characteristics of the differential Eq. (45) discussed above may be employed as indicated by von Kármán (see reference 12) to obtain a solution of the equation. Returning to Eq. (44), $w(r)$ is expanded as a series in the functions ϕ_n

$$w(r)/q(r) = \sum_{n=1}^{\infty} A_n \phi_n(r) \quad (47)$$

The coefficients A_n may be determined by a method analogous to that used in determining the coefficients of a Fourier series, and as in the case of Fourier constants, the determination is made possible by the orthogonality condition, Eq. (46), plus the normalizing condition,

$$\int_0^R q(r)[\phi_n(r)]^2 dr = 1 \tag{48}$$

Eq. (48) merely has the effect of fixing the amplitude of the ϕ function, so that the magnitude of the A_n's is set. Multiplying both sides of Eq. (47) by $\phi_n(r)q(r)$, the formula for A_n is obtained as

$$A_n = \int_0^R w(r)\phi_n(r)dr \tag{49}$$

The solution to Eq. (44) may also be expanded as a series

$$M = \sum_{n=1}^{\infty} a_n\phi_n(r) \tag{50}$$

Substituting Eqs. (47) and (50) into Eq. (44),

$$\sum_{n=1}^{\infty} a_n \frac{d^2\phi_n(r)}{dr^2} - \mu q(r) \sum_{n=1}^{\infty} a_n\phi_n(r) = q(r) \sum_{n=1}^{\infty} A_n\phi_n(r) \tag{51}$$

Now, since each function ϕ_n satisfies Eq. (45) for $\mu = \lambda_n$,

$$\frac{d^2\phi_n(r)}{dr^2} + \lambda_n q(r)\phi_n(r) = 0$$

or

$$d^2\phi_n(r)/dr^2 = -\lambda_n q(r)\phi_n(r) \tag{52}$$

Putting Eq. (52) into Eq. (51),

$$-\sum_{n=1}^{\infty} a_n[\lambda_n q(r)\phi_n(r) + \mu q(r)\phi_n(r)] = \sum_{n=1}^{\infty} q(r)A_n\phi_n(r)$$

which is satisfied if

$$a_n = -A_n/(\lambda_n + \mu) \tag{53}$$

Thus,

$$M = -\sum_{n=1}^{\infty} A_n\phi_n(r)/(\lambda_n + \mu) \tag{54}$$

A result entirely analogous to Eq. (38) is obtained for the special case.

The rigid blade bending moment is readily obtained as

$$M_R = -\sum_{n=1}^{\infty} A_n\phi_n(r)/\lambda_n \tag{55}$$

The bending moment for the perfectly flexible blade is

$$M_f = -\sum_{n=1}^{\infty} A_n\phi_n(r)/\mu \tag{56}$$

Now according to Cierva's formula

$$M = \frac{-\sum_{n=1}^{\infty} \frac{A_n\phi_n(r)}{\lambda_n} \sum_{n=1}^{\infty} \frac{A_n\phi_n(r)}{\mu}}{\sum [(A_n/\lambda_n) + (A_n/\mu)]\phi_n(r)} \tag{57}$$

Again, it may be seen that Cierva's method agrees with the "exact" solution only if the loading can be described by a single characteristic function ϕ_n or if the loading is expressed as a series of such functions and Cierva's method applied to each term separately. While it is possible to determine the $\phi_n(r)$ functions by a number of analytical and numerical methods, it is not suggested that this constitutes a practical method of analysis. The main reason for consideration of this method here is that it provides a mathematical foundation for Cierva's method and indicates its inherent limitations.

It may be concluded from our study that the accuracy of Cierva's method will depend upon the nature of the loading and upon the variation of the $q(r)$ function for the blade. For the case of $q(r)$ constant or constant ratio of centrifugal force to bending stiffness along the blade, which is of some practical value, the ϕ functions are of the form $\sin n\pi r/R$. Where the value of $q(r)$ does not vary greatly from a constant, ϕ_n should not vary greatly from the sinusoidal form. Thus, for a number of practical cases, Cierva's method will become more or less accurate as the loading curve deviates less or more from a sinusoidal form. Further, Cierva moments determined over parts of the blade where sinusoidal restrictions on loading are complied with are in better agreement with the true bending moment than Cierva moments over other parts of the blade.

What is actually done in applying Cierva's method as indicated in Eq. (57) is to apply to the entire series an average correction of the type indicated in Eq. (54) for each term in the series of "eigen" functions. If one term predominates, the Cierva method will automatically give a correction nearly corresponding to this term. It is not necessary, of course, to know which term does predominate, or even what the "eigen" functions are, in order to apply the Cierva method. If no one "eigen" function predominates in the loading, the error in applying Cierva's method will be somewhat greater, but the procedure will always lead to a mean correction. For this reason, it is much more satisfactory for application to arbitrary loadings than any single factor correction formula such as Hohenemser's. The single factor correction formula generally corresonds to a single characteristic (or "eigen") function; if it is applied to a loading in which other "eigen" functions predominate, errors of larger magnitude will result. This may be readily realized by looking back at Eq. (38) for the blade of constant Q_r/EI. If a single term correction formula were derived on the basis of a first harmonic loading ($n = 1$) and then applied to an arbitrary loading in which the third harmonic ($n = 3$) predominated, the tremendous error is apparent.

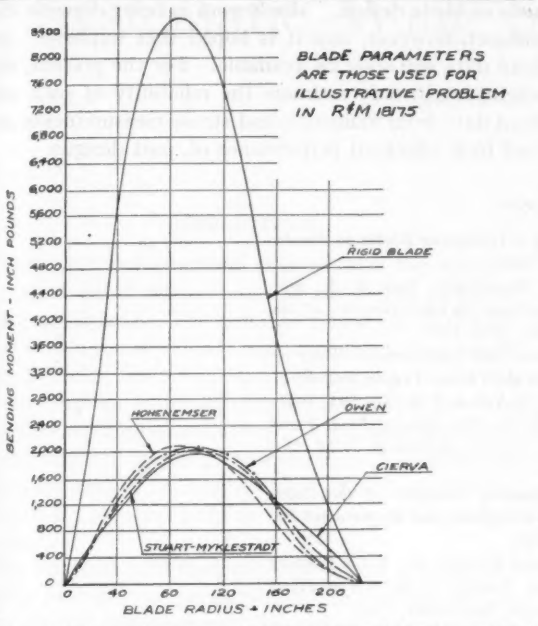

FIG. 4. Blade bending moments by various methods. Blade of constant section.

COMPARISON OF VARIOUS METHODS

Numerical computations were carried out by several methods in order to compare the accuracy of the method and the amount of labor involved. First, the blade of constant section chosen by Owen[1] for his illustrative problem was investigated by comparing Owen's solution with those obtained by the Cierva, Hohenemser, and Stuart-Myklestad methods. The results are shown in Fig 4

Owen's "exact" solution and the Stuart-Myklestad solution are found to be in good agreement. Owen's results show slightly higher moments over most of the blade, particularly in the region of maximum moment, than those obtained by the Stuart-Myklestad method. This is due to the fact that Owen neglects the change in β from the rigid blade value, whereas the Stuart-Myklestad method accounts for the change.

The Cierva method compares favorably with the more precise methods over the first 65 per cent of the blade. It is considerably in error on the conservative side on the outer 35 per cent of the blade. Near the point of maximum moment, the Cierva method differs from the Stuart-Myklestad value by about 4 per cent on the unconservative side

Hohenemser's method shows the poorest agreement with the Stuart-Myklestad curve over most of the blade length and, in fact, does not indicate the correct point of maximum moment, which the other methods all do. This is, of course, a result of the fact that the curve obtained by the Hohenemser method must be of the same shape as the rigid blade moment curve. It is of interest to note that the Hohenemser curve differs from the more precise solutions first on the conservative side, then on the unconservative side, in such a way as to make the root mean square error small, which is in fact the basis of its derivation.

In evaluating the merits of the various methods from a design standpoint, it should be remembered that with a flapping hinge, the design of the spar of constant section will be based on the maximum centrifugal force at the root or the combination of centrifugal force and bending moment at some point near the point of maximum moment. Thus, the failure of Cierva's method to predict correctly the moments on the outer part of the blade will be of little importance. It may then be concluded that, for blades of constant section and blade properties, Cierva's method is a completely satisfactory engineering design method. Where greater accuracy is desired, the revised Stuart-Myklestad seems to offer the quickest "exact" solution and is more suited to manipulation by engineering personnel than the collocation, energy methods, type solutions, or successive approximations.

For the case of typical step tapered spar, a comparison of Cierva's method with the Stuart-Myklestad solution for hovering is shown in Fig. 5. It may be seen that over most of the inner part of the blade the Cierva solution underestimates the moment by a maximum of 16 per cent in one spot. On the outer part of the blade, the Cierva moments are as much as 250 per cent too high at $r/R = 0.65$ and still diverging. This is more serious in a step tapered spar than in a spar of constant section, since the outboard sections are designed largely by the value of the moment there. If weight is not too important, the spar could be designed by Cierva's method allowing an appreciable margin over the inboard 50 per cent of blade and using the calculated values over the outer 50 per cent. This is also a good basis for preliminary design. For an "exact"

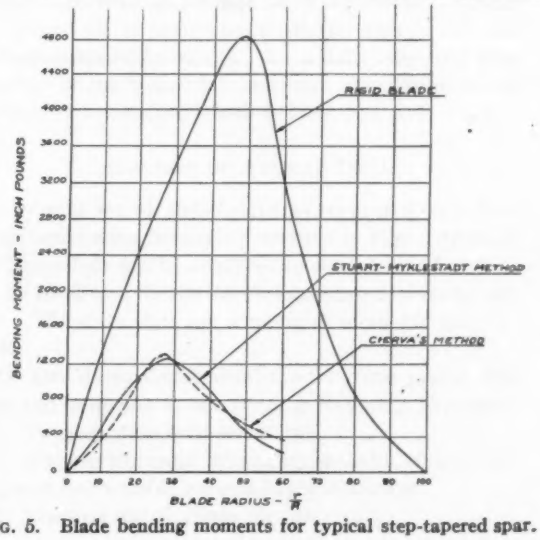

FIG. 5. Blade bending moments for typical step-tapered spar.

solution, to obtain the minimum section, the revised Stuart-Myklestad method appears to be required.

It should be kept in mind that the air-load data must be fairly reliable to justify accurate methods of blade design. At present, this is probably the greatest weakness of blade design. Much work is being done on the subject, however, and it is hoped that improved air-load data will soon be available. For the present, the engineer can only estimate the reliability of such air-load data from deflection and strain measurements on, and from observed performance of, past designs.

References

[1] Owen, J. B. B., *The Stressing of Gyroplane Blades in Steady Flight*, British R. & M. No. 1875, 1939.

[2] Hufton, P. A., Nutt, A. E. Woodward, Bigg, F. J., and Beavan, J. A., *General Investigation into the Characteristics of the C 30 Autogyro*, British R. & M. No. 1859, 1938.

[3] Wheatley, J. B., *An Analytical and Experimental Study of the Effect of Periodic Blade Twist on the Thrust, Torque, and Flapping Motion of an Autogyro Rotor*, N.A.C.A. T.R. No. 591, 1937.

[4] Beavan, J. A., and Lock, C. N. H., *The Effect of Blade Twist on the Characteristics of the C 30 Autgoyro*, British R. & M. No. 1727, 1936.

[5] Wheatley, J. B., *An Aerodynamic Analysis of the Auto-Rotor with a Comparison Between Calculated and Experiment Results*, N.A.C.A. T.R. No. 487, 1934.

[6] Klemin, A., Walling, W. C., and Wiesner, W., *Rotor Bending Moments in the Plane of Flapping*, Journal of the Aeronautical Sciences, Vol. 9, No. 11, pp. 411–418, September, 1942.

[7] *Principles of the Galerkin Method*, British R. & M. 1848, 1938.

[8] Hohenemser, K., *Zur Festigkeit von umlaufenden und quer zur Drehebene belasteten Staben, die gelenkig an die Drehachse angeschlossen sind*, Ingenieur-Archiv, BD VIII, Heft 3, pp. 203–213, June, 1937.

[9] Stuart, J., *A Tabular Method of Propeller Blade Stress Analysis*, Journal of the Aeronautical Sciences, Vol. 10, No. 4, pp. 115–118, April, 1943.

[10] Myklestad, N. O., *Letter to the Editor*, Journal of the Aeronautical Sciences, Vol. 10, No. 10, p. 319, October, 1943.

[11] Courant, R., and Hilbert, D., *Methoden Der Mathematischen Physik*, Vol. I; Julius Springer, Berlin, 1931.

[12] von Kármán, Th., *Use of Orthogonal Functions in Structural Problems*, Stephen Timoshenko 60th Anniversary Volume; The Macmillan Company, New York, 1938.

[13] de la Cierva, J., *New Developments of the Autogyro*, Journal of The Royal Aeronautical Society, Vol. 39, 1935.

[14] von Kármán, Th., and Biot, M., *Mathematical Methods in Engineering*; McGraw-Hill Book Company, Inc., New York, 1940.

Systematic Wing Section Development

GEORGE S. SCHAIRER*
Boeing Aircraft Company

Introduction

THE AIRPLANE DESIGNER is faced with the selection of an airfoil section early in the design phases of each new airplane. The airfoil section is one of the airplane design items which is seldom changed once an airplane is built. This is necessary because so much of a modern airplane is intimately associated with the wing structure and changing the airfoil is usually tantamount to designing and building a new airplane. Therefore it is important that a reasonably good choice of airfoil is made in the shortest possible time at the start of each design.

The designer finds that the wing on the average airplane is probably the primary factor in defining the airplane general arrangement. First of all the span, area, dihedral, sweep, and taper are important. Then the airfoil section itself is important. The section usually varies from root to tip and this variation is also important. Some of the more significant airfoil factors are:

(1) *Drag.* The drag of a wing is principally controlled by the airfoil section and its surface condition.

(2) *Lifts.* The primary purpose of a wing is to produce lift. The lift characteristics usually control the stability.

(3) *Moments.* The moment of the wing is structurally important and affects the stability.

(4) *Stalling.* The airfoil section usually defines the stalling characteristics of an airplane.

(5) *Compressibility.* The airfoil section is the primary factor determining the effect of Mach Number on airplane characteristics.

(6) *Flaps.* The ability of an airfoil to be highly flapped is frequently important.

(7) *Ailerons.* Aileron design is intimately associated with airfoil design.

(8) *Structure.* Airfoil proportions, particularly thickness, are important in defining structure.

(9) *Construction.* Airfoil proportions greatly affect the simplicity and ease of construction.

(10) *Landing Gear.* In many airplanes the wing is called upon to house the landing gear and this imposes space requirements upon the airfoil.

(11) *Wing Volume.* The wing is usually called upon to house fuel and sometimes engines. The volume requirement will frequently design wing thickness.

(12) *Deicing.* The problem of wing deicing is directly related to leading edge shape.

(13) *Flutter.* The flutter characteristics of an airplane are frequently controlled by airfoil proportions.

Tested Airfoils

The airplane designer has almost a limitless number of tested airfoils to choose from. The National Advisory Committee for Aeronautics has been active since its beginning in presenting data on airfoils. Many of these airfoils were tested in systematic series and the results have been presented in reports such as N.A.C.A. T.R. Nos. 460 and 610. In view of the large number of airfoils tested it would seem that the field should be well covered and little room for improvement should remain. Such a stand does not bear much investigation. There is still much to be learned about the behavior of airfoils. A great deal of theoretical work has been done to predict and explain the flow over airfoils. It has been found that theory and experiment agree very well in flows where separations do not exist. In addition, thick boundary layers cause divergence of experiment from theory. These theories, in general, are primarily for incompressible flows, and extensions to include the effects of compressible fluids are only satisfactory when no part of the flow approaches sonic conditions. However, most airplanes are designed to operate without flow separation on the airfoil except when approaching the stall and are flown at speeds where compressibility effects are reasonably accounted for by theory. This means that, with usable airfoils, it is possible to predict by theory all of their characteristics except the stall and compressibility effects. A partially empirical presentation of the basic characteristics of common airfoils is given by Jacobs and Rhode in N.A.C.A. R.T. No. 631.

Analysis of Airfoil Data

A typical set of airfoil data as measured in a two-dimensional wind tunnel is presented in Figs. 1 through 7. These data will be analyzed to show how a few tests can be used to indicate the characteristics of many airfoils. The data that are sometimes available may include:

(1) Two-dimensional wind-tunnel data giving lift, drag, and moments at one or more Reynolds Numbers.

(2) Pressure distributions for (1).

(3) Two-dimensional wind-tunnel data giving lift, drag, and moments at various Mach Numbers.

(4) Pressure distributions for (3).

Presented at the Aerodynamics Session, Fourteenth Annual Meeting, I.A.S., New York, January 29–31, 1946.

* Staff Engineer, Aerodynamics and Powerplants.

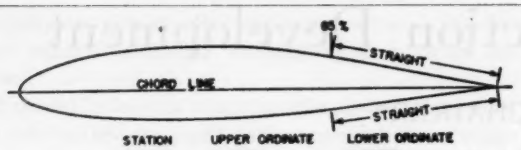

STATION % CHORD	UPPER ORDINATE % CHORD	LOWER ORDINATE % CHORD
0	.395	0
.50	1.580	1.110
.75	1.880	1.350
1.250	2.365	1.755
2.50	3.235	2.480
5.00	4.450	3.400
7.50	5.340	4.010
10	6.080	4.505
15	7.215	5.240
20	8.039	5.730
25	8.572	6.025
30	8.870	6.125
35	8.980	6.105
40	9.000	6.035
45	8.920	5.925
50	8.635	5.685
55	8.125	5.310
60	7.420	4.815
65	6.575	4.235
70	5.640	3.635
75	4.700	3.029
80	3.760	2.423
85	2.820	1.818
90	1.880	1.211
95	.942	.606
100	0	0

LEADING EDGE RADIUS = 1.975
α_c = 5° 6'

FIG. 1. B.A.C. No. 53, airfoil and ordinates.

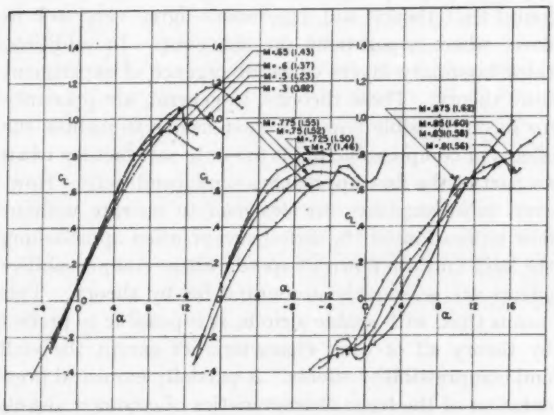

FIG. 2. C_L vs. α at various Mach Numbers. B.A.C. No. 53 airfoil. Note: Number in parentheses indicates R.N. in millions.

(5) Effects of surface condition and turbulence on characteristics as measured in two-dimensional wind tunnels or in flight.

(6) Three-dimensional test data on wings incorporating the airfoil.

The sample data presented in Figs. 1–6 do not include all possible tests but are sufficiently complete to be useful in understanding some of the phenomena to be encountered. An analysis of the pressure data explains many things. In many ways, pressure data are easier to use when the pressures at any point are plotted versus angle of attack or normal force coefficient which

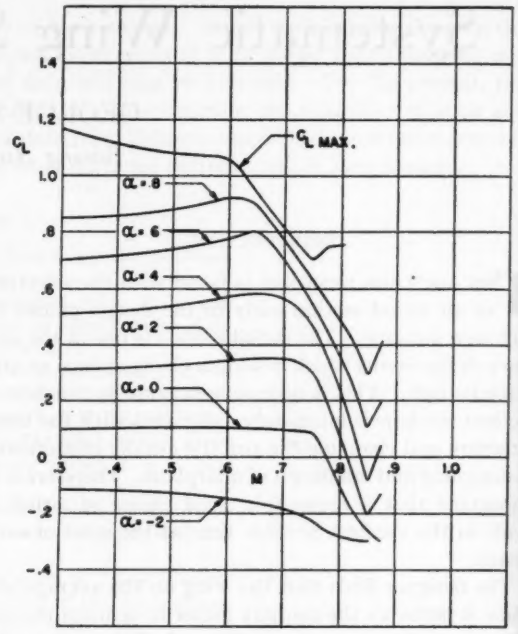

FIG. 3. C_L vs. Mach Numbers. B.A.C. No. 53 airfoil. Cross-plot of Fig. 2.

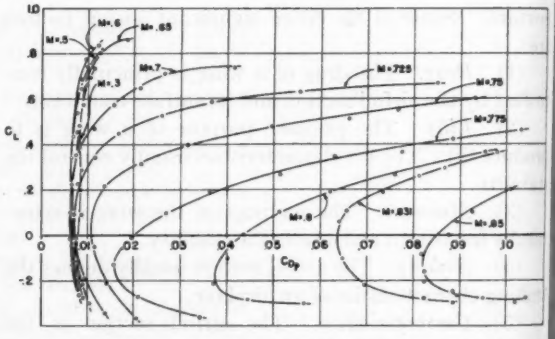

FIG. 4. C_D vs. C_L at various Mach Numbers. B.A.C. No. 53 airfoil. Drags measured by wake survey.

is usually even better. The data of Fig. 6 are replotted versus normal force coefficient in Fig. 7. It will be noticed that, for nearly all points, the variation of pressure coefficient with normal force coefficient is approximately linear. Theory, however, indicates that the velocity and not the pressure should be linear. The pressures can be converted to velocities by the use of Bernouli's equation, which indicates that the square root of the pressure coefficient will be the ratio of velocity to free-stream velocity. The velocity ratio or square root of the pressure coefficient is plotted versus normal force coefficient in Fig. 8. In this plot the variations are more nearly linear. Theory indicates, and experiment confirms, that the variation of velocity coefficient with lift is nearly identical at each per cent chord station for all airfoils. In general, differences occur only in the

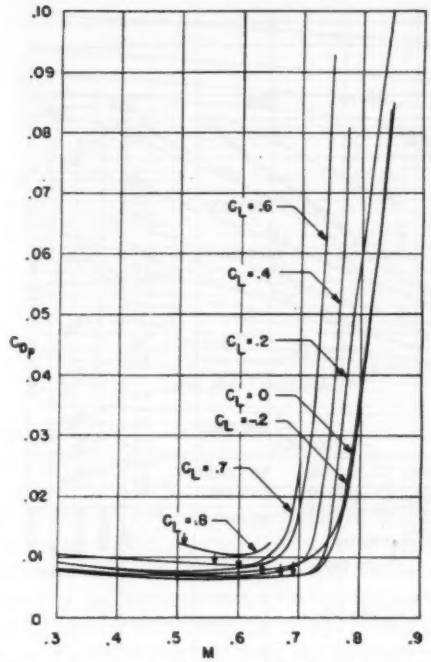

FIG. 5. C_D vs. Mach Numbers. B.A.C. No. 53 airfoil. Cross-plot of Fig. 4.

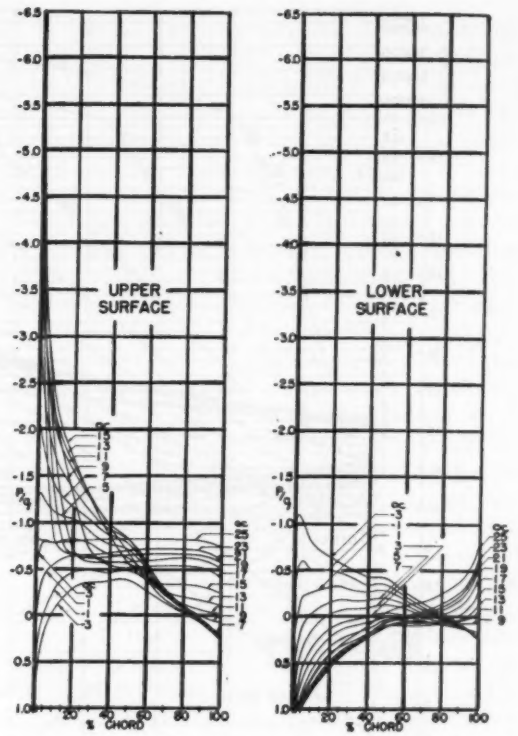

FIG. 6. Pressure distribution over B.A.C. No. 53 airfoil. M = 0.10, R.N. = 1.43×10^6.

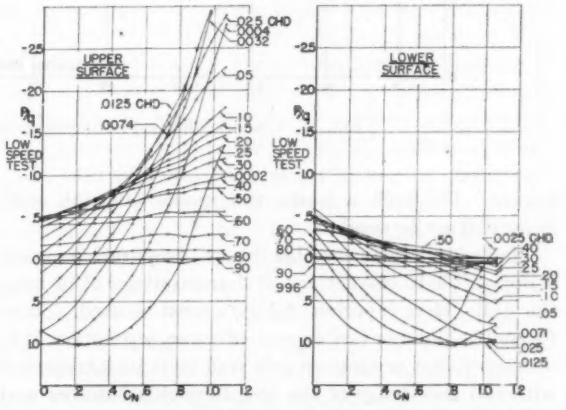

FIG. 7. Surface pressure P/q vs. C_N for B.A.C. No. 53 airfoil. M = 0.10, R.N. = 1.43×10^6.

first 1 or 2 per cent of airfoil chord. Since pressures are more useful experimentally, it is convenient to plot pressures on graph paper with a distorted scale so that a vertical scale is linear in velocity ratio rather than pressure. Examination of pressure data on a large number of airfoils indicates that appreciable variations in the pressures from those given by extrapolations using standard slopes of velocity with lift occur only when separation begins. The pressures or velocities at zero lift are a function of the airfoil shape. If the airfoil were symmetrical, the pressures or velocities would be symmetrical and, therefore, any differences from symmetry can be ascribed to the camber. From tests on a few airfoils it is possible to determine the velocities for many camber lines and thickness variations. For moderate variations in camber or thickness ordinates the velocities can be assumed to be proportional to the ordinate when all ordinates are uniformly increased or decreased.

The characteristics of the airfoil without separation can be related to the physical shape by means of the pressure distributions. The slope of lift curve for infinite aspect ratio must be estimated from experimental data but is not susceptible to much variation. The moment coefficient is constant about some aerodynamic center. The value of this moment coefficient will be independent of aerodynamic center at zero lift and is therefore a function only of the camber. From the pressure data the moment coefficient for each camber line can be computed. The aerodynamic center is defined by the variation of pressures with lift, and, since this is nearly identical for all airfoils, there will be little variation of aerodynamic center between airfoils with the center usually lying just ahead of the quarter chord. The effect of camber on the angle of attack for zero lift is obtainable directly from the camber data. Drags cannot be computed so easily. When separation does not exist, the drags will be determined primarily by the relative amounts of laminar and turbulent flow. In some cases pressures will define the transition point, but in nearly all practical cases the transition will be determined by constructional details and by such items as

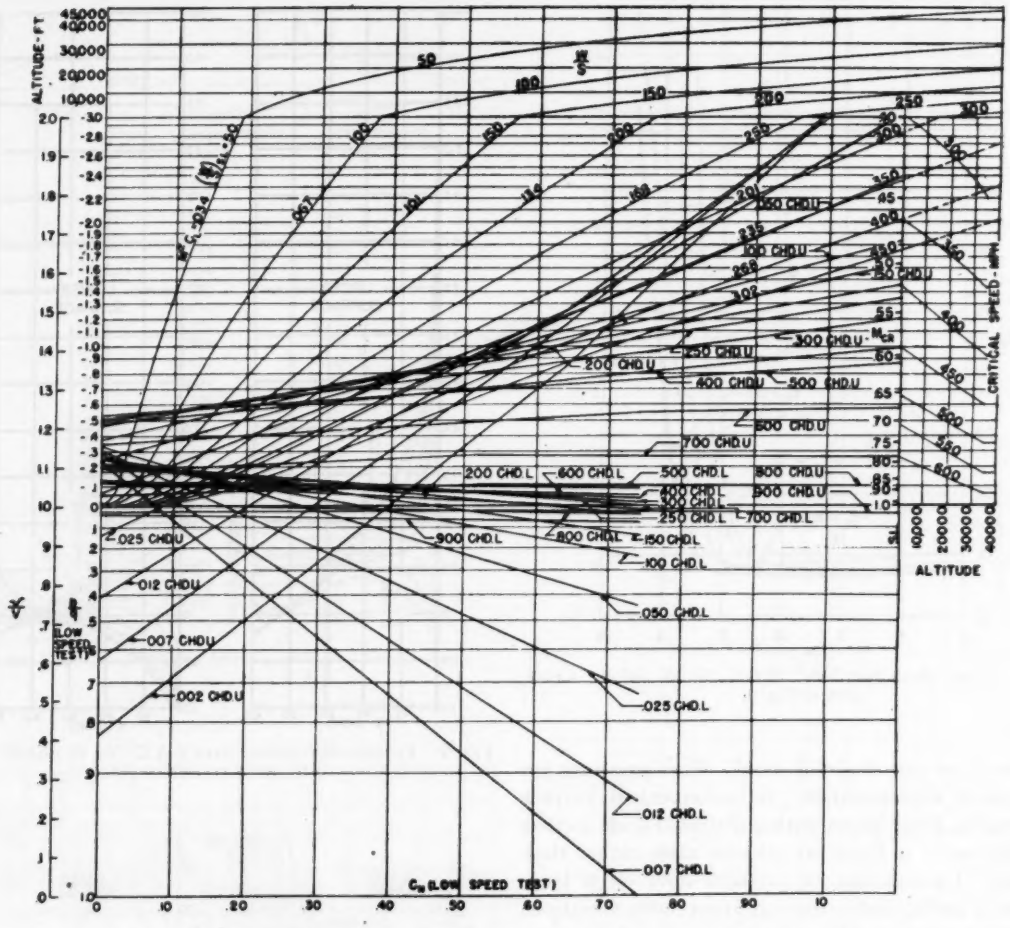

FIG. 8. Compressibility plotting form with data from Fig. 7. B.A.C. No. 53 airfoil.

deicers. On such a basis, the model and full-scale drags will not be similar.

The lack of any reasonable theory of separation makes it impossible to predict airfoil characteristics at or near the stall. Here experimental data must be used. Since Reynolds Number has a great effect on separation, it is necessary that separation and stall tests be intrepreted with full knowledge of the test Reynolds Number and possible effects of its variation. Much information on this subject has been given by the N.A.C.A. in reports such as T.R. No. 586. Some classes of airfoils are susceptible to Reynolds Number effects, while others are not. In general, increasing the Reynolds Number increases the maximum lift and delays separation. The stall characteristics eventually deteriorate at high Reynolds Number. If all other things remain equal, it will usually be desirable to use an airfoil not greatly affected by Reynolds Number, since in this case wind-tunnel tests of a complete model can be expected to give reliable stability and control data. Although drag savings, indicated by model tests in regions where separation exists, may not actually exist full scale, it will nearly always be conservative to use the airfoil that shows desirable characteristics at model scale. In such cases it will not be necessary to call upon Mr. Reynolds to correct in the airplane deficiencies found in the model which are attributed to him. Experience has shown that seldom are difficulties encountered full scale which cannot be found in tests of a model with a span of 7 to 9 ft., as are currently used for nearly all development testing. The converse is not always true. Model defects do not always show up full scale, but to assume that they will not is dangerous. In most cases, the tuft appearance of separations and the stalls is not greatly affected by Reynolds Number. Usually, the difference between good and bad stall characteristics lies in the rate of progress and location of the separation. These can be easily evaluated in model tests and are important criteria to be examined.

COMPRESSIBILITY

Compressibility characteristics can be evaluated very well in most cases from two-dimensional tests. Fig. 9

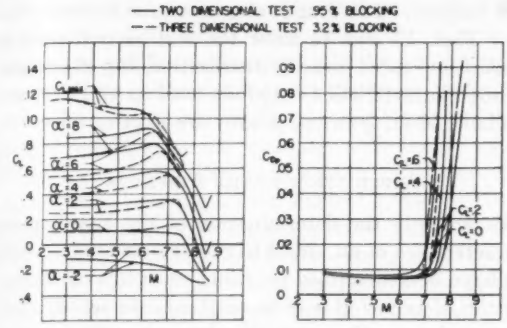

FIG. 9. Comparison of two-dimensional and three-dimensional airfoil tests. B.A.C. No. 53 airfoil.

compares two-dimensional with three-dimensional airfoil data for the B.A.C. No. 53 airfoil. The lift data are by forces in both cases. The drag data are by force in the three-dimensional case and by wake survey in the two-dimensional case. Excellent agreement has been found in several such cases. When the three-dimensional test conditions are not favorable, better results can be obtained two dimensionally. Such a case is shown in Fig. 10 where the three-dimensional model results were badly affected by blocking in at least one case. None of the data presented in this report has been corrected in any way for blocking. It is of great interest to be able to predict the compressibility characteristics. Using the relationship of von Kármán for the critical Mach Number (Mach Number for attainment of supersonic flow), it is possible to compute Mach Numbers for which supersonic flow is just attained. Using the Kármán-Tsien relationship to predict this critical Mach Number and the Glauert relationship to compute lift coefficient, it is possible to obtain estimates of the critical Mach Number and the lift coefficient at that Mach Number corresponding to a given low-speed pressure peak and lift coefficient. A convenient chart for making such calculations has been developed. For each low-speed pressure peak value there will be a critical Mach Number in accordance with the Kármán-Tsien relationship. At this Mach Number the lift coefficient is increased over the low-speed value by the Glauert relationship.

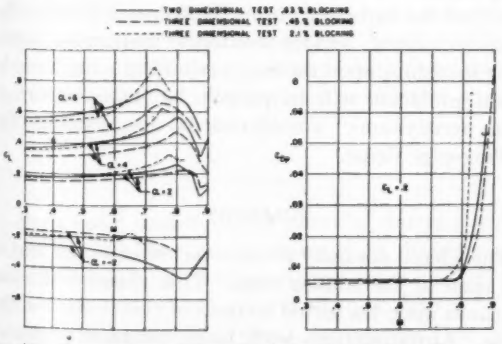

FIG. 10. Comparison of two-dimensional and three-dimensional airfoil tests. B.A.C. No. 100 airfoil.

In the application to an airplane, it is speeds and wing loadings that are of interest and not Mach Numbers and lift coefficients. Mach Number can be easily converted to speed as accomplished at the right of Fig. 8. By definition $W/S = (\rho/2)V^2C_L$. This is readily converted to $W/S = (\rho/2)a^2M^2C_L$. It can be shown that $a^2(\rho/2) = p(\gamma/2)$. Then $W/S = p(\gamma/2)M^2C_L$ or $W/S = (p/p_0)\ 1{,}485M^2C_L$. On Fig. 8 lines of constant M^2C_L have been drawn for conditions of lift coefficient and Mach Number at the start of supersonic flow. The lift coefficient scale at the bottom of the page is for low speeds as just explained. At the top of Fig. 8, scales are given to interpret M^2C_L as wing loading at various altitudes. This chart is used by plotting upon it either the envelope of pressure data or the complete pressure data, as in Fig. 8 and explained previously. The graph has been made to have a linear velocity ratio vertically. From this plot a given wing loading and altitude may be chosen at the top and followed downward along a constant M^2C_L line to the envelope of experimental data. Then, moving horizontally to the right, the critical Mach Number and speed at the altitude chosen can be read. In this manner the low-speed pressure data can be rapidly evaluated. It is interesting to note that in some cases the constant lift (M^2C_L) lines cross the airfoil data at two points. There is a high speed above which supersonic flow is obtained and a low speed below which it also occurs. The meaning of this is of great importance, for it can be seen that there is a wing loading above which supersonic flow will occur regardless of speed.

This method permits the determination of speeds at which supersonic flow should occur. These critical speeds are not necessarily related to the speed at which the drag starts to increase or to the stability critical speed. Actually, the drag starts to rise at about the point where supersonic flow starts. This drag rise comes about not only because of the shock, where the flow attempts to become subsonic again, but also because of separation in the flow. The pressure gradients are increased by Mach Number, and, if separation is imminent, this can cause a drag rise without the existence of supersonic flows. If separations are not likely, there may be no drag rise at all up to the point where supersonic flow starts. The relationship between predicted speeds and experimental values is shown on Fig. 5 for the data of Fig. 8.

The method for obtaining two-dimensional airfoil data at high Mach Numbers varies between various experimenters. An unusual method has been used by the Boeing Aircraft Company in their wind tunnel at Seattle. Two walls, 6 in. apart, are mounted vertically in the test section giving a test section 6 in. in span by 96 in. high. When 6-in. chord airfoils spanning the jet are tested in this tunnel, the blocking is small, permitting tests of 10 per cent thick airfoils to speeds above 0.92 Mach Number. Figs. 11 and 12 show the arrangement of this test section. The velocity be-

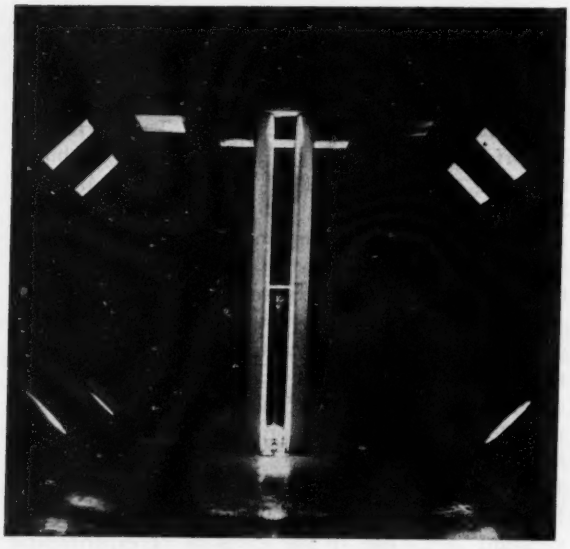

FIG. 11. High-speed two-dimensional end plates in test section of Boeing wind tunnel.

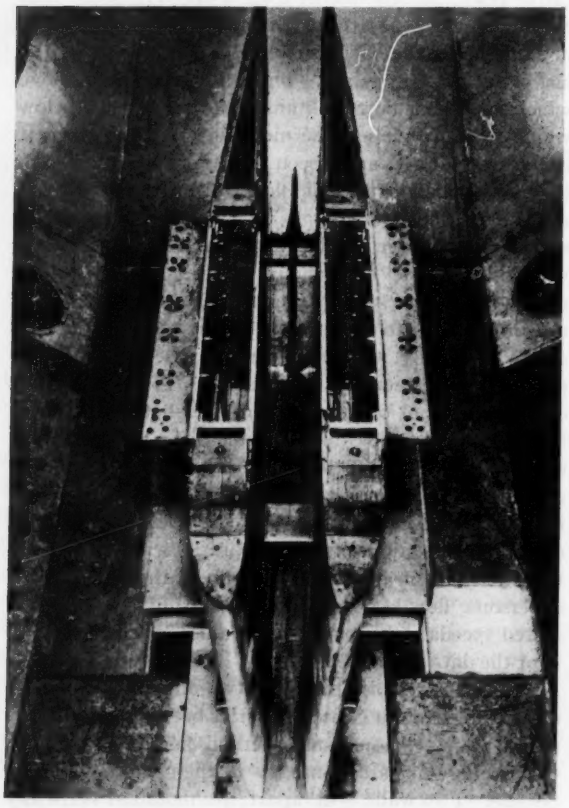

FIG. 12. Top view of high-speed two-dimensional test section with tunnel top removed.

tween the walls is uniform at all speeds and is about 50 per cent higher between the walls than in the tunnel proper. Lift, drag, and moment are measured on the force balance. The drag is also measured by wake survey. Figs. 13 and 14 show the test section used to measure low-speed pressure distribution, flap effects, and stalling characteristics. Airfoils used in this test section have 36-in. span and usually are of 24-in. chord.

APPLICATION TO THE AIRPLANE

So far, only the determination of the aerodynamic characteristics of an airfoil have been covered. Methods have been described by which the physical characteristics of an airfoil may be resolved into aerodynamic characteristics. However, the physical problems are of great importance in determining the airfoil. In most airplanes, the wing is called upon to be the backbone of the structure, to be the container of fuel and landing gear, and to be the hiding place for a high lift device, as well as to produce lift and lateral rolling control. The flexural rigidity of a wing is closely related to the ratio of span to root thickness. To keep equal rigidity when changing aspect ratio, it is necessary to thicken the root sections proportional to the aspect ratio increase. This leads to the use of high thickness ratios for the root sections of high aspect ratio wings. Most long-range airplanes have fuel volume requirements that are so severe that wing thickness is defined by the thickness necessary to provide the required internal volume. If the airplane is not expected to fly at high Mach Numbers, the maximum wing thickness may still be limited by aerodynamic considerations. The maximum possible thickness ratio has not yet been determined. The Boeing XPBB-1 used a constant chord inner wing with a thickness of 23 per cent. Entirely normal flow existed over this wing even with the extremely large deicers inflated.

LANDING GEAR AND FLAPS

The landing gear is frequently housed in the wing. This will often place severe limits upon the airfoil profile if the gear is to be held within the normal wing surface. Usually, a compromise is reached with portions of the landing gear protruding from the wing contour. The problem is more serious with wing flaps where the wing contour is usually chosen so as to contain all or nearly all the flap mechanism. Hollowness of either the upper or lower surface contours frequently works great hardships upon the flap mechanism. Such mechanism problems will frequently be more important than aerodynamic considerations in defining the trailing-edge shape.

AILERONS

The aileron normally fits into the outer 40 per cent of the span of the trailing edge. This places additional demands upon the airfoil sections of this portion of the wing. Airfoil sections with large included angles at the trailing edge tend to have thick boundary layers

at the trailing edge with a strong tendency toward local separation. This will greatly affect the aileron effectiveness and hinge moments. If the airfoil camber line has appreciable camber near the trailing edge, the aileron hinge moments are likely to be biased the same as they would by a full span tab with similar shape. This will cause the ailerons to float at other than neutral and will load the aileron control system. This is undesirable on military airplanes where battle damage may sever a control cable. It also causes added control system friction. When spring tab ailerons are used, it is important for the ailerons to float at neutral. The other aerodynamic effect of the airfoil on the aileron is the effect of bulging or hollow contours on hinge moment. Optimum results are obtained with nearly flat surfaces. For all of these reasons, it appears desirable to use an airfoil that has flat surfaces in the region of the aileron with a fairly small included angle.

The use of flat surfaces to form the trailing edge of airfoils has much to be said for it, although it places limitations upon the camber and thickness shapes that can be used, since both will automatically become straight in the region where flats are used. In general, such limitations are entirely acceptable. The effect of such a change in airfoils near the trailing edge cannot have any great effect upon drag because the boundary layer in this region tends to be flat even with curved airfoils. This has been borne out in two-dimensional airfoil tests conducted at Boeing. When the wing has a constant thickness ratio, flat surfaces are useful in that the trailing edge becomes two flat planes. This permits simplified structural design and is particularly useful when flaps or ailerons are not made of a constant per cent chord. In this case, it is possible to build constant chord flaps or ailerons with identical shapes along the span.

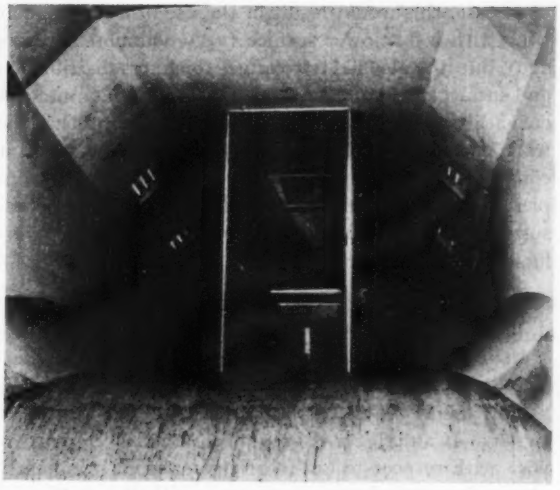

FIG. 13. Test section of Boeing wind tunnel with end plates for low-speed tests of 2-ft. chord = 3-ft. span airfoils.

FIG. 14. Wake survey rake behind flapped airfoil in test section of Fig. 13.

FLUTTER

The flutter and aileron reversal problem is intimately associated with the airfoil shape. The torsional rigidity that can be built into a wing is directly related to the cross section of the airfoil. Thin airfoils are fundamentally flexible and therefore undesirable from an aileron reversal standpoint. The flutter characteristics are also affected by the chordwise location of the structure in that this locates the mass center and the shear center to a great extent. This factor is not normally considered in the choice of an airfoil but may become important as speeds increase.

DEICING

Systematic studies of the effect of different airfoils upon deicing have not been made in deciding upon airfoils, but this may be important. Sharp leading edges should materially reduce the area to be deiced. There appears to be ample evidence to indicate that airfoil contour has much to do with the type of ice accumulations encountered. This problem should be studied in ice tunnels to determine the airfoil shape factors affecting icing.

STRUCTURE

The structural design of wings may frequently have important effects upon the airfoil choice. In the sim-

plest case, this would result in the use of a rectangular wing with a flat lower surface (very common 10 years ago), but it is also likely to affect thickness distribution and surface curvature. Peculiar twists and nonuniform curvature will frequently be so difficult to form that the wing incorporating them may be so distorted when it comes out of the shop as to definitely indicate some simpler shape would have given better aerodynamic results. This manufacturing problem must not be overlooked in choosing airfoils.

Stalling

Usually the first consideration in the choice of airfoils is the stalling problem. Stalling characteristics usually define the taper and twist of the wing for the designer. If a designer is prejudiced favorably or otherwise with respect to any particular airfoil, it is nearly always because of some experience with the stalling of an airplane using the airfoil. Although taper and twist are important, there can be little question that the airfoil is the most important single variable in the stalling problem. In multiengined airplanes, the propeller slipstreams will tend to prevent root stalling when any power is being used. The stall is thereby forced onto the tips, and the problem is not one of obtaining root stalling but one of having good stall characteristics with the stall first appearing at the tips. This is contrary to the popular conception wherein "tip stalling" is used to define bad stalling characteristics. In solving this problem, the airfoil shape is almost the only variable which can be varied. Airfoils with flat top lift curves give progressive stalls with more than sufficient warning to the pilot. The conventional approach to computing the stall by the use of spanwise lift curves has little if any significance when applied to wings with flat top lift curves. The application of flaps to airfoils materially changes their stall characteristics. This is likely to be important in the choice of airfoils and flaps. In any case, the airplane designer will normally use only those airfoils that for one reason or another he thinks will give a good stalling airplane. Although the stalling problem is of probably first importance in the choice of airfoils, it is the one concerning which the designer has probably the least factual information.

Conclusions

Each airplane and each designer will face different problems in the choice of airfoils. Some of the problems that are faced and some systematic methods for their study have been discussed. The properties of sections without supersonic flow or separation are readily predicted. The critical Mach Number can be estimated reasonably well, but the boundaries and characteristics of separated flow are not yet susceptible of estimation. Although these separation problems define the stall, which is of primary importance, experimental methods for determining stalling characteristics are questionable. Physical, structural, and arrangement problems will often define airfoils and their thickness in particular. Aileron and flap problems can have strong effects tending toward the use of airfoils with straight contours on their rear portions.

Exact and Approximate Solutions of Two-Dimensional Oblique Shock Flow

(*Continued from page 41*)

[5] Durand, W. F., *Aerodynamic Theory, Vol. III*, pp. 210–250; Julius Springer, Berlin, 1934.

[6] Busemann, A., *Aerodynamischer Auftrieb bei Uberschallgeschwindigkeit*, Luftfahrtforschung, Vol. 12, No. 6, pp. 210–220, October, 1935.

[7] Epstein, Paul S., *On the Air Resistance of Projectiles*, Proceedings of the National Academy of Science, Vol. 17, pp. 532–547, 1931.

[8] Taylor, G. I., *Applications of Ackeret's Theory of Aerofoils Moving at Speeds Greater Than That of Sound*, R. & M. No. 1467, British A.R.C., 1932.

[9] Hooker, S. G., *The Pressure Distribution and Forces on Thin Aerofoil Sections Having Sharp Leading and Trailing Edges, and Moving with Speeds Greater Than That of Sound*, R. & M. No. 1721, British A.R.C., 1936.

[10] Stack, John, Lindsay, W. F., and Littell, Robert E., *The Compressibility Burble and the Effect of Compressibility on Pressures and Forces Acting on an Airfoil*, N.A.C.A. Report No. 646, 1938.

[11] Vazsonyi, Andrew, *On Rotational Gas Flows*, Quarterly of Applied Mathematics, Vol 3, No. 1, pp. 29–37, April, 1945.

Force Measurements by Means of Resistance Wire Strain Gages

W. C. RANDELS* AND V. C. PLANE†
North American Aviation, Inc.

ABSTRACT

It is now common practice to measure forces by a spring in the form of a cantilever beam whose deflection is measured by resistance wire strain gages. In this paper, formulas and charts are given to aid in designing the beams. Several electrical circuits are analyzed. The results of some experiments on the effect of working voltage and temperature are presented.

NOTATION

F	=	applied force, lbs.
W	=	beam width, in.
$\Delta a/a$	=	unit strain in beam, in per in.
E	=	Young's modulus, lbs. per sq. in.
h	=	half thickness of beam, in.
x	=	distance from point of application of load, in.
δ	=	deflection, in.
M.A.	=	Mechanical advantage of lever system
R	=	resistance, ohms
R_1, R_2, R_3, R_4	=	gage resistances, ohms
R_1', R_2', R_3', R_4'	=	lead resistances, ohms
ΔR	=	change in resistance, ohms
s	=	strain sensitivity, $\Delta R/R = S(\Delta a/a)$
e	=	output voltage, volts
ϵ	=	input voltage, volts
r	=	meter resistance, ohms
i	=	output current, amp.
I	=	input current, amp.
ρ	=	shunt resistance, ohms
T	=	temperature, °C.
α, α'	=	temperature coefficient, ohms per °C.
L	=	applied load, lbs.
l	=	length of wire in gage, in.
D	=	diameter of wire, in.

INTRODUCTION

FOR SEVERAL YEARS resistance wire strain gages have been extensively used for measuring stresses in structural members. The methods used have been extensively covered in the literature. Recently, the aircraft industry and the National Advisory Committee for Aeronautics have been using resistance wire strain gages for measuring forces in both flight and model tests. These methods have now been sufficiently developed to offer possibilities of use in secondary force measuring systems, such as wind-tunnel balance systems and the like. In this paper it is proposed to present some of the principal considerations involved in such applications.

Presented at the Radio and Instruments Session, Fourteenth Annual Meeting, I.A.S., New York, January 29–31, 1946.

* Aeronautical Engineer.
† Research Analyst.

APPLICATIONS

Forces can be measured by springs whose deflection is measured by resistance wire strain gages. Two types of springs are commonly used—the cantilever beam and the ring. Of these, the cantilever beam offers more effective use of its surface area and usually presents no installation difficulties. This discussion will be confined to cantilever beams.

A constant strength beam of parabolic shape has the advantage that the average strain is equal to the maximum strain. In practice, two points are chosen on the parabola and a straight line drawn between them. For design purpose, it is sufficient to use the formulas for a constant strength beam. Corrections have been calculated and expressed graphically but their use has not been found necessary.

The handbook formula for stress in a constant strength beam is

$$F/W = {}^2/_3(\Delta a/a)E(h^2/x) \qquad (1)$$

The corresponding formula for deflection is

$$\delta^2(F/W) = (\delta/27)E(\Delta a/a)^3x^3 \qquad (2)$$

These formulas are graphed in Figs. 1 and 2. In practice the deflection and maximum load are usually specified and the length and width are set by practical considerations. The corresponding unit strain is determined from Fig. 1 and the beam thickness from Fig. 2. The quantity $\Delta a/a$ determines the sensitivity of the system. If this turns out to be too small, a suitable lever system will raise the sensitivity, for after a lever system is introduced, we have the new force and deflection at the beam. Then from Eq. (2)

$$F' = F/\text{M.A.},\ \delta' = \delta\text{M.A.}$$

$$\text{M.A. } \delta^2\frac{F}{W} = \delta'^2\frac{F'}{W} = \frac{8}{27}E\left(\frac{\Delta a}{a}\right)^3 x^3$$

which shows that the sensitivity for a given load and deflection varies as the cube root of the mechanical advantage.

The most useful electrical circuits are based on the Wheatstone bridge. It is most convenient to have all four arms of the bridge active. This makes temperature compensation simpler and, in some circuits, gives more sensitivity for a given amount of energy dissipated on

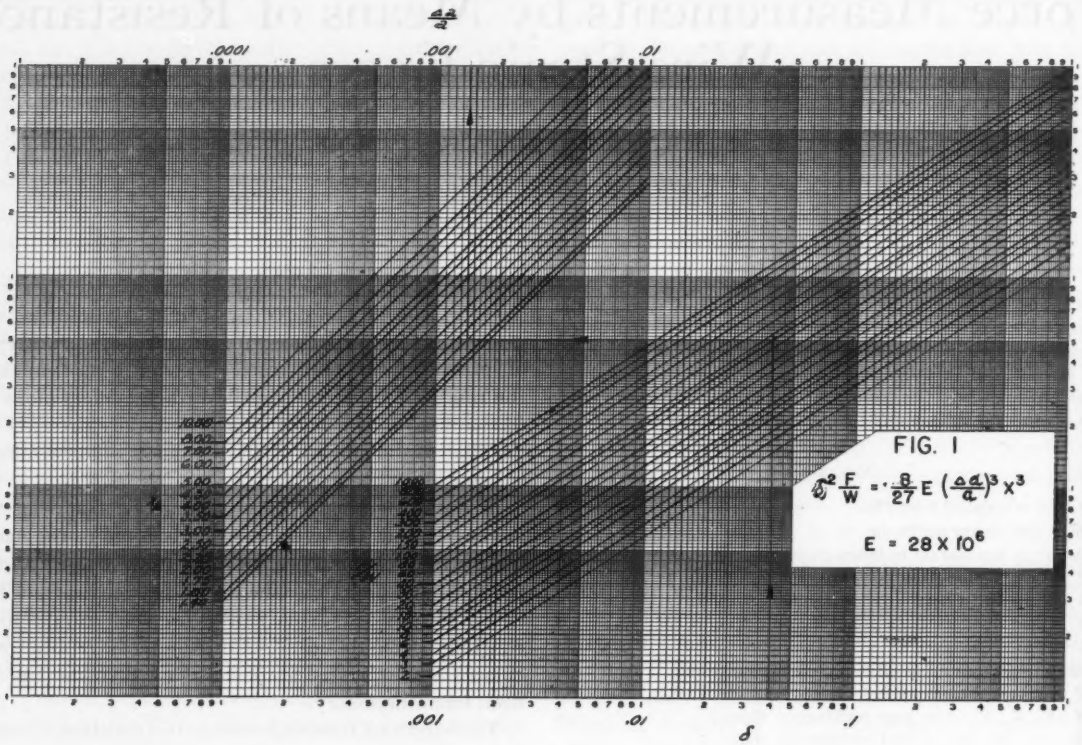
Δa/a
.0001
.001
.01
.001
.01
.1
δ
FIG. 1
δ² F/W = 8/27 E (Δa/a)³ x³
E = 28 x 10⁶

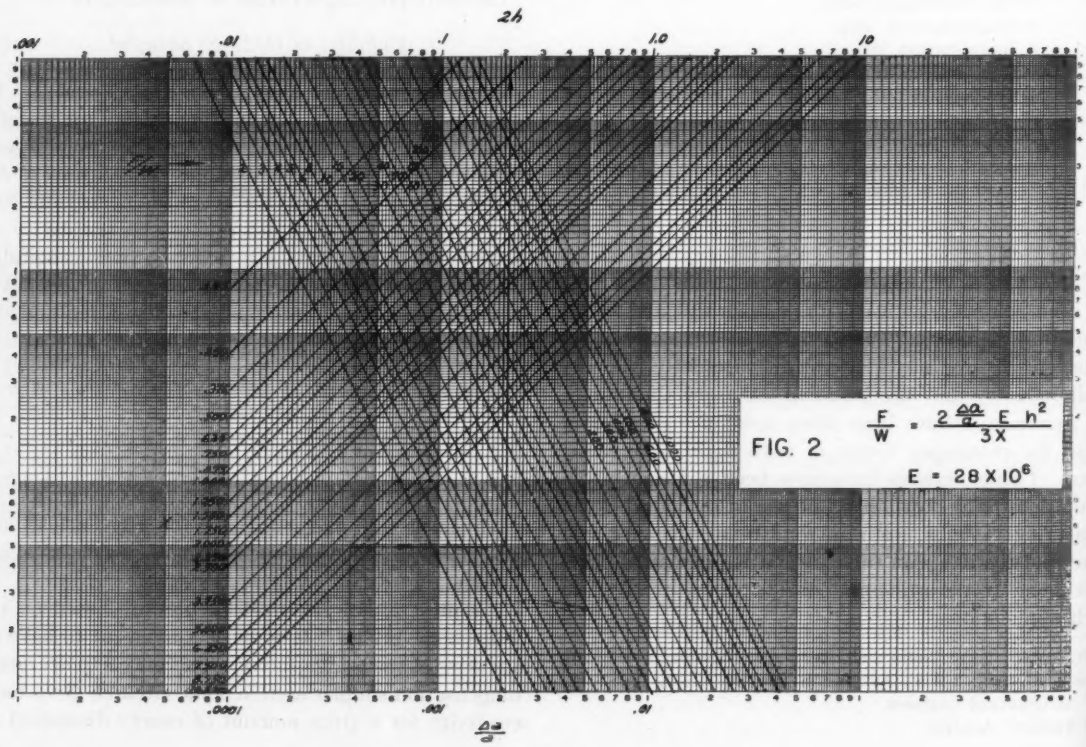
2h
.001
.01
.1
1.0
10
.0001
.001
.01
Δa/a
FIG. 2
F/W = 2 Δa/a E h² / 3x
E = 28 x 10⁶

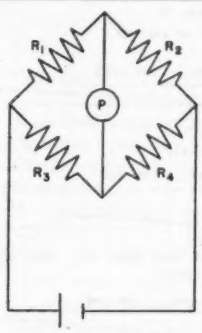

FIG. 3

$$e = s\frac{\Delta a}{a}\,\epsilon$$

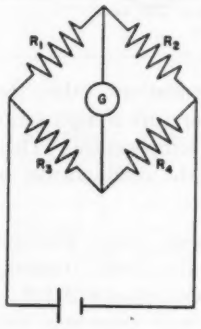

FIG. 4

$$i = \frac{s\frac{\Delta a}{a}}{1+\frac{r}{R}}\,I$$

$$e = \frac{s\frac{\Delta a}{a}\frac{r}{R}}{1+\frac{r}{R}}\,\epsilon$$

$$ei = \frac{\left(s\frac{\Delta a}{a}\right)^2\frac{r}{R}}{\left(1+\frac{r}{R}\right)^2}\,\epsilon I$$

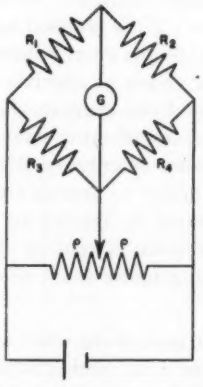

FIG. 5

$$s\frac{\Delta a}{a} = \frac{\frac{\Delta\rho}{\rho}\quad\frac{R}{\rho}}{\left(1+\frac{R}{\rho}\right)\left(2-\frac{1}{1+\frac{R}{\rho}}\right)}$$

the beam. Three circuits that have been used successfully are illustrated in Figs. 3, 4, and 5.

The circuit of Fig. 3 uses a potentiometer to measure the bridge unbalance. The sensitivity is given by

$$e = s(\Delta a\epsilon/a)$$

When used with modern self-balancing potentiometers, this is usually the most satisfactory arrangement. The sensitivity of the circuit is independent of the temperature. The zero drift with temperature, as will be seen later, is easily eliminated. If a potentiometer with a sensitivity of 0.01 millivolt is used with an applied voltage of five volts and gages with a gage factor of two, this setup will measure a $(\Delta a/a) = 1 \times 10^{-6}$, which for steel corresponds to a stress of 28 lbs. per sq.in.

The circuit of Fig. 4 uses a galvonometer or microammeter to measure the bridge unbalance. The sensitivity is given by the formulas

$$i = \{s(\Delta a/a)/[1 + (r/R)]\}I$$

$$e = \{s(\Delta a/a)(r/R)/[1 + (r/R)]\}\epsilon$$

$$ei = \{s(\Delta a/a)^2(r/R)/[1 + (r/R)]^2\}\epsilon I$$

The last of these, the power sensitivity, is the most important. The bridge and meter must be designed to go together. For maximum efficiency r and R should be equal. However, in this case, the circuit is usually overdamped, therefore any circuit of this type must be a compromise. With a commercial microammeter a sensitivity of $\Delta a/a = 1 \times 10^{-5}$ can easily be obtained. Much more sensitivity may be obtained with galvanometers. This circuit is used for measuring transient forces. At medium frequencies, the bridge output may be fed directly into a galvanometer. For high frequencies, amplifiers may be necessary because of the low sensitivity of high-frequency galvanometers. The sensitivity of the circuit depends on r/R and, hence, on the temperature; however, for the low temperature coefficient gages ordinarily used, this effect is negligible.

The circuit of Fig. 5 uses a galvanometer or potentiometer only as an indicator and the shunting resistance is varied to give a zero reading on the indicator. The sensitivity is given by

$$S\frac{\Delta a}{a} = \frac{(\Delta\rho/\rho)(R/\rho)}{[1 + (R/\rho)](2 - \{1/[1 + R/\rho]\})}$$

It has the advantage that the sensitivity is independent of the supply voltage and therefore a separate voltage reading is necessary. On the other hand, the calibration curve will be nonlinear and the sensitivity again depends on the temperature.

The circuit of Fig. 4 is the natural one to use when large temperature variations are expected. An analysis will be made of the temperature compensation problem for that circuit. For any circuit of this type, the voltage across the potentiometer is given by the formula

$$e = \{[R_1/(R_1 + R_2)] - [R_3/(R_3 + R_4)]\}\epsilon$$

If the resistances R_i are given increments ΔR_i, then to a first approximation the voltage will change by

$$\frac{de}{\epsilon} = \frac{R_2\Delta R_1 - R_1\Delta R_2}{(R_1 + R_2)^2} - \frac{R_4\Delta R_3 - R_3\Delta R_4}{(R_3 + R_4)^2}.$$

If the resistances R_i are in one piece and have the same temperature coefficient, then the change of resistance due to temperature is given by $\Delta R_i = \alpha R_i \Delta T$ and the change in meter reading is

$$\frac{de}{\epsilon} = \frac{\alpha R_2 R_1\Delta T - \alpha R_2 R_1\Delta T}{(R_1 + R_2)^2} - \frac{\alpha R_3 R_4\Delta T - \alpha R_3 R_4\Delta T}{(R_3 + R_4)^3} = 0$$

so that, under these assumptions, temperature compensation would be perfect. However, in practice it is

FIG. 6
EFFECT OF TEMPERATURE

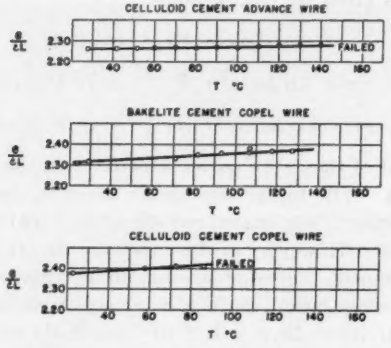

FIG. 7
EFFECT OF VOLTAGE

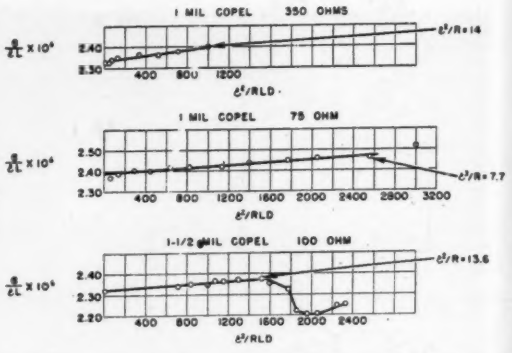

necessary to consider the effect of the leads which usually have a much different temperature coefficient from the gages. We denote the lead resistances by R_l' and their temperature coefficient by α' then

$$\frac{de}{\epsilon} = \frac{\Delta T(\alpha - \alpha')(R_2'R_1 - R_1'R_2)}{(R_1 + R_1' + R_2 + R_2')^2} - \frac{\Delta T(\alpha - \alpha')(R_4'R_3 - R_3'R_4)}{(R_3 + R_3' + R_4 + R_4')^2}$$

If we assume that the gages have approximately the same resistance R and that R_l' is small compared to R, then, neglecting higher order terms in R_l' and $(R_l - R)$

$$\frac{de}{\epsilon} = \frac{R_1' - R_2' - R_3' + R_4'}{4R} \Delta T(\alpha' - \alpha)$$

This shows that if the leads are approximately equal, the temperature compensation will be satisfactory. With only moderate care, the zero drift for 100°C. temperature change can be held to an amount corresponding to $\Delta a/a = 1 \times 10^{-5}$, and by trial-and-error adjustment of the leads values of one-fifth of this may be reached. Shunting resistance to give a suitable zero on the meter has the effect of changing the lead resistance and should be avoided. The zero can be controlled by selecting the gages or by adjusting the range of the potentiometer.

Since the sensitivity of a strain gage system depends on the applied voltage, it is desirable to know how much voltage can be safely used. This is a complicated problem since it depends considerably on the heat transfer characteristics of the installation. Also, the zero drift will depend on the temperature compensation and the uniformity of the gage temperature. Therefore, only experience can supply the final answer to this problem.

Fig. 6 shows the results of some tests. The beam had approximately 4 sq.in. effective heat transfer area. The area around the gages was wrapped with felt. Without this wrapping readings were extremely unstable, even at low voltages. The gages tested were two commercial Bakelite gages of different sizes and one homemade gage cemented with celluloid cement. In Fig. 6, $e/L\epsilon$ (which is proportional to s/E) is graphed against ϵ^2/RZD (which is proportional to the energy input per unit wire surface area). This choice of abscissa gives lines of about the same slope and this suggests that the wire temperature is the parameter affecting strain sensitivity. The breakdown point is entirely different on this scale but seems more nearly to depend on total energy input and therefore must be related to beam temperature. The breakdown point is marked by pronounced drifting of the reading under load, probably due to slipping.

In Fig. 7 the results of some tests of the effect of temperature are given. The value $e/L\epsilon$ (which is proportional to S/E) is graphed against temperature. One of the gages was a commercial Bakelite gage, one was a commercial celluloid gage, and the third, manufactured locally, used celluloid cement. The maximum temperature reached with the locally made celluloid gage (140°C.) was considerably above that quoted for similar commercial gages.

Letter to the Editor

(*Continued from page 24*)

three quantities depends on the Mach Number at which the heat is added. Eqs. (a) to (c) were used to obtain Fig. 1. Fig. 1 shows that at a Mach Number of zero all of the heat added to the fluid appears as additional enthalpy ($dU + dW$). As M is increased, a larger and larger proportion of the heat energy goes into kinetic energy of directed motion. At $M = 1/\sqrt{\gamma}$, all of the heat energy goes into kinetic energy of directed motion. For $1 > M > 1/\sqrt{\gamma}$, dE/dQ is greater than unity. In other words, all of the added heat energy and part of the internal energy of the fluid goes into kinetic energy of motion along the pipe.

(2) It is interesting to note that the condition for the vanishing of dT, which is the $\gamma M^2 = 1$, can be manipulated as follows:

$$\gamma M^2 = \gamma(u^2/a^2) = u^2/RT = 1$$

Therefore,

$$u^2/2 = RT/2 = {}^1/_3(\overline{C}^2/2)$$

where $\overline{C}^2$ is the mean square molecular speed of random (thermal) motion. Therefore, when $\gamma M^2 = 1$, the kinetic energy of the directed translatory motion along the pipe of 1 lb. of the gas is equal to the kinetic energy associated (under the assumption of equipartition of thermal energy) with each degree of freedom in translation of the molecules in 1 lb. of gas.

(3) The case of isothermal flow can also appropriately be discussed here. Binder has shown[2] that, for flow with friction and heat transfer, the limiting Mach Number for isothermal flow is $M = 1/\sqrt{\gamma}$. The physical reason for this limit can be derived. The method will only be outlined and the result given briefly.

It should be remembered that in the discussion in paragraph (1) of the present letter the effects of friction were neglected. The effects of friction are taken into account by adding a friction term to Eq. (4). The specific case of heat transfer by forced convection is treated by setting

$$m\,dQ = h(T_w - T_s)dS$$

where h = heat-transfer coefficient, T_w = temperature of wall, T_s = stagnation temperature of gas, and S = surface area of wall.

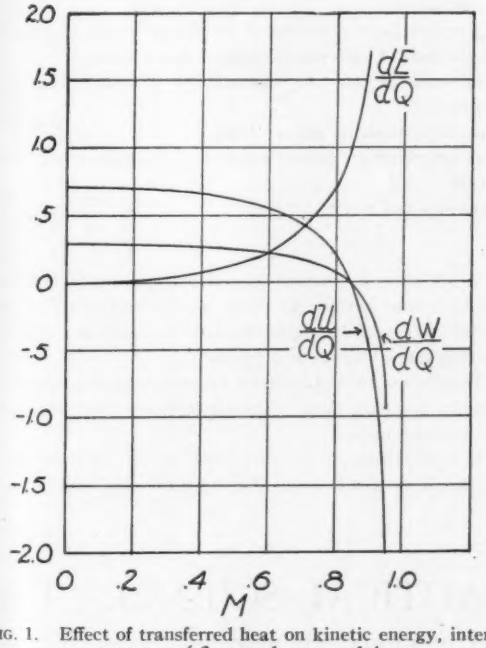

FIG. 1. Effect of transferred heat on kinetic energy, internal energy, and flow work. $\gamma = 1.4$.

The quantity h can then be eliminated in terms of the friction factor f by means of the relation

$$h/c_p\rho u = f/2$$

It can then be shown that the condition for isothermal flow, $dT = 0$, is that

$$\frac{T_w}{T_s} = 1 - \frac{\gamma(\gamma - 1)M^4}{(\gamma M^2 - 1)\{1 + [(\gamma - 1)/2]M^2\}}$$

This equation was employed to obtain Fig. 2, which shows T_w/T_s as a function of M for constant temperature. As M approaches $1/\sqrt{\gamma}$ from below, the value of T_w/T_s required for isothermal flow approaches infinity. For $M > 1/\sqrt{\gamma}$, negative values of T_w/T_s are required. Inasmuch as T_w and T_s are here based on the absolute temperature scale, negative values are physically impossible. They are shown by the dashed curve in Fig. 2.

What occurs is this. For all subsonic Mach Numbers, friction causes the temperature to decrease. For Mach Numbers up to $1/\sqrt{\gamma}$, the addition of heat to the fluid causes the temperature to increase. It is possible for the two effects to cancel each other and for the temperature to remain constant. At $M = 1/\sqrt{\gamma}$ the addition or the subtraction of heat does not affect the temperature; therefore, the temperature must decrease because of friction. For $1 > M > 1/\sqrt{\gamma}$, the extraction of heat causes the temperature to rise, but heat cannot be extracted by forced convection at a rate that is great enough to cancel the effect of friction. Therefore the temperature cannot remain constant.

(4) There is a misstatement on page 539, column 2, section 3(b), of the reference paper which should be corrected. The correct statement is: In the supersonic case, when heat is added, u decreases and p and ρ increase.

REFERENCES

[1] Hicks, Bruce L., *Addition of Heat to a Compressible Fluid in Motion*, N.A.C.A. A.C.R. No. E5A29, 1945. (This report has been declassified.)
[2] Binder, R. C., *Limiting Isothermal Flow in Pipes*, A.S.M.E. Trans., Vol. 66, No. 3, pp. 221–223, April, 1944.

GEORGE P. WOOD
Physicist
Langley Memorial Aeronautical Laboratory
N.A.C.A.

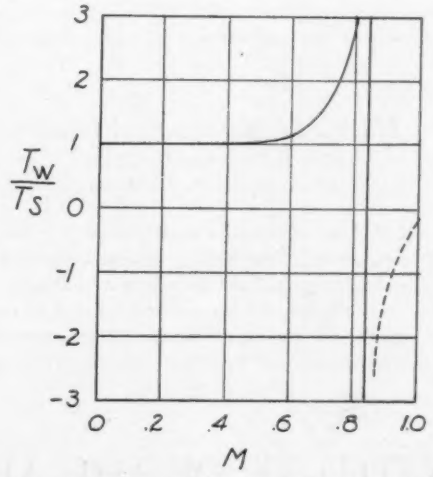

FIG. 2. Ratio of wall temperature to gas stagnation temperature as a function of Mach Number for isothermal flow. $\gamma = 1.4$.

Services of the Libraries of the Institute of the Aeronautical Sciences

The services of the Libraries are available to all members of the Institute, to Corporate Members, to advertisers in the AERONAUTICAL ENGINEERING REVIEW and AERONAUTICAL ENGINEERING CATALOG, and, under usual library limitations, to the public. Four specialized services are available.

The Paul Kollsman Lending Library

This lending library service makes available, *without charge*, the latest and more important aeronautical books.

Members may request the loan of any aeronautical or technical book they wish to borrow. Through an exchange agreement with the Engineering Societies Library, any book on general engineering may be borrowed from its great collection of over 160,000 volumes.

A photostating service is available at usual library rates.

Applications for membership in the library and further information will be sent on request.

The W. A. M. Burden Reference Library

This reference library contains over 12,000 aeronautical books, magazines, pamphlets, and reports gathered from world-wide sources and is one of the most complete aeronautical libraries in the world. Material from this library is not available for loan but may be used for reference purposes.

The Pacific Aeronautical Library

6715 Hollywood Boulevard
Los Angeles 28, California

Established in cooperation with the aircraft companies the library serves. The leading aircraft companies in or near Los Angeles participate in its support and operation.

This service library for aeronautical research is available to the public for reading privileges. Source material includes aerodynamic and structural research reports, as well as books on drafting, production methods, history, and allied sciences. It furnishes books, periodicals, and pamphlet material to the participating aircraft companies to supplement their engineering libraries.

Technical Information Service

This service has experienced personnel under the supervision of trained aeronautical engineers to compile any information desired. The services range from listing specialized reference books to the preparation of exhaustive bibliographies, digesting of reports, and general surveys of any aeronautical subject. Some of the available services are:

Bibliographies on any aeronautical subject.
Reports on any aeronautical subject.
Digests of aeronautical books, papers, periodicals, and references.
Translations.
Engineering investigations of special aeronautical subjects.
Biographies of individuals engaged in aeronautics.
Photostats of any aeronautical or general engineering material.
Microfilms made on special order.
Photographs made from the Institute's photographic collection.
Drawings and tracings made.

In addition to the services mentioned any commission which comes within the scope of the Service will be accepted. Special arrangements may be made for work requiring several weeks or months.

Translators are available for accurate transcriptions of all foreign language data. Translations are carefully edited by trained engineers.

Reproductions of any material in the collections of the Institute may be ordered at standard photostat rates.

INSTITUTE OF THE AERONAUTICAL SCIENCES, INC.
2 EAST 64TH STREET, NEW YORK 21, N.Y.